Western Graduate&PostdoctoralStudies

Western University
Scholarship@Western

Electronic Thesis and Dissertation Repository

10-19-2017 12:30 PM

The Recurrence-Based Analysis of Intracranial Pressure

Mahnaz Rabbani, *The University of Western ontario*

Supervisor: Dr. Mark Daley, *The University of Western Ontario*
Co-Supervisor: Dr. Lindi Wahl, *The University of Western Ontario*
A thesis submitted in partial fulfillment of the requirements for the Master of Science degree in Computer Science
© Mahnaz Rabbani 2017

Follow this and additional works at: https://ir.lib.uwo.ca/etd

Recommended Citation

Rabbani, Mahnaz, "The Recurrence-Based Analysis of Intracranial Pressure" (2017). *Electronic Thesis and Dissertation Repository*. 5156.
https://ir.lib.uwo.ca/etd/5156

This Dissertation/Thesis is brought to you for free and open access by Scholarship@Western. It has been accepted for inclusion in Electronic Thesis and Dissertation Repository by an authorized administrator of Scholarship@Western. For more information, please contact wlswadmin@uwo.ca.

Abstract

Modern computational approaches tied together with the power of mathematical science has pushed us closer to reach a deeper understanding of complex dynamical systems. Real-world biological and physiological systems now can be studied on account of the accessibility to fast, cheap and powerful computers. In particular, the field of neuroscience and brain data analysis has grown significantly in the recent years. Recurrence plots (RPs) are a relatively new approach for the analysis of non-linear, non-stationary and noisy data. Rooted in topological properties of the system, RP visualizes the recurrence states of the dynamical system. Armed with the recurrence quantification measures, RP is even more rigorous in exploring and quantifying real-world dynamical system.

In the present work, we benefit from the RP and RQA methods to study the behavior of intracranial pressure (ICP) waveforms. ICP is defined as the fluid pressure inside the skull which carries important information associated with the status of the patient. Our main goal is to detect sudden changes or extreme regime changing in these signals. Patterns appearing in RP can shed light on fundamental characteristics of the system. Our results suggest distinguishable patterns in the RPs of some subjects which are not detectable in the raw ICP signals. This work sets up the workflow for using RP analysis in online ICP monitoring of brain-injured patients.

Keywords: intracranial pressure (ICP) analysis, recurrence plot (RP), recurrence quantification analysis (RQA)

Acknowledgments

I wish to express my sincere appreciation to my supervisors, Dr. Mark Daley and Dr. Lindi Wahl, for giving me the opportunity to work under their invaluable supervisions. I wish to give my gratitude to my colleagues especially James Hughes, and the examining committee, in particular, Dr. Douglas Fraser for his insightful comments.

I owe infinite thanks to my lovely parents, Reza and Maryam, and my sisters, Reihaneh and Parisa, for their continuous support and encouragement. I am in particular thankful beyond words to my older sister, Reihaneh, for all the love, attention, encouragement and support she gave me. Lastly, I would like to thank my dear friend Sina, for supporting me through my research.

Table of Contents

Abstract i

Acknowledgments ii

Table of Contents iii

List of Figures v

1 Introduction and Background 1
- 1.1 Primary and secondary brain injury 1
- 1.2 Intracranial pressure 3
  - 1.2.1 ICP hypertension 3
  - 1.2.2 ICP monitoring 4
  - 1.2.3 ICP waveform 5
- 1.3 Previous work on ICP analysis 6
  - 1.3.1 ICP hypertension forecasting 7
  - 1.3.2 ICP waveform complexity and entropy 9
  - 1.3.3 ICP waveform nonlinearity 11
- 1.4 Recurrence plots 12
  - 1.4.1 Phase space and trajectories 13
  - 1.4.2 Poincaré recurrence theorem 14
  - 1.4.3 Takens' embedding theorem 14
  - 1.4.4 Recurrence plots definition 15
  - 1.4.5 Embedding dimension 16
  - 1.4.6 Norm and threshold 17
  - 1.4.7 Structures in recurrence plots 17
  - 1.4.8 Recurrence quantification analysis (RQA) 19
- 1.5 Thesis Statement and Contribution 22

2 Methodology and Results 23
- 2.1 The MIMIC II data set 23
  - 2.1.1 Clinical database 24
  - 2.1.2 Waveform database 25
  - 2.1.3 Data preprocessing 25
  - 2.1.4 Dataset limitations 26
- 2.2 Recurrence plots 27

2.2.1 Structures in RPs 29
2.2.2 RQA 31
2.2.3 Anomalous Subjects 35
2.2.4 Novelty Curve of RP 36

3 Discussion and Conclusion **44**

Bibliography **47**

Appendix **51**

A Comprehensive Results **52**

List of Figures

Figure 1.1: The normal ICP waveform 6

Figure 2.1: Time series of subject 3094054 27
Figure 2.2: RP of subject 3094054 30
Figure 2.3: RP of subject 3105502 31
Figure 2.4: RP of subject 3779174 32
Figure 2.5: RP of subject 3646209 33
Figure 2.6: Distributions of different RQA measures 34
Figure 2.7: Anomaly subject in $ENRT_V$ 36
Figure 2.8: Anomaly subject in $ENRT_V$ 37
Figure 2.9: Anomaly subject in DIV 38
Figure 2.10: Anomaly subject in L_{max} 39
Figure 2.11: Anomaly subject in DIV 40
Figure 2.12: Anomaly subject in DIV 41
Figure 2.13: Novelty curve of ICP 42
Figure 2.14: Novelty curve of RP 43

Figure A.1: Distributions of RQAs for all subjects 52
Figure A.2: Distributions of different RQA measures 53
Figure A.3: Novelty curves of subject 3029993 54
Figure A.4: Novelty curves of subject 3033031 55
Figure A.5: Novelty curves of subject 3083337 56
Figure A.6: Novelty curves of subject 3094054 57
Figure A.7: Novelty curves of subject 3096171 58
Figure A.8: Novelty curves of subject 3105502 59
Figure A.9: Novelty curves of subject 3169632 60
Figure A.10: Novelty curves of subject 3262086 61
Figure A.11: Novelty curves of subject 3269261 62
Figure A.12: Novelty curves of subject 3289177 63
Figure A.13: Novelty curves of subject 3367596 64
Figure A.14: Novelty curves of subject 3379471 65
Figure A.15: Novelty curves of subject 3460047 66
Figure A.16: Novelty curves of subject 3463681 67
Figure A.17: Novelty curves of subject 3505904 68
Figure A.18: Novelty curves of subject 3516004 69
Figure A.19: Novelty curves of subject 3555523 70
Figure A.20: Novelty curves of subject 3562822 71

Figure A.21: Novelty curves of subject 3582988 72
Figure A.22: Novelty curves of subject 3599360 73
Figure A.23: Novelty curves of subject 3600995 74
Figure A.24: Novelty curves of subject 3607634 75
Figure A.25: Novelty curves of subject 3623238 76
Figure A.26: Novelty curves of subject 3645431 77
Figure A.27: Novelty curves of subject 3646209 78
Figure A.28: Novelty curves of subject 3662063 79
Figure A.29: Novelty curves of subject 3721988 80
Figure A.30: Novelty curves of subject 3738640 81
Figure A.31: Novelty curves of subject 3779174 82
Figure A.32: Novelty curves of subject 3781713 83
Figure A.33: RQA results of subject 3029993 84
Figure A.34: RQA results of subject 3033031 85
Figure A.35: RQA results of subject 3083337 86
Figure A.36: RQA results of subject 3094054 87
Figure A.37: RQA results of subject 3096171 88
Figure A.38: RQA results of subject 3105502 89
Figure A.39: RQA results of subject 3169632 90
Figure A.40: RQA results of subject 3262086 91
Figure A.41: RQA results of subject 3269261 92
Figure A.42: RQA results of subject 3289177 93
Figure A.43: RQA results of subject 3367596 94
Figure A.44: RQA results of subject 3379471 95
Figure A.45: RQA results of subject 3460047 96
Figure A.46: RQA results of subject 3463681 97
Figure A.47: RQA results of subject 3505904 98
Figure A.48: RQA results of subject 3516004 99
Figure A.49: RQA results of subject 3555523 100
Figure A.50: RQA results of subject 3562822 101
Figure A.51: RQA results of subject 3582988 102
Figure A.52: RQA results of subject 3599360 103
Figure A.53: RQA results of subject 3600995 104
Figure A.54: RQA results of subject 3607634 105
Figure A.55: RQA results of subject 3623238 106
Figure A.56: RQA results of subject 3645431 107
Figure A.57: RQA results of subject 3646209 108
Figure A.58: RQA results of subject 3662063 109
Figure A.59: RQA results of subject 3721988 110
Figure A.60: RQA results of subject 3738640 111
Figure A.61: RQA results of subject 3779174 112
Figure A.62: RQA results of subject 3781713 113
Figure A.63: RP and novelty curve of subject 3029993 115
Figure A.64: RP and novelty curve of subject 3033031 116
Figure A.65: RP and novelty curve of subject 3083337 117

Figure A.66: RP and novelty curve of subject 3094054 118
Figure A.67: RP and novelty curve of subject 3096171 119
Figure A.68: RP and novelty curve of subject 3105502 120
Figure A.69: RP and novelty curve of subject 3169632 121
Figure A.70: RP and novelty curve of subject 3262086 122
Figure A.71: RP and novelty curve of subject 3269261 123
Figure A.72: RP and novelty curve of subject 3289177 124
Figure A.73: RP and novelty curve of subject 3367596 125
Figure A.74: RP and novelty curve of subject 3379471 126
Figure A.75: RP and novelty curve of subject 3460047 127
Figure A.76: RP and novelty curve of subject 3463681 128
Figure A.77: RP and novelty curve of subject 3505904 129
Figure A.78: RP and novelty curve of subject 3516004 130
Figure A.79: RP and novelty curve of subject 3555523 131
Figure A.80: RP and novelty curve of subject 3562822 132
Figure A.81: RP and novelty curve of subject 3582988 133
Figure A.82: RP and novelty curve of subject 3599360 134
Figure A.83: RP and novelty curve of subject 3600995 135
Figure A.84: RP and novelty curve of subject 3607634 136
Figure A.85: RP and novelty curve of subject 3623238 137
Figure A.86: RP and novelty curve of subject 3645431 138
Figure A.87: RP and novelty curve of subject 3646209 139
Figure A.88: RP and novelty curve of subject 3662063 140
Figure A.89: RP and novelty curve of subject 3721988 141
Figure A.90: RP and novelty curve of subject 3738640 142
Figure A.91: RP and novelty curve of subject 3779174 143
Figure A.92: RP and novelty curve of subject 3781713 144

Chapter 1

Introduction and Background

1.1 Primary and secondary brain injury

Brain injuries are a major cause of death in the adult population under 45 years of age worldwide (Jennett, 1996). Roughly speaking, 1.5 million individuals suffer from Traumatic Brain Injury (TBI) in the United States annually. In Canada, unintentional events including head-injuries were ranked in the top five causes of death from 2009 to 2013[1].

According to Brain Injury Canada, annually 160,000 Canadians are affected by brain injuries. Statistics show that TBI is more common in males, particularly young men (Stein, 2001), and often occurs as a result of impacts to the head in road accidents, falls and assaults. The reality that so many disabilities and even deaths result from such events involving young people is troubling given that TBI imposes many social and financial costs on society, estimated near $200 million (based on 1991 dollars) annually in the United States (Runge, 1993).

TBI outcome most often is directly correlated with the severity of the primary injury; nonetheless, secondary brain injury also plays an important role. Primary injury is defined as the direct damage of the physical impact to the intracranial contents and occurs at the time of the incident, while secondary brain injury is defined as the damage and pathological conditions that develop over time as a result of primary injuries and could occur shortly after the primary injury or many days after admission to the intensive care unit (ICU) (Mendelow et al., 2005).

---

[1] Statistics Canada. Table 102-0561-Leading causes of death, total population, by age group and sex, Canada, annual, CANSIM (database).

Secondary brain injury is caused by cerebral ischemia, cerebral hypoxia, inflammation, seizure, etc. Cerebral or brain ischemia occurs when there is not enough blood flow to the brain to fulfill the metabolic need for oxygen. Subsequently, this lack of oxygen leads to damage and death of brain tissues. The damage could be to a specific region of the brain (focal ischemia), or to larger areas (global ischemia). Cerebral hypoxia occurs when the oxygen flow to the brain decreases. The causes could be a reduction in blood flow (brain ischemia) or a problem in breathing or blood oxygenation, etc. Brain herniation occurs when the intracranial pressure (ICP; will be explained in the next subsection) increases above the normal value. Sustained elevated ICP can cause serious damage to the brain which may result in moderate to severe disability or even death. ICP elevation occurs when intracranial contents are compressed and relocated due to the pressures caused by brain swelling, usually by a brain tumor, head injury or stroke.

Unlike primary brain damage, some types of secondary brain injury can be preventable. Actively monitoring the patients can lead to an early and accurate diagnosis of secondary brain injury which is a key factor in treatment and subsequently preventing further damage to the brain. ICP is one of the commonly monitored physiological measures in criticality brain-injured patients. Although there is abundant research that supports ICP monitoring and recommends it as one of the important indicators in management guidelines for TBI, still some studies reject any difference in the outcome of patients with ICP monitoring (Cremer et al., 2005; Dang et al., 2015).

1.2 Intracranial pressure

Intracranial pressure (ICP) is simply the fluid pressure inside the cranium. According to the Monro-Kellie doctrine (Neff and Subramaniam, 1996), the skull is similar to a closed box, containing a fixed volume of incompressible intracranial components. ICP is defined as the pressures of these intracranial components: brain matter, cerebrospinal fluid (CSF), and cerebral blood. The ICP value depends on age, body position, and health condition and is altered by sneezing, coughing, Valsalva maneuver, etc. In a healthy adult, ICP is normally between 7-15 mmHg in a supine position (Brain et al., 2007). In young children and infants, ICP is lower at 3-7 mmHg and 1.5-6 mmHg, respectively (Greenberg and Arredondo, 2006). Although the ICP may drop below the normal value, above-normal ICP is a more common and threatening condition.

1.2.1 ICP hypertension

ICP could be increased in pathological conditions caused by disease or impact to the head, for instance when an abnormal object, such as a tumor or a hematoma, is added to the incompressible matter within the skull. Following the initial ICP increase, the auto-regulation system controls and balances this increase by decreasing the cerebral blood and fluid inside the skull. However, the auto-regulation mechanism is able to keep the pressure equilibrium for only a short period of time, after which the ICP elevation could cause damage to the brain tissue. Sustaining ICP values over 20 to 25 mmHg for more than at least five minutes is considered ICP hypertension and can cause severe brain damage if untreated.

Following severe TBI, it is very likely that patients develop ICP hypertension and the correlation between intracranial hypertension and TBI outcome is well established (Juul et al., 2000; Kim, 2011; Mayer and Chong, 2002). It has been shown that increased ICP is associated with poor outcomes in TBI (Miller et al., 1977; OṔhelan et al., 2009) and has a mortality rate of 20% (Fakhry et al., 2004).

According to a study by OṔhelan et al. (2009), ICP hypertension occurs in four distinguishable patterns in TBI patients: early, late, bimodal and continuous. Early/late ICP hypertension is defined as when the pressure increases within/after 72 hours of TBI. Bimodal ICP involves two separate increases, first in the early stage and then again in the late stage, while in the continuous pattern the ICP increases continuously and does not abate once it has begun. Although it is a common belief that most secondary brain injuries develop in the first 72 hours after primary injury, Johnston et al. (1970) suggest that ICP monitoring should be continued after the first 72 hours even in patients for whom ICP is normal during this period of time. The authors found that 17% of the patients in their dataset developed an increased ICP described by the late pattern, with a peak time of 7 days post-injury.

1.2.2 ICP monitoring

ICP monitoring is one of the brain-specific monitoring criteria in the neurocritical care unit. ICP monitoring usually is applied on comatose patients, patients suspected of primary and secondary brain injuries, patients suffering from stroke or tumor, and patients with neurological problems which have remained undiagnosed by other medical examinations. Two types of ICP monitoring exist: invasive and noninvasive operations.

External ventricular drain (EVD) is the most common invasive ICP measurement. EVD is a moderately invasive ICP procedure in which a medical professional inserts a catheter into the lateral ventricular region of the patient's skull. The pressure is then recorded at a specific frequency and the bedside monitor displays the values. The monitoring time varies depending on ICU medical staff choices, however, a minimum of 30 seconds is needed for a standard ICP recording. EVD may include some risks, such as bleeding, infection, brain tissue damage and brain herniation.

Some examples of noninvasive techniques includes Transcranial Doppler Ultrasonography (TCD), Tympanic Membrane Displacement (TMD), and Optic Nerve Sheath Diameter (ONSD). In general, these methods attempt to estimate the ICP value from noninvasive measures that are correlated with the ICP. However, up to this date, the accuracy of noninvasive techniques tend to have high inter-subject variability and are not adequate enough to replace invasive procedures (Raboel et al., 2012).

1.2.3 ICP waveform

The ICP waveform is composed of three components: the pulse waveform, the respiratory waveform, and the slow waveform. These components overlap in the time domain, but are separated in the frequency domain (Czosnyka and Pickard, 2004). In the time domain and on a scale of milliseconds, the ICP waveform displays three upstrokes in one wave. These are P_1, the percussion wave, which represents atrial pulsation; P_2, the tidal wave, which represents intracranial compliance; and P_3, the dicrotic wave, which represents aortic valve closure.

ICP waveforms can display four clinical statuses: normal, A, B, or C waves. In a normal ICP waveform, P_1 and P_3 should have the highest and lowest upstrokes respectively, and P_2 should be in the middle. If P_2 is higher than P_1, the patient suffers from intracranial hypertension (Kirkness et al., 2000).

The A wave (or plateau wave) is the most alarming type of ICP waveform and represents secondary brain injuries such as ischemia. This wave is recognized with an abrupt elevation in ICP to 50-80 mmHg that persists for more than five minutes. In B and C waves, elevations of ICP also occur, where in the former the increase is semi-periodic to 20-30 mmHg, while in the latter the increase is to a maximum of 20 mmHg with a frequency of 4-8 per minute (Lundberg et al., 1965).

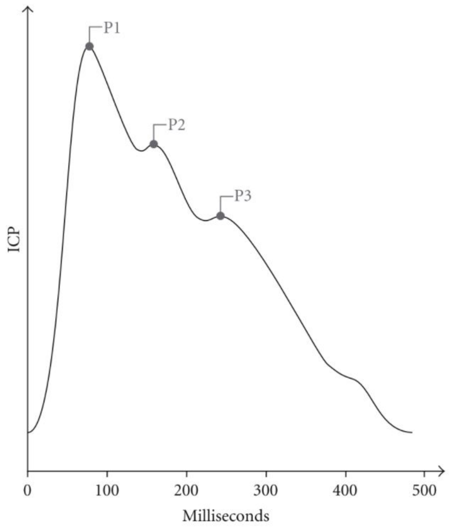

Figure 1.1: Simplified ICP waveform in a healthy person. Percussion, tidal, and dicrotic waves are tagged with P_1, P_2, and P_3, respectively.

Although the ICP mean value is important and helpful in clinical diagnoses, exploring the ICP waveform could reveal much more information about the dynamics of this system that are useful for prognostic and diagnostic applications. Like other complex biological systems, the ICP waveform represents a low-dimensional projection of a complex, high-dimensional system of its underlying components and their interactions. Any small change in these components will affect the whole system.

1.3 Previous work on ICP analysis

As mentioned in the previous section, researchers have made many efforts to study and explore ICP signals (Di Ieva et al., 2013). However, compared to other brain data, such as EEG, ICP research still has a long way to go, particularly in signal processing. Although today most physicians and researchers appreciate the importance of ICP monitoring, there are concerns that the only information currently used in clinical decisions is the mean ICP value, ignoring other types of potentially important information the signal carries regarding cerebrospinal pathophysiology (Czosnyka et al., 2007). The majority of studies utilizing machine learning and data mining techniques have attempted to provide a proactive manner for treatment of brain-injured patients by forecasting intracranial hypertension (ICH) and intracerebral hemorrhage from the ICP waveform. Moreover, some studies have focused on the correlation between the complexity of ICP signals and patient outcomes. Here, we provide a review of some of the most important previous work on ICP analysis.

1.3.1 ICP hypertension forecasting

It has been more than 30 years since scientists first tried to develop a framework for predicting ICP hypertension (IH), and a number of predictive features of the ICP time series have been suggested in the literature.

A fairly recent work on ICP analysis is an algorithm titled Morphological Clustering and Analysis of Intracranial Pressure (MOCAIP), proposed by Hu et al. (2009). The MOCAIP pipeline applies various data analysis methods (described below), signal processing and optimization techniques. The authors propose and validate this algorithm for analyzing continuous ICP waveforms. The inputs of this algorithm are the ICP and ECG signals and the outputs are the noise-filtered ICP signals with the sub-peaks identified. The authors claim that the algorithm improves the quality of the ICP signals by filtering noise as well as optimally determining the three sub-peaks in an ICP pulse.

Briefly, the algorithm consists of five main stages: pulse detection, pulse clustering, legitimate pulse recognition, peak detection and peak designation. In the pulse detection step, ECG beats are found using a method known as ECG QRS detection (Afonso et al., 1999). At this stage, the authors use an algorithm presented in their previous work (Hu et al., 2008) to construct the ICP pulse. The pulse clustering step filters out noise and artifacts to achieve filtered representative pulses instead of raw pulses. First, the pulses are clustered using Euclidian distance. Then the dominant pulse is defined as the average of the largest cluster and will be used for future analyses. However, it is possible that the dominant pulse can be completely noise (for example when the probe is detached) and should be removed from further analyses in the legitimate pulse recognition phase. In the peak detection and peak designation phases, three sub-peaks are detected for each legitimate dominant pulse using 24 MOCAIP metrics. Lastly, the algorithm is validated by comparing its results with the expert observations of a healthcare professional. Another study used experimental assessment to evaluate this methodological framework. The authors observed high specificity and low sensitivity of detecting IH for this framework (Hu et al., 2010).

In another study, the authors apply the MOCAIP algorithm, as well as a quadratic classifier (QDC), to forecast intracranial hypertension, which they define as any ICP time window during which pressure exceeds 20 mmHg for a minimum of 5 minutes. The authors claim that the ICP signal prior to intracranial hypertension could be differentiated from normal ICP signals. They provide a quantitative method by which to differentiate benign ICP elevations from possibly dangerous plateau waves (Hamilton et al., 2009).

Specifically, Hamilton et al. (2009) consider four different segments of the ICP signal: the beginning of intracranial hypertension and 5, 20 and 25 minutes before the IH starts. Then for each of these four segments, they determine a combination of metrics with the most predictive power among the 24 metrics of the MOCAIP algorithm. In this study, the authors used data from 37 patients hospitalized at the UCLA Medical Center. Patients had conditions that required ICP monitoring, such as hydrocephalus (accumulated cerebrospinal fluid in the skull) and shunt malfunction problems. The authors proposed a method by which to forecast potentially harmful ICP elevations in order to prevent erroneous diagnoses of plateau waves and over-treatment. Their results offer a forecasting horizon of five minutes with 90% sensitivity and 75% specificity.

So far, we have reviewed the studies that have considered ICP signals in the time domain where usually the focus is to detect the three sub-peaks in the waveform. It is worth mentioning that besides the more commonly used time domain analysis, there is another type of ICP analysis that focuses on the frequency domain of the signals. However, Holm and Eide (2008) claim that the time domain analysis is a better approach. The authors compared the frequency domain and time domain methods and concluded that applying the former causes a significant information loss due to heavy data compression.

1.3.2 ICP waveform complexity and entropy

It's not a straightforward task to define complexity, however, it can be considered as a characteristic of a dynamical system that makes it able to react to even extremely small changes in that system. Several studies have explored the complexity of the ICP waveform during the course of intracranial hypertension and the correlation of this complexity with patient outcome. Hornero et al. (2005, 2006) used Approximate Entropy to study the complexity of ICP signals during the course of acute ICP hypertension (ICP spike). In general, entropy is a measure of the predictability and randomness of a stochastic process. Approximate Entropy (ApEn), which was used by the authors, is one of the common techniques for measuring the regularity of experimental data, particularly medical data such as heart rate. ApEn could be applied to systems with little or no prior knowledge, allowing it to analyze relatively short and noisy time series. ApEn is model independent and scale invariant and in other applications this metric has been shown to reveal patterns that are indistinguishable and hidden by other classic time series analyses.

Hornero et al. (2005, 2006) studied the ICP data of seven pediatric patients (ages between 4.5 to 15.5) with severe TBI. They define normal ICP as less than 20-25 mmHg and IH as ICP of more than 25 mmHg for a minimum of 5 minutes. They found

11 ICP spikes in these seven subjects using a spike detection algorithm. The authors evaluated the approximate entropy during the period of ICP spikes and observed that the complexity of ICP decreases in IH periods. They also estimated the approximate entropy for various synthetic signals with different properties, such as sinusoid pulse noise, noise power and noise bandwidth, in order to gain a better insight into ApEn itself.

The decrease in ICP complexity has also been demonstrated in another study wherein the authors measured the complexity with Lempel-Ziv (LZ) complexity (Hornero et al., 2007). The LZ algorithm is mostly popular for its data compression applications. Beside, LZ is also associated with Kolmogorov complexity (Kolmogorov, 1965) and used as a measure of complexity and randomness for discrete-time biological signals. The LZ algorithm represents the rate of new patterns that occur in the system over time; hence, a higher value of LZ complexity means a more complex system.

In spite of the popularity of LZ complexity metric, there are some criticisms of applying the classic LZ to physiological data. In the classic LZ algorithm (CLZ) the original time series is transformed into a binary sequence, using a threshold which is often the median or mean of the series. This transformation may result in the loss of useful information or altering the dynamical properties of the data (Zhang et al., 2016). Various extensions have been proposed in order to improve the CLZ algorithm. For instance, the multistate LZ complexity algorithm proposed by Sarlabous et al. (2009). Hu et al. (2006) also investigated the effect of the data size on LZ complexity and proposed a new normalization scheme that is almost independent of the length of the data sequence.

Hornero et al. (2007) proposed preliminary results for the possibility of IH detection from non-invasive signals such as pulse oximetry coupled with ICP. In another study, the authors observe that the outcomes in patients with TBI correlate with ICP waveform complexity (Lu et al., 2012). The authors applied multiscale entropy analysis and showed that patients who display reduced complexity of mean ICP waveform are more likely to have poor outcomes.

1.3.3 ICP waveform nonlinearity

Nonlinearity is one of the fundamental properties of almost all real-world systems, and intracranial pressure is not excluded from this fact. A nonlinear or complex system consists of different components that interact with each other in a nonlinear manner. Any small change in a nonlinear system can lead to a dramatic change in the whole system. In contrast to linear systems, nonlinear systems are far more difficult to predict and so cannot be easily understood. Nonlinear systems are almost always irreducible, which means in order to study their behavior, the whole system must be considered at once and it is typically uninformative to study any nonlinear system by examining its parts individually (Goldberger, 1996).

Traditional techniques often fail when applied to nonlinear and complex systems. Therefore, researchers have applied modern statistical physics and mathematics in order to study these systems. One example of these studies is work by Stanley et al. (1999) in which notable physiologic structures in heart rate dynamics were discovered that were undetectable with traditional methods. The authors found that the non-equilibrium behavior of the healthy heart is altered by pathological conditions such as congestive heart failure.

The dynamic of the ICP waveform is also nonlinear and complex, and these characteristics require further study using nonlinear approaches and considering all underlying parameters. One of the nonlinear techniques that researchers have applied to ICP waveforms is fractal analysis (Burr et al., 2008; Fan et al., 2010; Sourina et al., 2010). Fractal analysis determines the self-similarity properties of irregular and complex systems. In other words, the property of self-similarity means that the object (spatial or temporal) displays the same shape/pattern at different scales. Fractal dimension (FD) is the measure that describes fractal analysis quantitatively. Different methods compute the FD; however, in biomedical studies, the box-counting method is the most commonly used.

Sourina et al. (2010) applied fractal analysis to the ICP waveforms of 9 patients before and after decompressive craniectomy surgery in order to detect the transition phases in each patient's status. The authors concluded that the fractal dimension value is a reasonable indicator for determining whether surgery is required.

1.4 Recurrence plots

Dynamical systems are ubiquitous in the natural world and consequently our daily lives. Thus, understanding, analyzing and forecasting these systems are crucial tasks in many fields of science. These real-world systems are mostly nonlinear, non-stationary in time, noisy, and often comprise many coupled variables. In addition, according to Chaos theory, some of these systems are very sensitive to the initial conditions and a very small perturbation of initial conditions results in dramatic alterations in the system. Such systems defy complete and precise prediction due to the complexity raised from these characteristics.

Supposing many of the real-world systems are rule-driven and deterministic, short-term and approximate prediction for them via mathematical modeling and computational solutions has been the focus of research. With the emergence of cheap powerful computers many of these systems can be numerically approximated with arbitrary resolution. However, predictions are always limited to the short term due to uncertainties in the initial conditions. In order to overcome this challenge, other methods are needed to discover the invariant properties of a dynamical system which are independent of the initial conditions.

In contrast to linear approaches that are mostly well-established and acknowledged, nonlinear methods are still controversial. Common nonlinear methods, such as calculating the Lyapunov exponent, different entropy methods such as Kolmogorov-Sinai entropy, and correlation dimension, have been proposed for the study of systems that are stationary in time. More recently, different methods have been introduced to study non-stationary real-world dynamics. Recurrence plots and recurrence quantification analysis, used in this work, are relatively new methods for studying nonlinear systems with regard to the topology of the system. Recurrence plot theory is founded on the Poincaré recurrence theorem (Poincaré, 1890), and Takens' embedding theorem (Takens et al., 1981). Therefore, in order to have a better understanding of the RPs method, these two important theorems are introduced very briefly in the following subsections.

1.4.1 Phase space and trajectories

Trajectories and their representations in phase space are fundamental concepts in the study of nonlinear systems from the topological point of view. The phase space of a dynamical system is defined as all the possible states that the system could be found in. For one/two dimensional systems with one/two variable(s) the phase space is respectively a line (phase line) or a 2-D plane (phase plane). Now, consider a system with d variables. At time t, the system and its velocity are described by:

$$\vec{x(t)} = (x_1(t), x_2(t), ..., x_d(t)), \tag{1.1}$$

$$\dot{\vec{x(t)}} = \frac{dx(t)}{dt}. \tag{1.2}$$

The phase space of this system is a d-dimensional space wherein as time evolves the vector $\vec{x(t)}$ moves in the direction of its velocity and forms the phase space trajectories. In any time t, the velocity field $\dot{\vec{x(t)}}$ is tangent to the vector $x(t)$. Accordingly, knowing $\dot{\vec{x(t)}}$ makes it possible to determine the phase space trajectories of $\vec{x(t)}$ without having the exact expression of it or being necessary to find $x(\vec{t})$ via integration.

Phase space trajectories reveal significant information regarding the behavior of underlying system. Recurrence plots were initially proposed in order to study the phase space trajectories of a high dimensional system, with the goal of providing a two-dimensional visualization tool for such systems and gaining a deeper understanding of their temporal dynamics (Marwan, 2008).

1.4.2 Poincaré recurrence theorem

The Poincaré recurrence theorem (Poincaré, 1890) is often the first concept that is explained in ergodic theory. Roughly speaking, this theorem states that a measure-preserving system[2] will recur to a state close to its initial state, after a sufficiently long but finite time. The proof of this theorem is beyond the scope of this thesis.

1.4.3 Takens' embedding theorem

Phase space reconstruction plays a critical role in exploring the real-world time series. In such systems, is not possible to determine all involved variables, as they are not always known or measurable. Instead, often only one observation of the process is available which is a discrete time series. Takens' theorem (Takens et al., 1981) opened a new chapter in the study of nonlinear systems by providing the essential theoretical bases for analyzing real-world and experimental time series.

Takens et al. (1981) proved that phase space reconstruction is still possible having only a single observation of a dynamical system; in a way that the new system does preserve the topological structure and properties of the original system. Takens' theorem was indeed a specific case of the Whitney embedding theorem (Whitney, 1936) and proved that a phase space can be reconstructed with the time-delayed versions of a single time series.

---

[2] (X, T, μ) is a measure-preserving system if (X,μ) is a measure space and $T : X \to X$ preserves μ.

Roughly speaking, Takens' theorem states that a phase space of a dynamical system can be reconstructed[3] (under certain conditions) in a way that the topological properties of the original system are preserved.

Time delay embedding is one of the common methods for phase space reconstruction. Assume the observation time series with sampling time of Δt is vector $u_i = u(i\Delta t)$, where $i = 1, \dots ,N$. Then with the time delay embedding technique:

$$\vec{x_i} = \sum_{j=1}^{m} u_{i+(j-1)\tau} e_j \tag{1.3}$$

where τ is the time delay and m is the embedding dimension (Marwan et al., 2007).

1.4.4 Recurrence plots definition

Recurrence is a fundamental concept in dynamical systems and is defined as the recurrence of the system to the (almost) same state after finite time. The original intuition of recurrence was introduced in the 19th century, however, it was not until 1987 that Eckmann proposed the recurrence plot (Eckmann et al., 1987). In addition to recurrence plots, other techniques such as first return maps, space time separation plots, and recurrence time statistics, are all based on the recurrence concept.

Recurrence plots are powerful visualization tools to display the recurrence states of a dynamical system in a temporal manner. Moreover, these plots are able to shed light on other characteristics of the system due to their associations with many fundamental properties of the system, such as Pesins dimension, Lyapunov exponents, Hausdorff dimension and various types of entropy. Armed with the powerful method of recurrence plots, we are able to analyze short, noisy and non-stationary time series, which are hard to study with other methods.

---

[3] This reconstruction is guaranteed when $m > 2D + 1$, where m is the embedding dimension and D is the correlation dimension of the attractor.

Recurrence plots are based on a binary square matrix $R_{i,j}$, for i,j= $1, 2, ..., N$:

$$R_{i,j} = \begin{cases} 1, & \text{if } x_i \approx x_j \\ 0, & \text{otherwise} \end{cases}$$

Webber Jr and Marwan (2015) defined $R_{i,j}$ as:

$$R_{i,j}^{m,\varepsilon_i} = \Theta(\varepsilon_i - \|x_i - x_j\|), x_i \in \mathbb{R}^m, i, j = 1...N \tag{1.4}$$

Where N is the number of states or data points, ε_i is the threshold (will be explained later), $\|.\|$ is the norm, and Θ is the Heaviside function. Both axes of the recurrence plot are time, and the recurrence points ($R_{i,i} = 1$) make the main diagonal line called the line of identity (LOI). The threshold (ε_i) and norm are two important factors in constructing insightful RPs for a dynamical system and choosing them properly is a crucial task.

1.4.5 Embedding dimension

Eckman originally defined the RPs on a reconstructed phase space and an embedded system, hence, the original definition of RP includes two embedding variables, the embedding dimension and time delay. In general, finding the proper embedding variables for a system is not a trivial task.

More recently, some studies have demonstrated that the RP can be constructed on a non-embedded system and still display the same (or similar) results as the embedded system (Iwanski and Bradley, 1998; March et al., 2005; Marwan et al., 2007). Thiel et al. (2004) investigated this matter with an example where they demonstrated that the correlation dimension and Rényi entropy statistics of a dynamical system estimated from its RPs stay invariant with the change of the embedding dimension.

1.4.6 Norm and threshold

Defining appropriate choices for threshold and norm is essential in constructing RPs and depends mainly on the properties of the dynamical system under study (Marwan et al., 2007). Different types of norms make different shapes of neighborhoods. The L_1-norm, the L_2-norm, and the L_∞-norm are three of the most commonly used norms that respectively find the least, the most, and an intermediate number of neighbors for a particular state. The L_∞-norm is more efficient computationally and more common as a result.

The choice of threshold is more influential on the RPs and needs to be chosen carefully. Improper choices of threshold can result in spurious recurrences in the case of a large threshold, or lead to the loss of real recurrence states in the case of small threshold. Some rules for a proper choice of threshold have been proposed. For example Mindlin and Gilmore (1992) suggested a few percent of the maximum of phase space diameter for the threshold value, while Zbilut and Webber (1992) stated that this value should be more than 10% of the maximum of phase space diameter.

1.4.7 Structures in recurrence plots

As mentioned before, RPs are visualization tools for displaying the recurrence states of trajectories of a dynamical system in a temporal manner. RPs exhibit specific patterns which shed light on important information about the trajectories and behavior of the system associated with the recurrence properties. The RPs' patterns are categorized in large and small scale patterns. The following are the typical patterns that appear in RPs and their brief interpretation (Marwan et al., 2007).

Large-scale patterns

- **Homogeneous** RPs represent that the underlying dynamical system is a stationary system. e.g stationary random time series.

- **Diagonal lines** in RPs represent periodic and quasi-periodic systems. The RPs of such systems often display diagonal oriented checkerboard structures. The frequencies of the system can be determined based of these patterns.
- **Drift** in RP represents a non-stationary systems with variables that are changing slowly. This slow change results in a pattern that is paling (or darkening) away from the main diagonal.
- **White areas or bands:** in RPs represent sudden changes or extreme events in systems.

Small-scale patterns

Besides large-scale patterns of RPs, small-scale patterns (also called texture) are another means of extracting information from RPs. These patterns are also the ground of the quantification analysis which will be introduced in the next section.

- **Single recurrence points** in RPs can happen in the case that a state is rare, experiences extreme fluctuation or happens for a very short time.
- **Diagonal lines** which are parallel lines to the LOI, happen when two parts of trajectories are (almost) parallel. Assuming k is the diagonal line length, for $k = \{1, ..., l\}$, mathematically this corresponds to: $R_{i+k,j+k} = 1$.
- **Vertical/horizontal lines** in RPs occur when a state does not have alteration for a period of time, or alters very slowly. Assuming k is the vertical line length, for $k = \{1, ..., m\}$: $R_{i,j+k} = 1$.

Even supposing the mentioned patterns and their explanations have been introduced and discussed in various articles, still a proper interpretation of these patterns requires a decent background and can be somewhat subjective in some cases. This challenge can be overcome with the more objective approach to RPs, recurrence quantification analysis, which we introduce in the following section.

1.4.8 Recurrence quantification analysis (RQA)

A few years following the introduction of RPs, Webber and Zbilut proposed several quantification measures in order to standardize and facilitate the interpretation of these graphical tools (Webber and Zbilut, 1994; Zbilut and Webber, 1992). These measures made the RP method more rigorous since they enhanced it with well defined quantitative descriptions. Recurrence quantification analysis (RQA) is applied to estimate the complexity of the nonlinear system. These measures are related to the RP's recurrence density, diagonal and vertical lines. Here, we introduce the RQA formulas with a brief explanation for each one (Marwan et al., 2007). It should be mentioned that the LOI is usually excluded form RQA analyses. In the following, N is defined as the number of data points which is the number of phase space points.

- **Recurrence rate** measures the density of the recurrence points in the system.

  $$RR = \frac{1}{N^2} \sum_{i,j=1}^{N} R_{i,j} \tag{1.5}$$

  where $R_{i,j}$ is the recurrence matrix. The average number of neighbors for each point is also defined as:

  $$N_n = \frac{1}{N} \sum_{i,j=1}^{N} R_{i,j} \tag{1.6}$$

- **Determinism** measures the percentage of the recurrence points of the diagonal lines.

$$DET = \frac{\sum\limits_{l=l_{\min}}^{N} lP(l)}{\sum\limits_{l=1}^{N} lP(l)} \tag{1.7}$$

where $P(l)$ is the histogram of the lengths of the diagonal lines. Systems with deterministic behavior display long diagonal lines, while chaotic systems often includes short or no diagonal lines. A high DET value indicates a more predictable and less complex system.

- **Average diagonal line length** measures the average time that two segments of the trajectory are in a same neighborhood.

$$L = \frac{\sum\limits_{l=l_{\min}}^{N} lP(l)}{\sum\limits_{l_{\min}}^{N} lP(l)} \tag{1.8}$$

- **Longest diagonal line length** measures the maximum length of diagonal lines.

$$L_{\max} = \max\left(\{l_i;\ i = 1, \ldots, N_l\}\right) \tag{1.9}$$

where N_l is the number of diagonal lines in the recurrence plot and l_i is the length of the diagonal line. Accordingly, Divergence is defined as:

$$DIV = \frac{1}{L_{\max}} \tag{1.10}$$

A high DIV value indicates that the diagonal lines are short and the trajectory segments diverge fast.

- **Entropy** measures the Shannon entropy (and accordingly the complexity) of the RP in regard to the diagonal lines.

  $$ENTR = -\sum_{l=l_{min}}^{N} p(l) \ln p(l) \tag{1.11}$$

  where $p(l)$ is the probability of finding a diagonal line with the length of l in the RP, $p(l) = P(l)/N_l$.

- **Laminarity** measures the percentage of the recurrence points of the vertical lines.

  $$LAM = \frac{\sum\limits_{v=v_{\min}}^{N} vP(v)}{\sum\limits_{v=1}^{N} vP(v)} \tag{1.12}$$

  where $P(v)$ is the histogram of the lengths of the vertical lines.

- **Longest vertical line length** measures the maximum length of vertical lines.

  $$V_{\max} = \max\left(\{v_i;\ i = 1, \ldots, N_v\}\right) \tag{1.13}$$

  where N_v is the number of vertical lines in the recurrence plot and v_i is the length of the vertical line.

- **Trapping time** measures the average of the vertical lines' length.

  $$TT = \frac{\sum\limits_{v=v_{min}}^{N} vP(v)}{\sum\limits_{v=v_{\min}}^{N} P(v)} \tag{1.14}$$

  The TT value measures the mean time that a system is trapped in a particular state.

1.5 Thesis Statement and Contribution

Here we propose a novel approach for analysis of ICP waveform in brain-injured patients. To our knowledge, this is the first study that applies recurrence plots and recurrence quantification analysis to ICP data. The research question of this thesis is to determine whether these methods have the potential of analyzing the ICP data for identification of ICP hypertension. If so, they may be capable of revealing information and should be further studied.

In the next chapter we present our results which are the RPs and RQA measures of all 30 available subjects. We then discuss the results and findings. Our main finding can be summarized as "the recurrence plots and recurrence quantification analysis are capable of being used in ICP waveform analysis."

Chapter 2

Methodology and Results

2.1 The MIMIC II data set

This study is based on version 3 of the MIMIC-II (multiparameter intelligent monitoring in intensive care II) database (Saeed et al., 2011). MIMIC-II is one part of an ongoing industrial and academic collaboration between MIT, Philips Healthcare, and Beth Israel Deaconess Medical Center and is funded by the National Institutes of Health (NIH). The goal is to provide open source ICU databases for researchers and scientists by promoting patient monitoring and treatment in intensive care units. MIMIC-II is freely accessible via the Physionet website.

The Physionet website provides physiological databases (PhysioBank), related software and tools (PhysioToolkit) and related articles and publications (PhysioNet Library) (Goldberger et al., 2000). PhysioBank offers over four terabytes of data, organized into more than 80 databases including MIMIC-II. PhysioBank's record search is a powerful method through which users can find their desired datasets with specific properties.

The MIMIC-II dataset contains clinical records from tens of thousands of neonate and adult patients who have been hospitalized in different intensive care units of a single teaching hospital in the years 2001 to 2007. The data is anonymized completely, which means all patient, family, and staff identifiers have been removed and all dates have been changed for the sake of legal standards. The MIMIC-II is contained within three databases: a clinical database (with restricted access), a waveform database (with unrestricted access) and a matched database, which is a continuous effort to match the waveform database with the corresponding clinical database.

The MIMIC-III database (Johnson et al., 2016) is a more recent project that has been started to extend the MIMIC-II database and to update it by adding more recent data from the years 2008 to 2012. On the MIMIC-III dataset, besides appending new data, the previous raw data has been regenerated in order to achieve better quality, accuracy and ease of use. The MIMIC-III is an ongoing project and its waveform dataset was not available at the time of this study; therefore, we have used the MIMIC-II database for our analyses.

2.1.1 Clinical database

The MIMIC-II clinical database was gathered from hospital archives and patient bedside monitoring. This database consists of clinical records for 32,536 subjects regarding the following information: general (patients' admissions/discharges/death dates, patient demographics, etc), physiological, medications, lab tests, fluid balances (intake and output such as solutions/blood and urine/blood loss, respectively), notes and reports. As mentioned previously, considering the sensitivity of this information, all the data have been anonymized, the dates have been switched with fake dates (although the time intervals have not been changed), and access to this database is restricted to registered users of the Physionet website.

2.1.2 Waveform database

The MIMIC-II waveform database contains physiological waveforms and numeric time series of physiological measurements for approximately 13,500 ICU patients. The lengths of the recorded signals and time series depend on the decisions that the ICU medical staff have made for each patient. Mostly, the durations of the recordings are a few days in length; nonetheless, shorter and longer lengths (hours or weeks, respectively) also exist.

The waveforms were recorded at 125Hz and contain the following: electrocardiographic (ECG, measure of heart electrical activity), continuous blood pressure (BP), plethysmogram (PLETH, measure of changes in blood volume) and respiration (RESP). The ECG waveform itself includes: AVF, AVL, AVR, I, II, III, MCL, MCL1, V_1, and V_2. The BP waveform includes: invasive arterial blood pressure from two of the radial arteries (ABP and ART), cerebral perfusion pressure (CPP), central venous pressure (CVP), femoral artery pressure (FAP), intracranial pressure (ICP), left atrial pressure (LAP), pulmonary arterial pressure (PAP), right atrial pressure (RAP), uterine arterial pressure (UAP) and uterine venous pressure (UVP).

Besides the mentioned signals, the MIMIC II waveform database also contains records of numeric sampling over time. The sampling happens once per second or once per minute; however, in the case of irregular sampling, the most recent value has been recorded. These records contain temperature, heart rate (HR), cardiac output (CO), carbon dioxide (CO2), respiration rate, oxygen saturation (SpO2), diastolic/systolic/mean blood pressure, etc.

2.1.3 Data preprocessing

For the data preparing process, the pipeline of an article by Hughes et al. (2017) is followed and the same dataset is used. First, subjects with ICP recordings were distinguished from others, and from those with ICP, subjects with a “consistent set” of waveforms were selected. A total of 30 subjects were selected (time series of these subject IDs are included in the appendix.) with the following recordings: RESP, PLETH, ECG-II, ECG-V, ECG-AVR, ABP, and ICP. In order to have a comprehensive analysis, and acknowledging all the underlying parameters, we consider all available signals, in addition to the ICP. Here, each point is a length-seven vector of values for different measurements at each timestamp. This assumes that the waveforms are aligned in time, which is a true assumption as all the signals have the same frequency (125 samples per second) according to the data documentation.[1]

Although the signals are polluted with artifacts from different sources (explained in the next subsection), we did not apply filters to the signals as suggested by Hughes et al. (2017), in order to preserve them in a raw state. However, down-sampling by a factor of five and z-score normalization were applied to the data. An example of waveforms for one subject (3094054) is displayed in Figure 2.1. It should be mentioned that in all figures the ICP is in mmHg and normalized.

2.1.4 Dataset limitations

Similar to other physiological data, ICP signal is noisy and polluted with high-frequency and low-frequency artifacts. High-frequency noise is mainly caused by the sensors or the process of converting analog signals to digital. Meanwhile, the low-frequency noise is caused by coughing, sneezing or patient movements. According to the MIMIC II documentation, another source of noise is the gap intervals which occurred when the staff did not restart the monitoring machine for a new patient, or when the recording probe was disconnected from the patient temporary.

Another constraint of the MIMIC-II dataset is that the signals are not labeled with patients' status. In other word, waveforms are not tagged with any information regarding the onset and termination of patient's critical events (e.g ICP hypertension

---

[1] The ECG signals were not sampled at the same frequency originally. However, these signals have been reconstructed and are consistent with other signals.

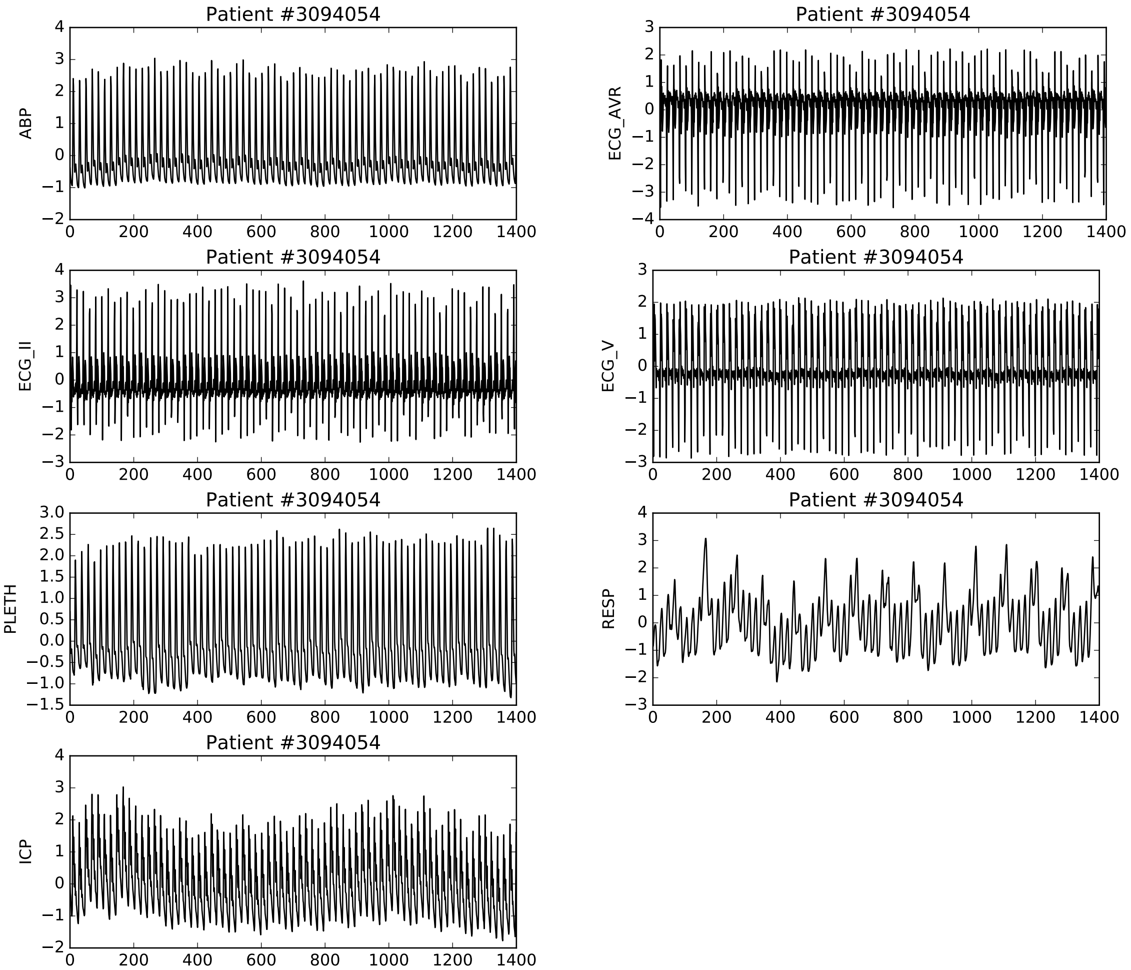

Figure 2.1: Time series of seven waveform recordings for subject 3094054: RESP, PLETH, ECG-II, ECG-V, ECG-AVR, ABP, and ICP.

in the case of ICP waveform). Moreover, the clinical dataset contains important and useful information of the patients such as the patient demographics, received treatments and the patent's outcome. However, only a few number of subjects possess matched clinical and waveform datasets. The process of matching is in progress and more matched records may be added in the future.

2.2 Recurrence plots

The recurrence plots for all 30 subjects has been generated. Moreoever, the global recurrence plot which is the un-thresholded recurrence plot (or more simply the plot based on the distance matrix (Zbilut and Webber, 2006)) is also generated. The RPs of some of the subjects are included in the next subsection, however, the complete list of figures can be found in the Appendix. The RP parameters that are used in these plots are as the following:

- N is the number of data points which is equal to 1400 in our study. It should be mentioned that each data point in our dataset is a vector of length seven. At time t, this vector contains the values of the following waveforms at that time: RESP, PLETH, ECG-II, ECG-V, ECG-AVR, ABP, ICP readings.

- ε, the threshold, is set to 2. As suggested in the literatures (Schinkel et al., 2008), we set the threshold as 10% of the maximal phase space diameter. This value varies for different subjects with $1 \pm .5 < \varepsilon < 2$. We set the ε as the upper bound which is 2. The reason of choosing the upper bound is that we want to minimize the effect of noise on the potential patterns in RPs because noise would alter these structures and a higher threshold may prevent noisy alterations and preserve the larger patterns (Marwan et al., 2007).

- The norm considered is the L_2-norm which is the Euclidean norm. Therefore, the distance of two data points is the Euclidean distance of two vectors of lengths seven.

- Lastly, although the original definition of RP, equation 1.4, is based on the theory of the reconstruction of phase space and includes two embedding parameters; we do not apply embedding to our system. The reason, as mentioned in Section 1.4.5, is that the non-embedded system can also display similar patterns in its RP.

2.2.1 Structures in RPs

The PR usually exhibit periodic patterns, whereas abrupt changes indicate a regime change in the dynamics of the system. For example, Figure 2.2 illustrates the structure observed in same subject as of Figure 2.1. The associated ICP and ECG-II waveforms also are provided in the top of the RP in order to make the comparison of RP and the raw signals possible.

As mentioned in the previous chapter, white regions or bands in the RP indicate abrupt fluctuations in the system. Determining these sudden changes are really important in our study since they may be a sign of sudden change in the status of the patient in, for instance, ICP hypertension.

In Figure 2.2 white bands are visible, the one at approximately time point $t = 160$ is more obvious which is a sign of visible change in that moment. This change is also visible in the raw ICP signal.

Similar white bands are observable in RPs of eight subjects out of all the 30 subjects studied. While most RPs display periodic dynamics, these eight subjects exhibit peculiar and surprising patterns in their RPs which are not always apparent in their ICP signals. We specifically we plot the RPs for three more subjects here in Figure 2.3, Figure 2.4, and Figure 2.5. The RP plots of all subjects are provided in the appendix.

Figure 2.3, we see how subject 3094054 displays an extreme alteration in its RP. A clear white band exists right before time point 200. The interesting point here is that this event can not be detected form the raw ICP signal, which proves the significance of RP.

In Figure 2.4, the RP shows two periods of rare states close to data points 400 and 1200. This may be an indication of regime change in these periods. These events are visible in the raw ICP signal too.

Finally, we review one more subject in Figure 2.5 which exhibits a similar white

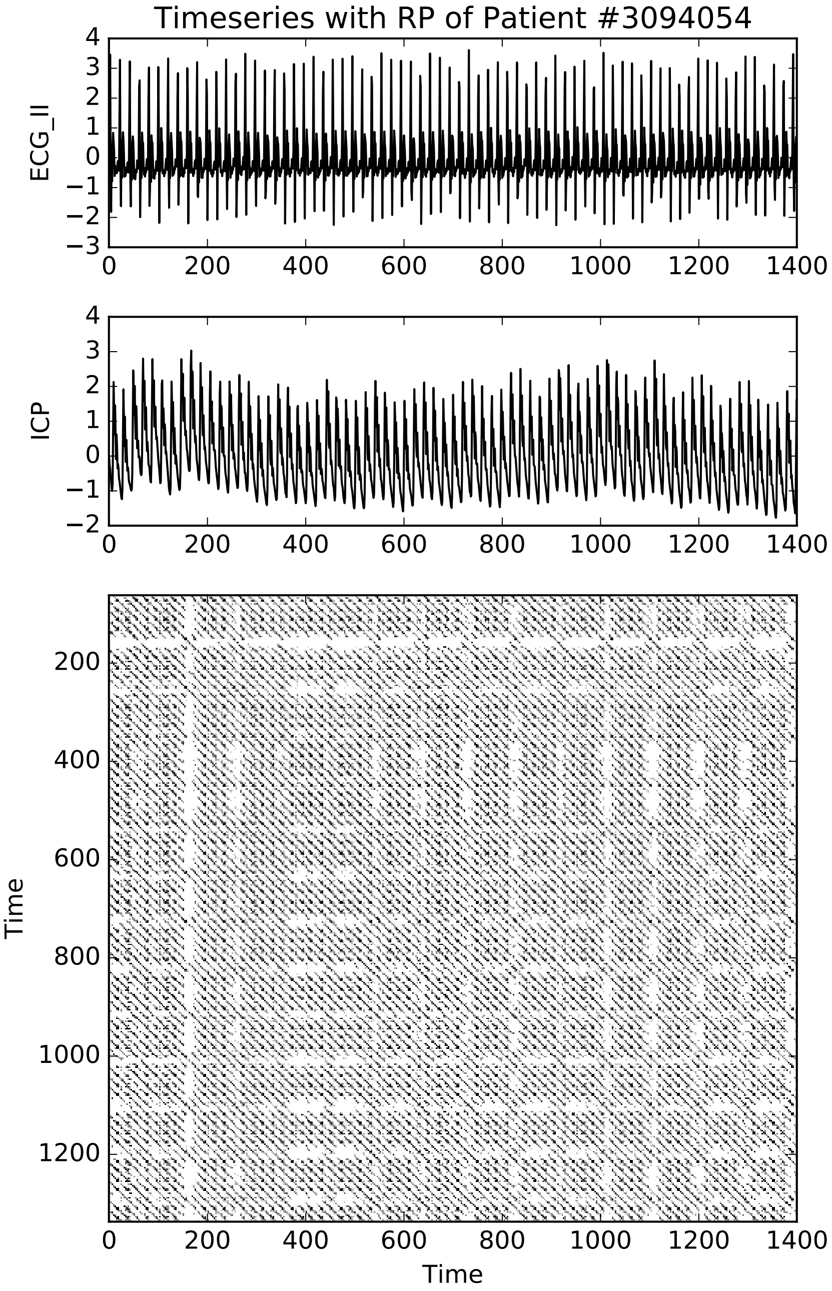

Figure 2.2: Top to bottom, respectively: ECG and ICP signals and RP of patient with ID 3094054. The data have the length 1400 (N = 1400). RP parameters are m = 1, $\epsilon = 2$. At time point near t = 160 there is a white band which represents an abrupt change in the signal data. This change can also be detected in the raw ICP signal.

band in its RP plot, whereas we see a change in the periodic patterns before $t = 1000$; this however is not detectable when looking at the raw timeseries.

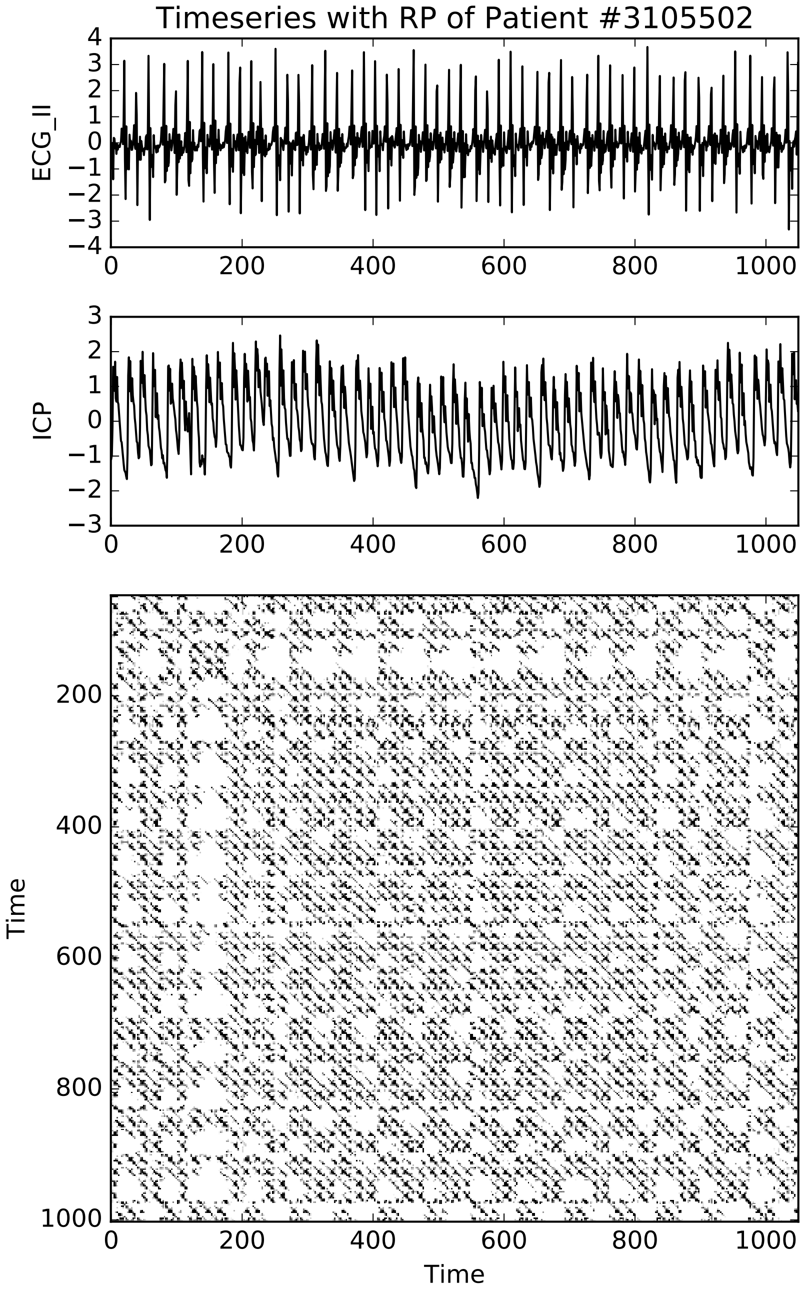

Figure 2.3: RP, ICP and EEG signals of patent with ID 3105502. The white band close to time point 200 is a sign of extreme change in the system. This information is not obvious in the raw ICP signal and emphasizes the utility of RP methods in highlighting abnormalities and regime changes in such complex dynamic systems.

2.2.2 RQA

Although eyeballing the RP plots is possible, particularly in our case that the number of subjects is not large, it is valuable to quantify the change in periodic patterns and

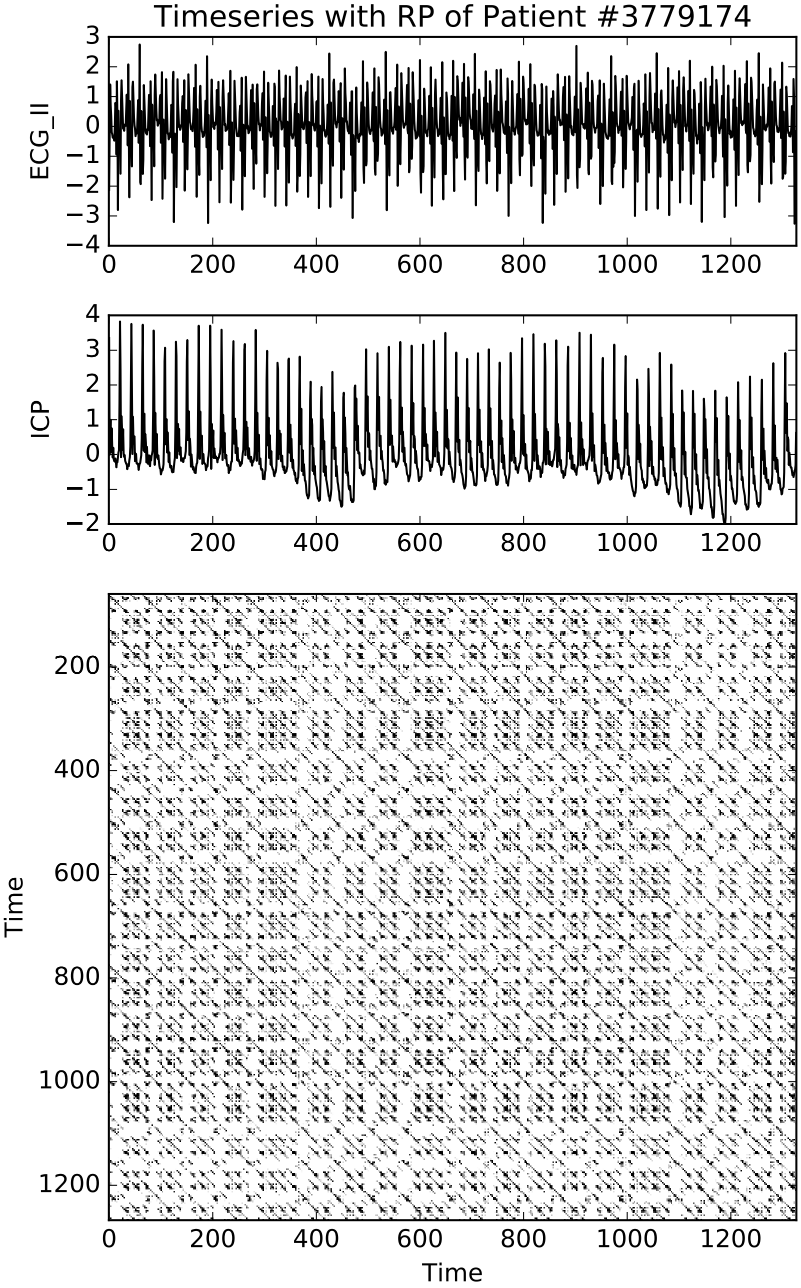

Figure 2.4: RP, ICP and EEG signals of patent with ID 3779174. Two periods of rare states around data points 400 and 1200 are displayed in the RP. Regime changing events could be interpreted in these periods. Raw ICP signal also displays these events.

surprisingness of observed dynamics. Therefore, we continue with the recurrence plot analysis measures which are defined to quantify these changes given an RP matrix.

In more details, we calculate eleven RQA measures for each subject: *RR*: Re-

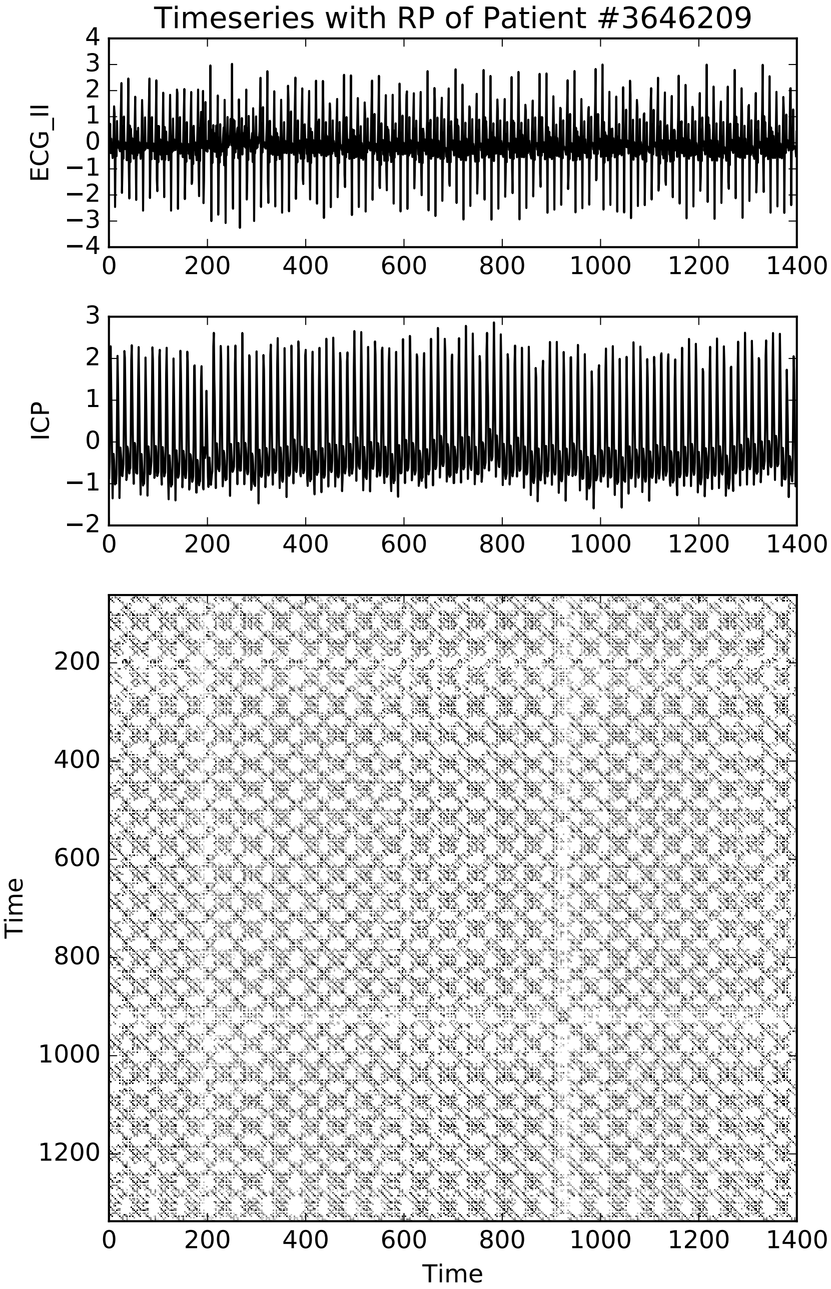

Figure 2.5: RP, ICP and EEG signals of patent with ID 3646209. Here, we also see a possible change as a white band, although less preeminent compared to the last subjects.

currence Rate, DET: Determinism, L: Average diagonal line length, L_{max}: Longest diagonal line, DIV: Divergence of diagonal lines, $ENTP_L$: entropy of diagonal lines, LAM: Laminarity, TT: Trapping time, V_{max}: maximum vertical line, and $ENTP_V$:

entropy of vertical lines. For their definition please refer to the previous Chapter. The distribution of statistics of these RQA measures across all the subjects are calculated and the results are given in Table 2.1, whereas Figure 2.6 shows the distribution in boxplot format.

RQA	median	mean	min	max	var	cov
RR	0.164	0.169	0.135	0.352	0.001	0.001
DET	0.647	0.640	.518	0.812	0.007	0.007
C_2	0.163	0.168	0.134	0.352	0.001	0.001
L	7.449	7.525	6.275	10.270	0.654	0.676
L_{max}	184	237	58	1197	39570	40934
DIV	0.005	0.006	0.001	0.017	0.0	0.0
$ENTP_L$	2,291	2.304	1.923	2.787	0.039	0.040
LAM	0.711	0.705	0.510	0.867	0.010	0.010
TT	4.551	4.693	3.386	7.776	0.788	0.815
V_{max}	7.00	8.433	5.000	14.000	6.712	6.944
$ENTP_V$	1.594	1.558	0.748	2.431	0.143	0.148

Table 2.1: Summary statistics of RQA measurements across subjects. The RQA measures include: RR, DET, C_2, L , L_{max}, DIV, $ENTP_L$, LAM, TT , V_{max}.

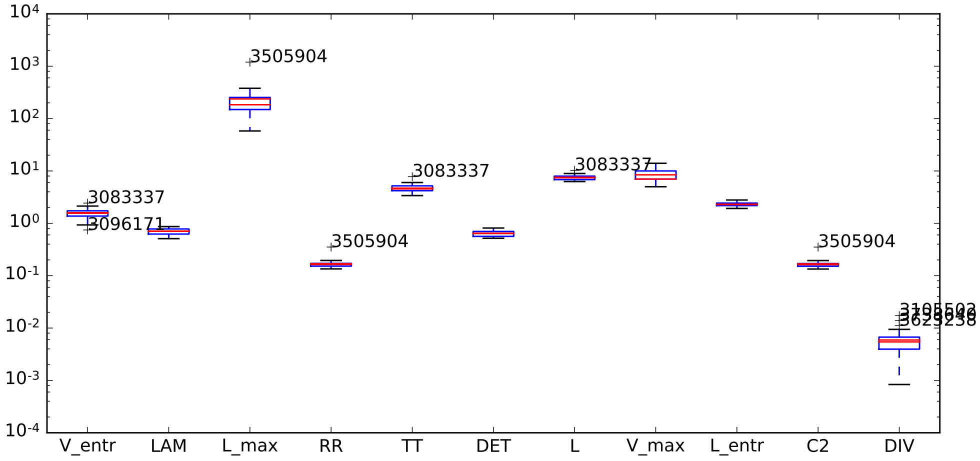

Figure 2.6: Distributions of different RQA measures

2.2.3 Anomalous Subjects

Using descriptive statistics of boxplot, shown in Figure 2.6, we can flag the subjects that deviate from the distribution and mark them as anomalies. To find the outliers, first the quartiles of the data are calculated and the interquartile range is computed from the upper and lower quartiles, which is $IQR = Q_3 - Q1$. Then the whiskers are plotted which extend to a point greater or lower than $1.5 * IQR$ from the upper and lower quartiles. Points outside of these are marked as outliers, which are those that $Q_1 - x$ or $x - Q_3$ is greater than $1.5 * IQR$.

The subjects with anomaly values have been identified and listed bellow:

- subject id 3096171 is a anomaly in $ENRT_V$ with value 0.747.
- subject id 3083337 is a anomaly in $ENRT_V$ with value 2.430.
- subject id 3505904 is a anomaly in L_{max} with value 1197.
- subject id 3505904 is a anomaly in RR with value 0.352.
- subject id 3083337 is a anomaly in TT with value 7.776.
- subject id 3083337 is a anomaly in L with value 10.27.
- subject id 3505904 is a anomaly in C_2 with value 0.352.
- subject id 3738640 is a anomaly in DIV with value 0.014.
- subject id 3623238 is a anomaly in DIV with value 0.011.
- subject id 3105502 is a anomaly in DIV with value 0.017.

Having these subjects flagged, we can now take a close look at their recurrence plots to investigate the patterns and see if the abrupt changes are present. In particular, Figure 2.7 to Figure 2.12 show the (bounded and unbounded) PR plots of these anomalies, along with the distribution of their diagonal and vertical lines which are used to quantify the patterns in them in the RQA measures.

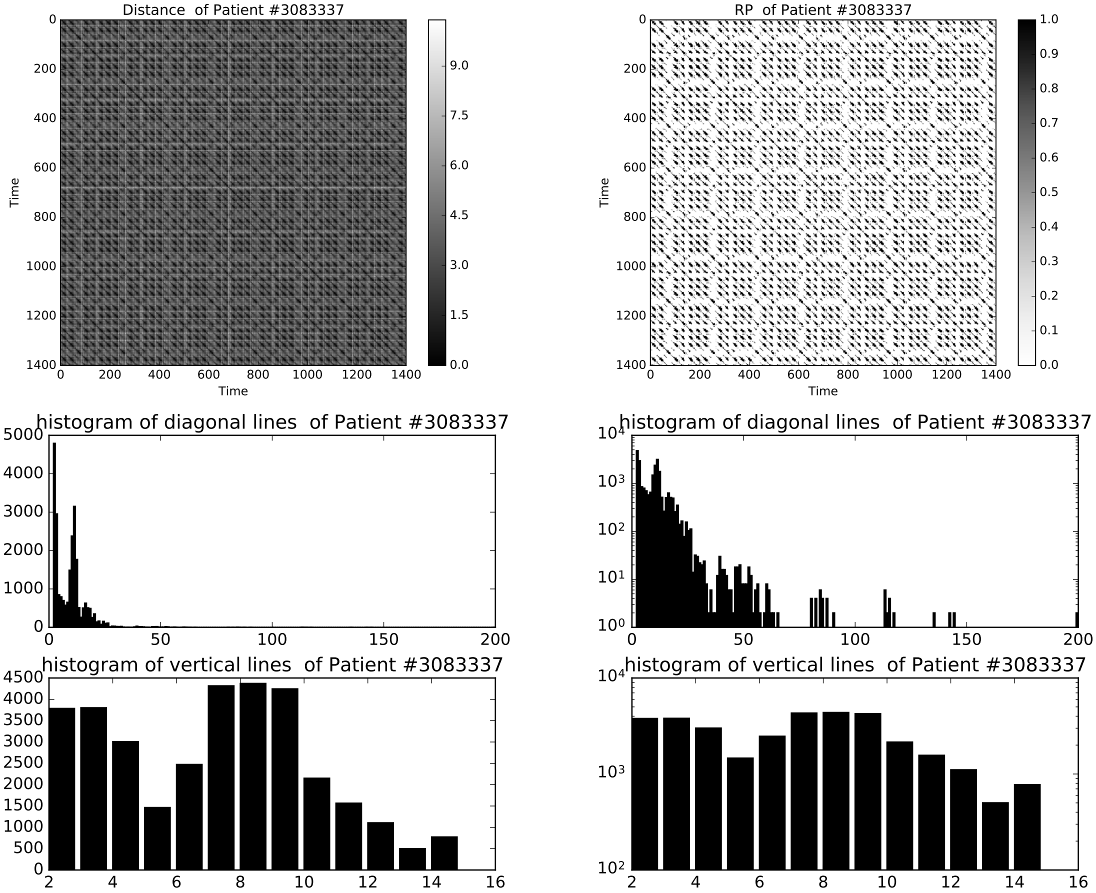

Figure 2.7: Anomaly in $ENRT_V$ for subject id 3083337 has value 2.43

2.2.4 Novelty Curve of RP

We further investigate the novelty curve for the original time series, as well as the distance matrix which is basis of the RPs. Figure 2.13 shows the novelty curve derivation steps taken from an original time-series. From top to bottom, the ICP waveform and four steps of amplitude squaring, windowing, differentiation, and half wave rectification are shown respectively. In the first step the amplitude of the each data point is squared. In the second step, each point is set to the mean of a window of size 10 points. In the next plot, the differentiation of each point and its previous

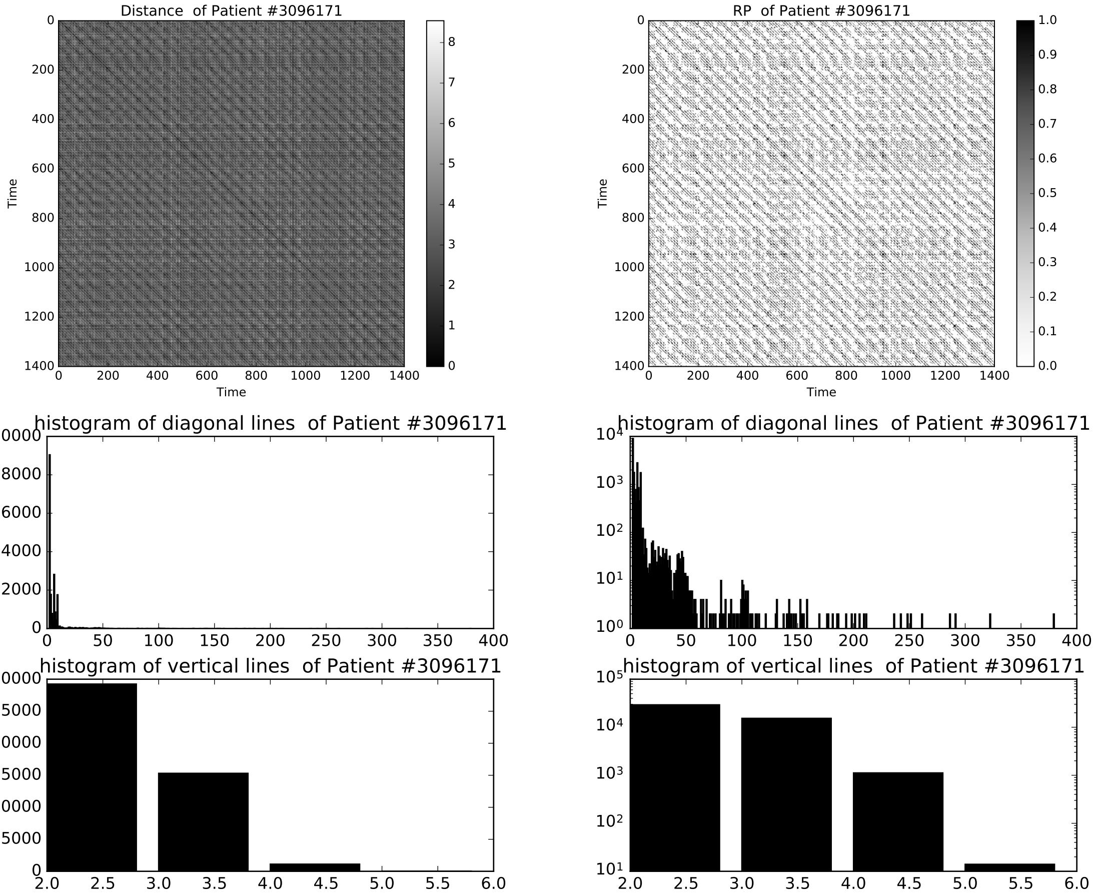

Figure 2.8: Anomaly in $ENRT_V$ for subject id 3096171 has value 0.75

point is computed. The last plot at the bottom shows the derived novelty curve after half wave rectification which filters out the negative points.

Figure 2.14 shows the novelty curve of the distance matrix for the subject previously showed in 2.5. In order to build the novelty curve of a matrix, the differentiation step is changed with Euclidean distance of subsequent columns. We can see the picks in the novelty curve at around $t = 200$, $t = 400$, and $t = 1000$. This shows that the picks at these novelty curves could also be used to detect changes in the PR plots.

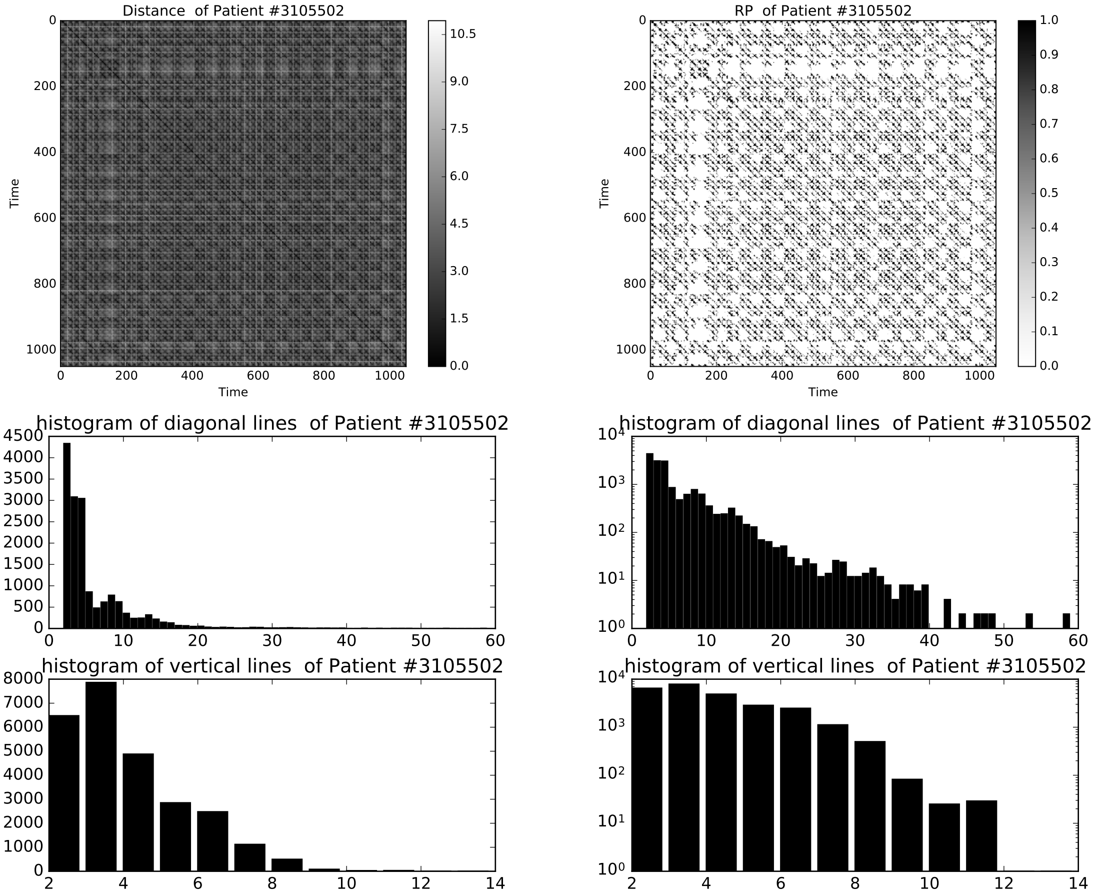

Figure 2.9: Anomaly in DIV for subject id 3105502 has value 0.018

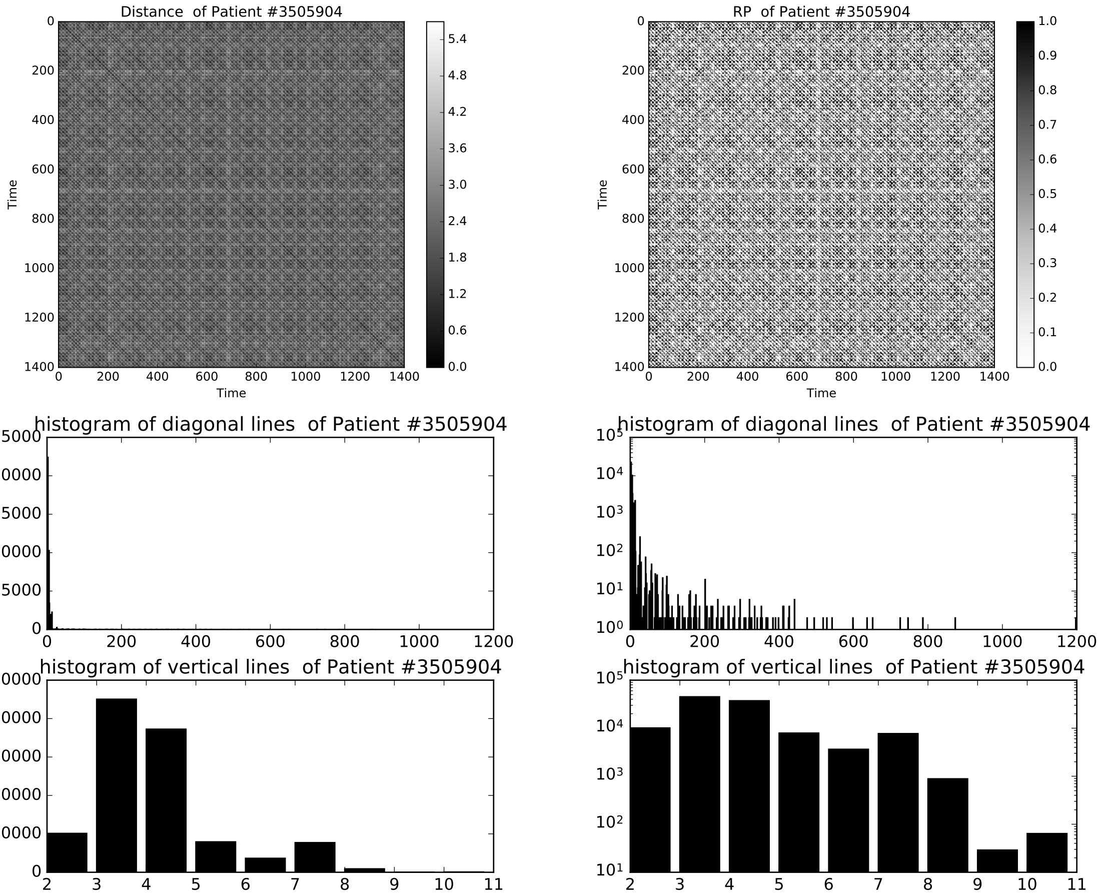

Figure 2.10: Anomaly in L_{max} for subject id 3505904 has value 1197

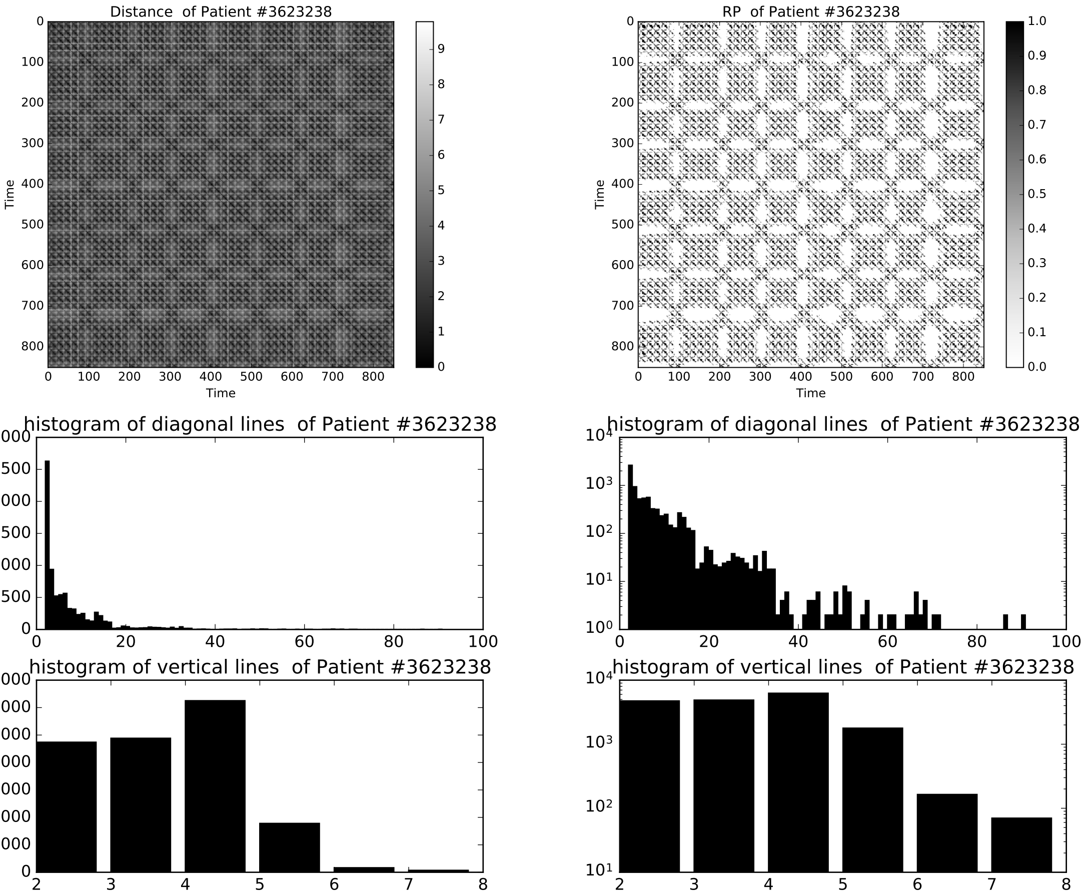
Distance of Patient #3623238

RP of Patient #3623238

histogram of diagonal lines of Patient #3623238

histogram of diagonal lines of Patient #3623238

histogram of vertical lines of Patient #3623238

histogram of vertical lines of Patient #3623238

Figure 2.11: Anomaly in DIV for subject id 3623238 has value 0.011

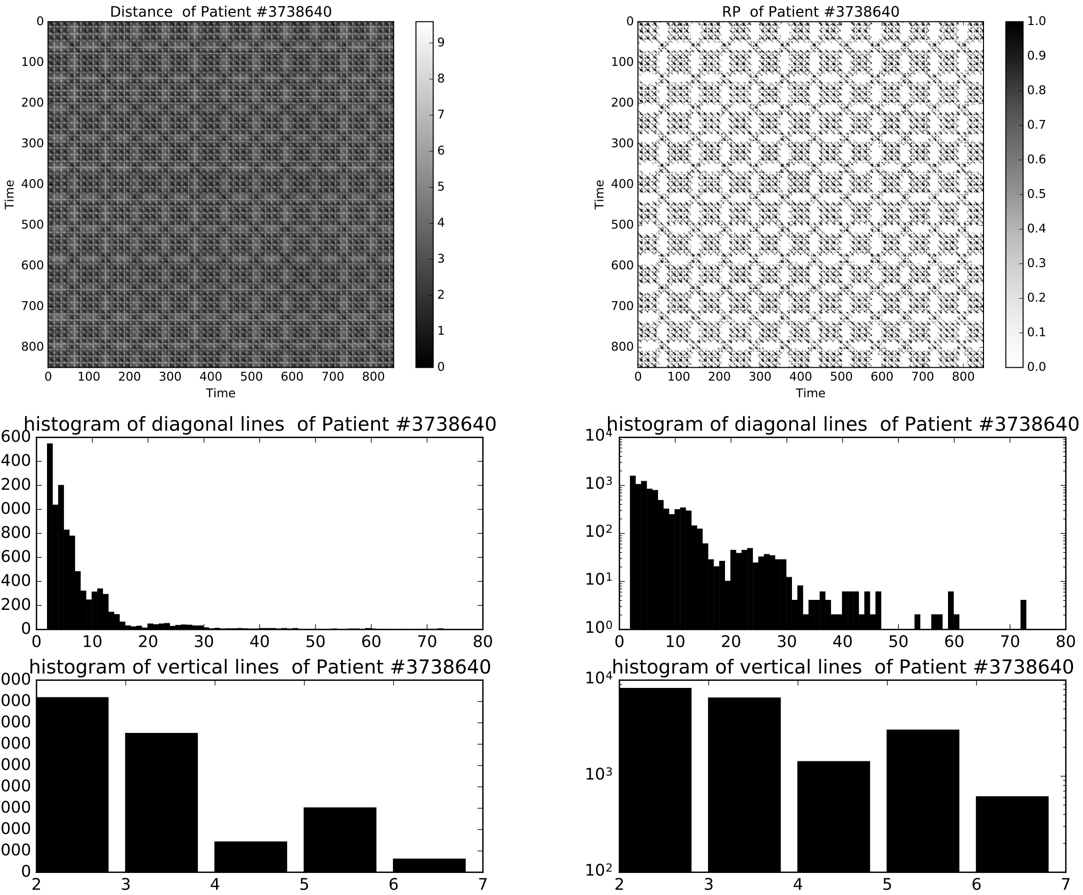

Figure 2.12: Anomaly in DIV for subject id 3738640 has value 0.014

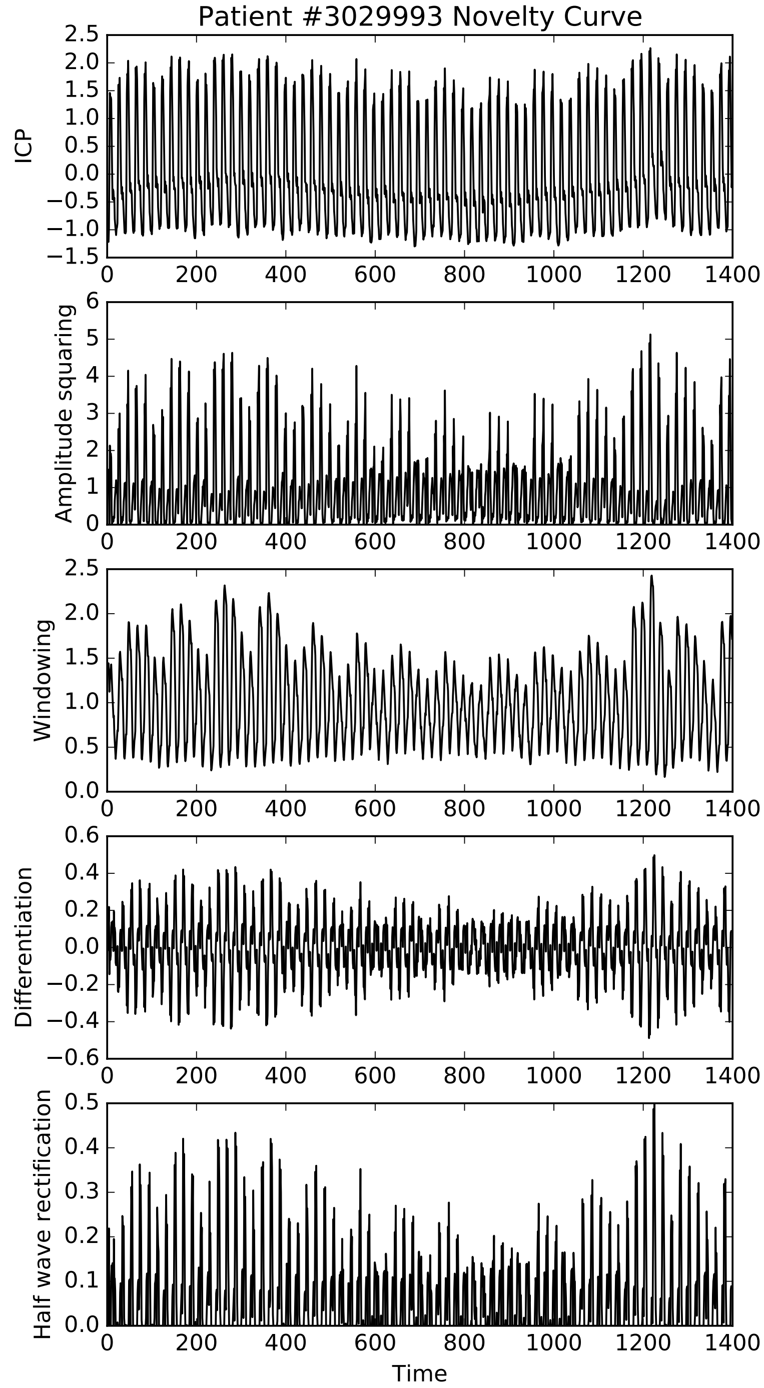

Figure 2.13: Novelty curve derivation from the original ICP time-series for subject 3029993

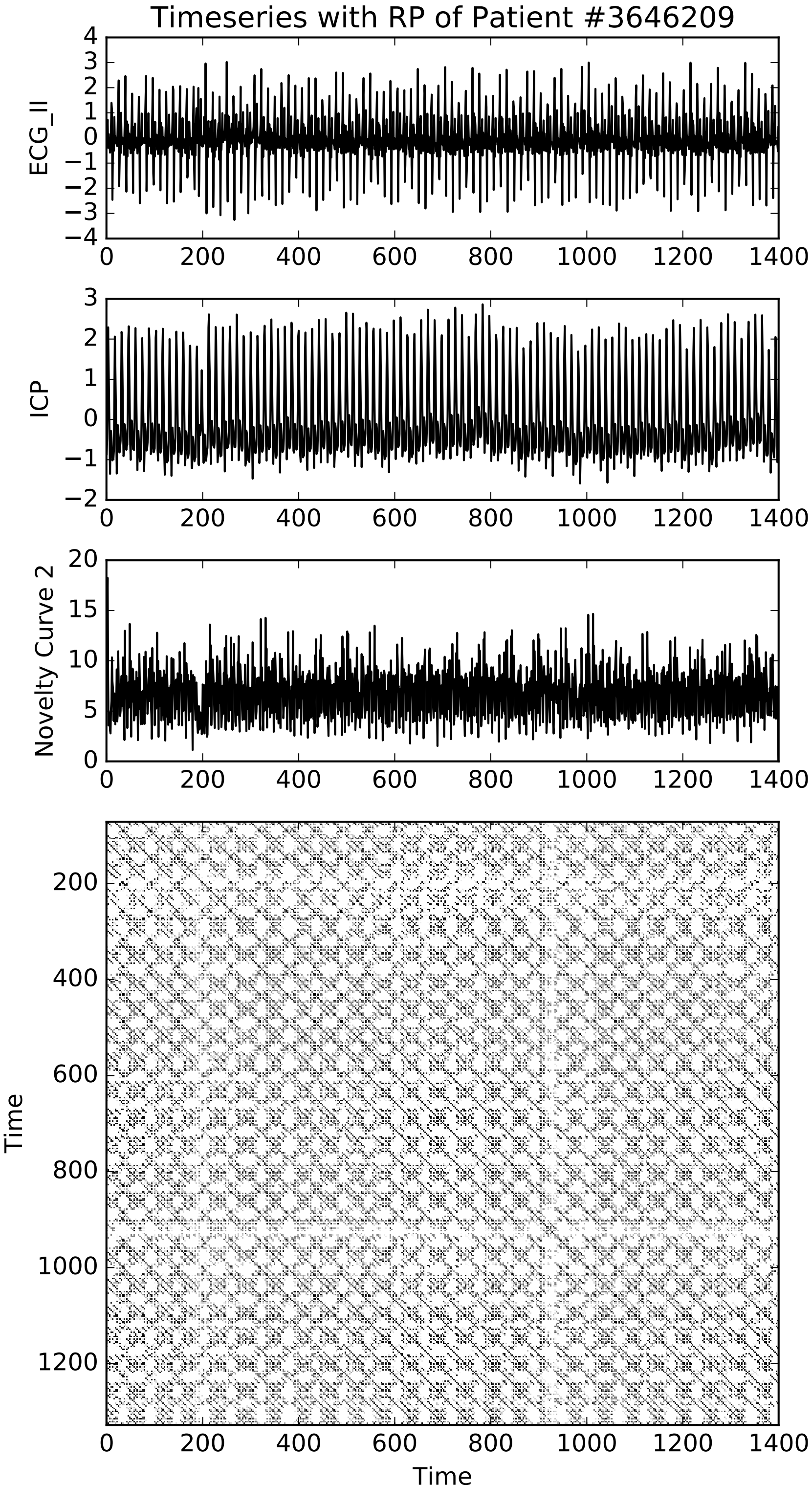

Figure 2.14: Novelty curve of the RP matrix.

Chapter 3

Discussion and Conclusion

This thesis is an effort to address the intriguing question: In what ways do the methods of recurrence plots and recurrence quantification analysis describe data form nonlinear systems; and are they capable of revealing insightful information about the dynamics complex dynamical systems and real-world time series? We investigate this question in a more specific clinical context using intracranial pressure signals obtained from human brain-injured patients; by narrowing it to one specific type of brain data: intracranial pressure waveform.

Intracranial pressure is simply the pressure inside the skull. This pressure is the result of incompressible components of the cranium: brain matter, cerebrospinal fluid (CSF), and cerebral blood. It is shown in the literature that the waveform of this pressure carries important information which can not be extracted with the scalar ICP value which is most commonly used by medical professionals. Various methods have been applied in order to explore and analyze these signals. We propose and use the Recurrence Plot (RP) and Recurrence Quantification Analysis (RQA) to study the dynamics of these waveforms.

The dataset used in this study only contains the physiological waveforms and not the clinical information such as the reason of admission and the outcome of patents.

Due to this constraint it is not easy to make interpretations of the RPs and the RQA results nor to make forecasts and predictions. However, we show that these methods clearly demonstrate the ability for analyzing these complex time series by visualizing them into simple 2D plots and elucidating information in the signals that may not be obvious in the signal itself, such as discontinuities in dynamics over time or descriptive statistics on the properties of the system's phase space.

We observe that the ICP waveforms can exhibit a rich variety of peculiar patterns in their RP which are hidden in the raw signal. Further study on this regard is needed to understand the relationship between these dynamic peculiarties and the corresponding clinical outcome of the patients. Also, it should be stated that our proposed analysis to spot changes might be too sensitive and further robustness experiments could be a potential further work.

The presented work is only a small step in the tough task of understanding the dynamics of ICP waveforms among a plethora of other clinical signals. This method of ICP analysis could be merged with other works in this area or extended in many different directions. One possible future direction is to use the recurrence approach to understand the relationship between the ICP signals and other biological measurements in order to develop non-invasive ICP monitoring framework with an acceptable accuracy. The phase space reconstruction of these dynamic signals can give insights into the relationships if biological signals. The second possible future work is to use this methods in real-time ICP monitoring. Combining this approach with other available methods and clinical data can allow medical experts to more easily understand the long-term behavior of the ICP waveforms instead of only the mean, scalar, ICP value. Another extensions to this work could be applying this method to a labeled ICP dataset in order to predict ICP hyperinflation. With appropriately labeled data, it is possible to compare different parts of the ICP waveform (normal signal, pre-hypertention and during hyperinflation) and train classifiers or apply machine learning techniques to identify healthy patterns or those that can lead to secondary injuries.

Bibliography

Afonso, V. X., Tompkins, W. J., Nguyen, T. Q., and Luo, S. ECG beat detection using filter banks. *IEEE transactions on biomedical engineering*, 46(2):192–202, 1999.

Brain, T. F. et al. Guidelines for the management of severe traumatic brain injury. VIII. Intracranial pressure thresholds. *Journal of neurotrauma*, 24:S55, 2007.

Burr, R. L., Kirkness, C. J., Mitchell, P. H., et al. Detrended fluctuation analysis of intracranial pressure predicts outcome following traumatic brain injury. *IEEE Transactions on Biomedical Engineering*, 55(11):2509–2518, 2008.

Cremer, O. L., van Dijk, G. W., van Wensen, E., Brekelmans, G. J., Moons, K. G., Leenen, L. P., and Kalkman, C. J. Effect of intracranial pressure monitoring and targeted intensive care on functional outcome after severe head injury. *Critical care medicine*, 33(10):2207–2213, 2005.

Czosnyka, M. and Pickard, J. D. Monitoring and interpretation of intracranial pressure. *Journal of Neurology, Neurosurgery & Psychiatry*, 75(6):813–821, 2004.

Czosnyka, M., Smielewski, P., Timofeev, I., Lavinio, A., Guazzo, E., Hutchinson, P., and Pickard, J. D. Intracranial pressure: more than a number. *Neurosurgical focus*, 22(5):1–7, 2007.

Dang, Q., Simon, J., Catino, J., Puente, I., Habib, F., Zucker, L., and Bukur, M. More fateful than fruitful? Intracranial pressure monitoring in elderly patients with traumatic brain injury is associated with worse outcomes. *journal of surgical research*, 198(2):482–488, 2015.

Di Ieva, A., Schmitz, E. M., and Cusimano, M. D. Analysis of intracranial pressure: past, present, and future. *The Neuroscientist*, 19(6):592–603, 2013.

Eckmann, J.-P., Kamphorst, S. O., and Ruelle, D. Recurrence plots of dynamical systems. *EPL (Europhysics Letters)*, 4(9):973, 1987.

Fakhry, S. M., Trask, A. L., Waller, M. A., Watts, D. D., et al. Management of brain-injured patients by an evidence-based medicine protocol improves outcomes and decreases hospital charges. *Journal of Trauma and Acute Care Surgery*, 56(3): 492–500, 2004.

Fan, J.-Y., Kirkness, C., Vicini, P., Burr, R., and Mitchell, P. An approach to determining intracranial pressure variability capable of predicting decreased intracranial adaptive capacity in patients with traumatic brain injury. *Biological research for nursing*, 11(4):317–324, 2010.

Goldberger, A. L. Non-linear dynamics for clinicians: chaos theory, fractals, and complexity at the bedside. *The Lancet*, 347(9011):1312–1314, 1996.

Goldberger, A. L., Amaral, L. A., Glass, L., Hausdorff, J. M., Ivanov, P. C., Mark, R. G., Mietus, J. E., Moody, G. B., Peng, C.-K., and Stanley, H. E. Physiobank, physiotoolkit, and physionet. *Circulation*, 101(23):e215–e220, 2000.

Greenberg, M. S. and Arredondo, N. Handbook of neurosurgery. 2006.

Hamilton, R., Xu, P., Asgari, S., Kasprowicz, M., Vespa, P., Bergsneider, M., and Hu, X. Forecasting intracranial pressure elevation using pulse waveform morphology. In *Engineering in Medicine and Biology Society, 2009. EMBC 2009. Annual International Conference of the IEEE*, pages 4331–4334. IEEE, 2009.

Holm, S. and Eide, P. K. The frequency domain versus time domain methods for processing of intracranial pressure (ICP) signals. *Medical engineering & physics*, 30(2):164–170, 2008.

Hornero, R., Aboy, M., Abásolo, D., McNames, J., and Goldstein, B. Interpretation of approximate entropy: analysis of intracranial pressure approximate entropy during acute intracranial hypertension. *IEEE transactions on biomedical engineering*, 52 (10):1671–1680, 2005.

Hornero, R., Aboy, M., Abasolo, D., McNames, J., Wakeland, W., and Goldstein, B. Complex analysis of intracranial hypertension using approximate entropy. *Critical care medicine*, 34(1):87–95, 2006.

Hornero, R., Aboy, M., and Abásolo, D. Analysis of intracranial pressure during acute intracranial hypertension using Lempel–Ziv complexity: further evidence. *Medical & biological engineering & computing*, 45(6):617–620, 2007.

Hu, J., Gao, J., and Principe, J. C. Analysis of biomedical signals by the Lempel-Ziv complexity: the effect of finite data size. *IEEE Transactions on Biomedical Engineering*, 53(12):2606–2609, 2006.

Hu, X., Xu, P., Lee, D. J., Vespa, P., Baldwin, K., and Bergsneider, M. An algorithm for extracting intracranial pressure latency relative to electrocardiogram R wave. *Physiological measurement*, 29(4):459, 2008.

Hu, X., Xu, P., Scalzo, F., Vespa, P., and Bergsneider, M. Morphological clustering and analysis of continuous intracranial pressure. *IEEE Transactions on Biomedical Engineering*, 56(3):696–705, 2009.

Hu, X., Xu, P., Asgari, S., Vespa, P., and Bergsneider, M. Forecasting ICP elevation based on prescient changes of intracranial pressure waveform morphology. *IEEE Transactions on Biomedical Engineering*, 57(5):1070–1078, 2010.

Hughes, J. A., Jackson, E. C., and Daley, M. Modelling Intracranial Pressure with Noninvasive Physiological Measures. In *Computational Intelligence in Bioinformatics and Computational Biology, 2017 IEEE Conference on*. IEEE, 2017.

Iwanski, J. S. and Bradley, E. Recurrence plots of experimental data: To embed or not to embed? *Chaos: An Interdisciplinary Journal of Nonlinear Science*, 8(4): 861–871, 1998.

Jennett, B. Epidemiology of head injury. *Journal of Neurology, Neurosurgery & Psychiatry*, 60(4):362–369, 1996.

Johnson, A. E., Pollard, T. J., Shen, L., Lehman, L.-w. H., Feng, M., Ghassemi, M., Moody, B., Szolovits, P., Celi, L. A., and Mark, R. G. MIMIC-III, a freely accessible critical care database. *Scientific data*, 3, 2016.

Johnston, I., Johnston, J., and Jennett, B. Intracranial-pressure changes following head injury. *The Lancet*, 296(7670):433–436, 1970.

Juul, N., Morris, G. F., Marshall, S. B., and Marshall, L. F. Intracranial hypertension and cerebral perfusion pressure: influence on neurological deterioration and outcome in severe head injury. *Journal of neurosurgery*, 92(1):1–6, 2000.

Kim, Y.-J. A systematic review of factors contributing to outcomes in patients with traumatic brain injury. *Journal of clinical nursing*, 20(11-12):1518–1532, 2011.

Kirkness, C. J., Mitchell, P. H., Burr, R. L., March, K. S., and Newell, D. W. Intracranial pressure waveform analysis: clinical and research implications. *Journal of Neuroscience Nursing*, 32(5):271–277, 2000.

Kolmogorov, A. N. Three approaches to the quantitative definition ofinformation'. *Problems of information transmission*, 1(1):1–7, 1965.

Lu, C.-W., Czosnyka, M., Shieh, J.-S., Smielewska, A., Pickard, J. D., and Smielewski, P. Complexity of intracranial pressure correlates with outcome after traumatic brain injury. *Brain*, 135(8):2399–2408, 2012.

Lundberg, N., Troupp, H., and Lorin, H. Continuous recording of the ventricular-fluid pressure in patients with severe acute traumatic brain injury: a preliminary report. *Journal of neurosurgery*, 22(6):581–590, 1965.

March, T., Chapman, S., and Dendy, R. Recurrence plot statistics and the effect of embedding. *Physica D: Nonlinear Phenomena*, 200(1):171–184, 2005.

Marwan, N. A historical review of recurrence plots. *The European Physical Journal-Special Topics*, 164(1):3–12, 2008.

Marwan, N., Romano, M. C., Thiel, M., and Kurths, J. Recurrence plots for the analysis of complex systems. *Physics reports*, 438(5):237–329, 2007.

Mayer, S. A. and Chong, J. Y. Critical care management of increased intracranial pressure. *Journal of Intensive Care Medicine*, 17(2):55–67, 2002.

Mendelow, A. D., Crawford, P. J., and Crawford, P. Primary and secondary brain injury. *Head injury. Pathophysiology and management. Hodder Arnold, London*, pages 73–92, 2005.

Miller, J. D., Becker, D. P., Ward, J. D., Sullivan, H. G., Adams, W. E., and Rosner, M. J. Significance of intracranial hypertension in severe head injury. *Journal of neurosurgery*, 47(4):503–516, 1977.

Mindlin, G. M. and Gilmore, R. Topological analysis and synthesis of chaotic time series. *Physica D: Nonlinear Phenomena*, 58(1-4):229–242, 1992.

Neff, S. and Subramaniam, R. Monro-Kellie doctrine. *Journal of neurosurgery*, 85 (6):1195–1195, 1996.

OṔhelan, K. H., Park, D., Efird, J. T., Johnson, K., Albano, M., Beniga, J., Green, D. M., and Chang, C. W. Patterns of increased intracranial pressure after severe traumatic brain injury. *Neurocritical care*, 10(3):280, 2009.

Poincaré, H. Sur le problème des trois corps et les équations de la dynamique. *Acta mathematica*, 13(1):A3–A270, 1890.

Raboel, P., Bartek, J., Andresen, M., Bellander, B., and Romner, B. Intracranial pressure monitoring: invasive versus non-invasive methodsa review. *Critical care research and practice*, 2012, 2012.

Runge, J. W. The cost of injury. *Emergency medicine clinics of North America*, 11 (1):241–253, 1993.

Saeed, M., Villarroel, M., Reisner, A. T., Clifford, G., Lehman, L.-W., Moody, G., Heldt, T., Kyaw, T. H., Moody, B., and Mark, R. G. Multiparameter Intelligent Monitoring in Intensive Care II (MIMIC-II): a public-access intensive care unit database. *Critical care medicine*, 39(5):952, 2011.

Sarlabous, L., Torres, A., Fiz, J. A., Gea, J., Galdiz, J. B., and Jané, R. Multistate Lempel-Ziv (MLZ) index interpretation as a measure of amplitude and complexity changes. In *Engineering in Medicine and Biology Society, 2009. EMBC 2009. Annual International Conference of the IEEE*, pages 4375–4378. IEEE, 2009.

Schinkel, S., Dimigen, O., and Marwan, N. Selection of recurrence threshold for signal detection. *The European Physical Journal-Special Topics*, 164(1):45–53, 2008.

Sourina, O., Ang, B.-T., and Nguyen, M. K. Fractal-based approach in analysis of intracranial pressure (ICP) in severe head injury. In *Information Technology and Applications in Biomedicine (ITAB), 2010 10th IEEE International Conference on*, pages 1–4. IEEE, 2010.

Stanley, H., Amaral, L. N., Goldberger, A., Havlin, S., Ivanov, P. C., and Peng, C.-K. Statistical physics and physiology: monofractal and multifractal approaches. *Physica A: Statistical Mechanics and its Applications*, 270(1):309–324, 1999.

Stein, D. G. Brain damage, sex hormones and recovery: a new role for progesterone and estrogen? *Trends in neurosciences*, 24(7):386–391, 2001.

Takens, F. et al. Detecting strange attractors in turbulence. *Lecture notes in mathematics*, 898(1):366–381, 1981.

Thiel, M., Romano, M. C., Read, P., and Kurths, J. Estimation of dynamical invariants without embedding by recurrence plots. *Chaos: An Interdisciplinary Journal of Nonlinear Science*, 14(2):234–243, 2004.

Webber, C. L. and Zbilut, J. P. Dynamical assessment of physiological systems and states using recurrence plot strategies. *Journal of applied physiology*, 76(2):965–973, 1994.

Webber Jr, C. L. and Marwan, N. *Recurrence quantification analysis*. Springer, 2015.

Whitney, H. Differentiable manifolds. *Annals of Mathematics*, pages 645–680, 1936.

Zbilut, J. P. and Webber, C. L. Embeddings and delays as derived from quantification of recurrence plots. *Physics letters A*, 171(3-4):199–203, 1992.

Zbilut, J. P. and Webber, C. L. Recurrence quantification analysis. *Wiley encyclopedia of biomedical engineering*, 2006.

Zhang, Y., Wei, S., Liu, H., Zhao, L., and Liu, C. A novel encoding Lempel–Ziv complexity algorithm for quantifying the irregularity of physiological time series. *computer methods and programs in biomedicine*, 133:7–15, 2016.

Appendix A

Comprehensive Results

A.1 Overall Results

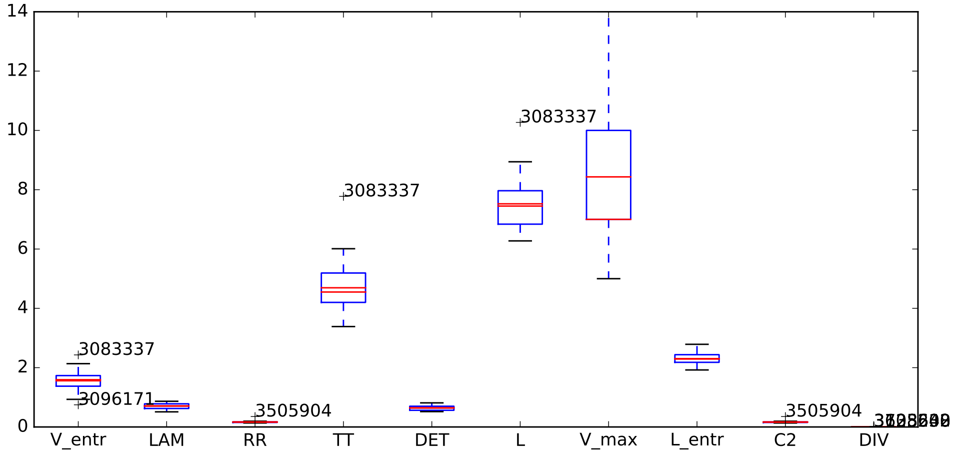

Figure A.1: Distributions of RQAs for all subjects, anomalies are flagged, actual scale of the figure provided in the main text.

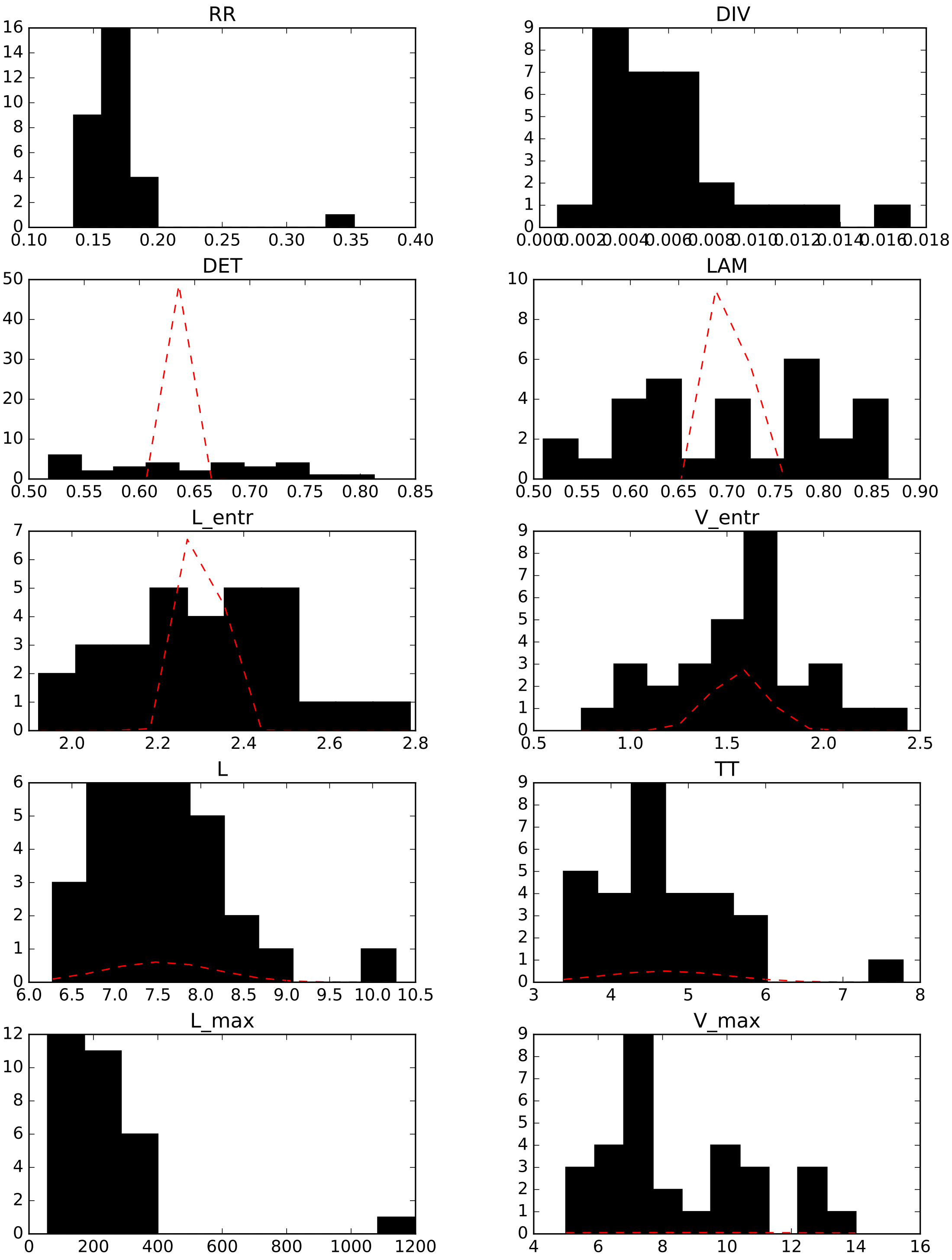

Figure A.2: Distributions of different RQA measures, from which the above box plot is generated. The red curve is the Gaussian with same mean and variance, which confirms these are not normal distributions.

A.2 Novelty Curves of All Patients

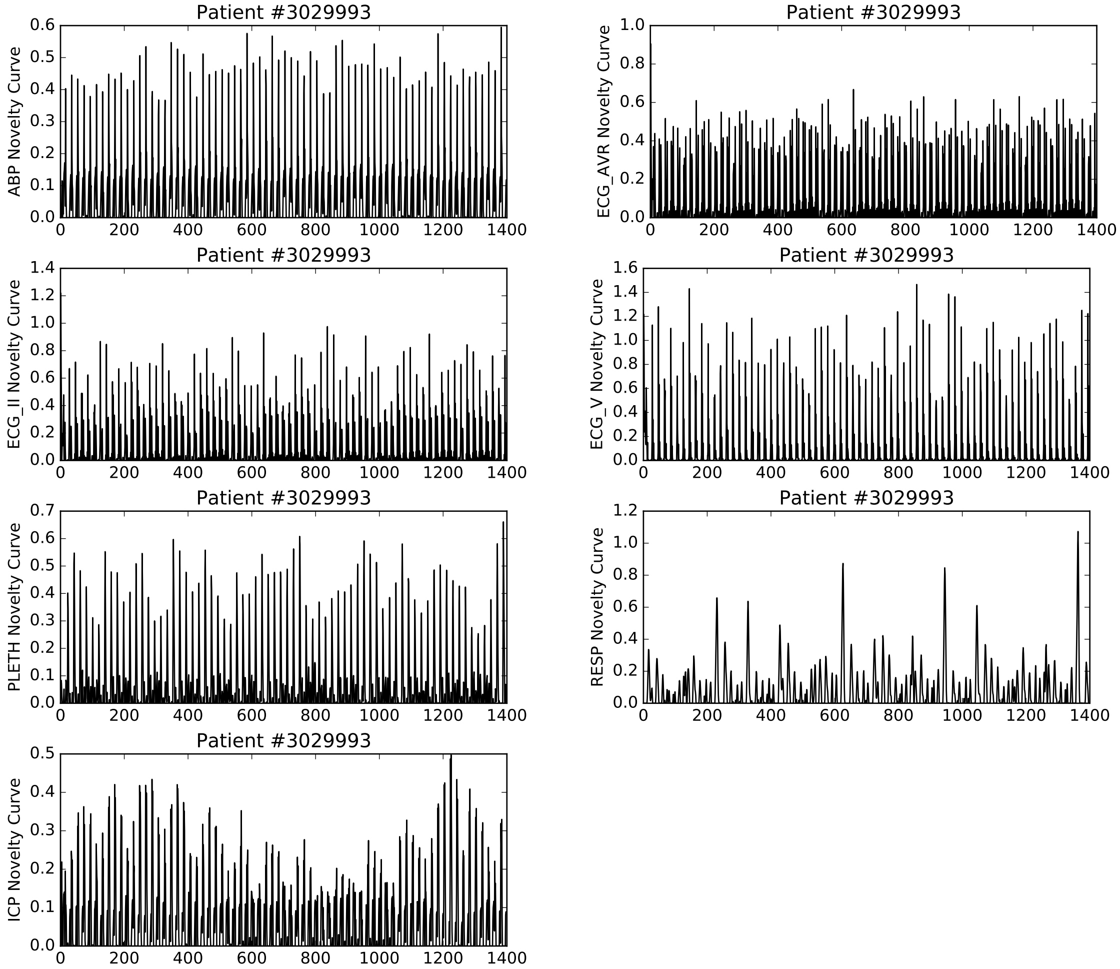

Figure A.3: Novelty curves of subject 3029993

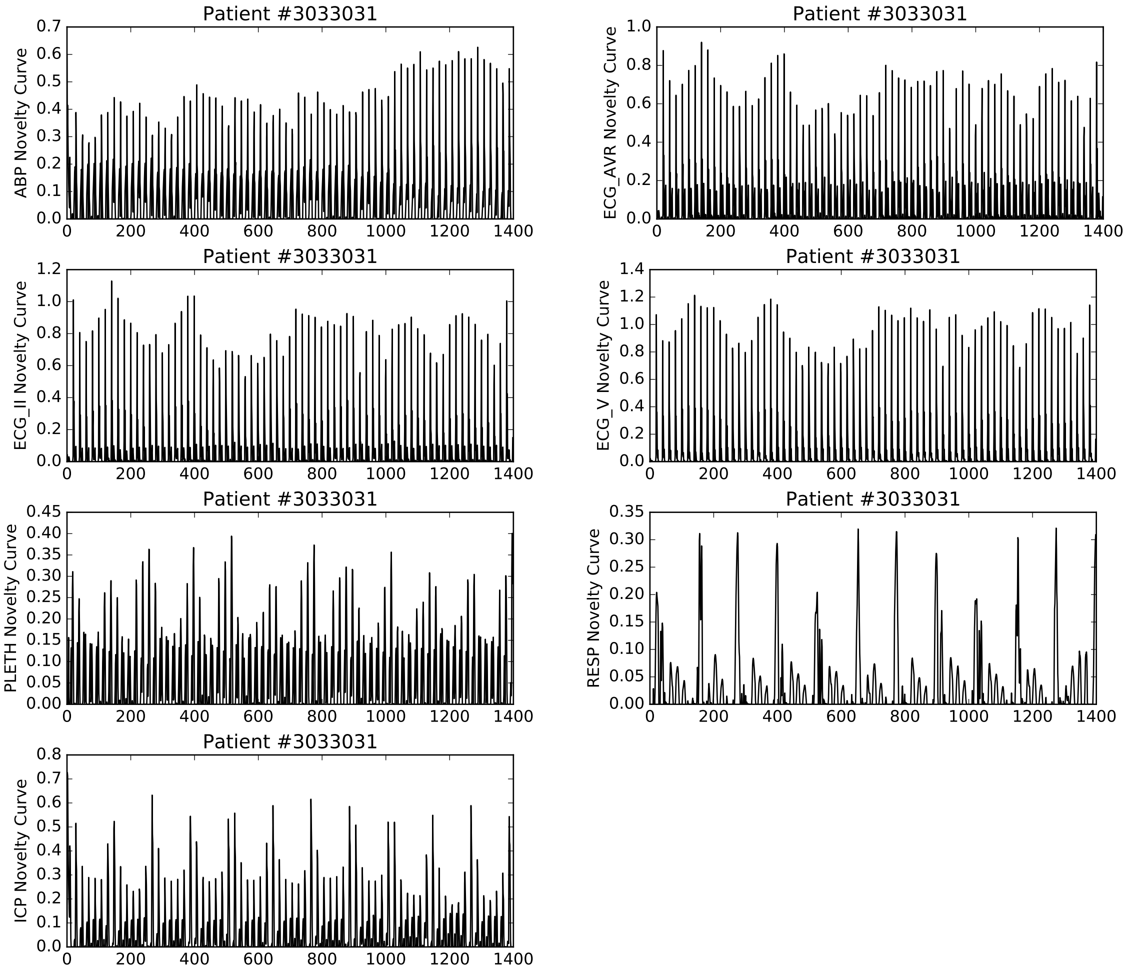

Figure A.4: Novelty curves of subject 3033031

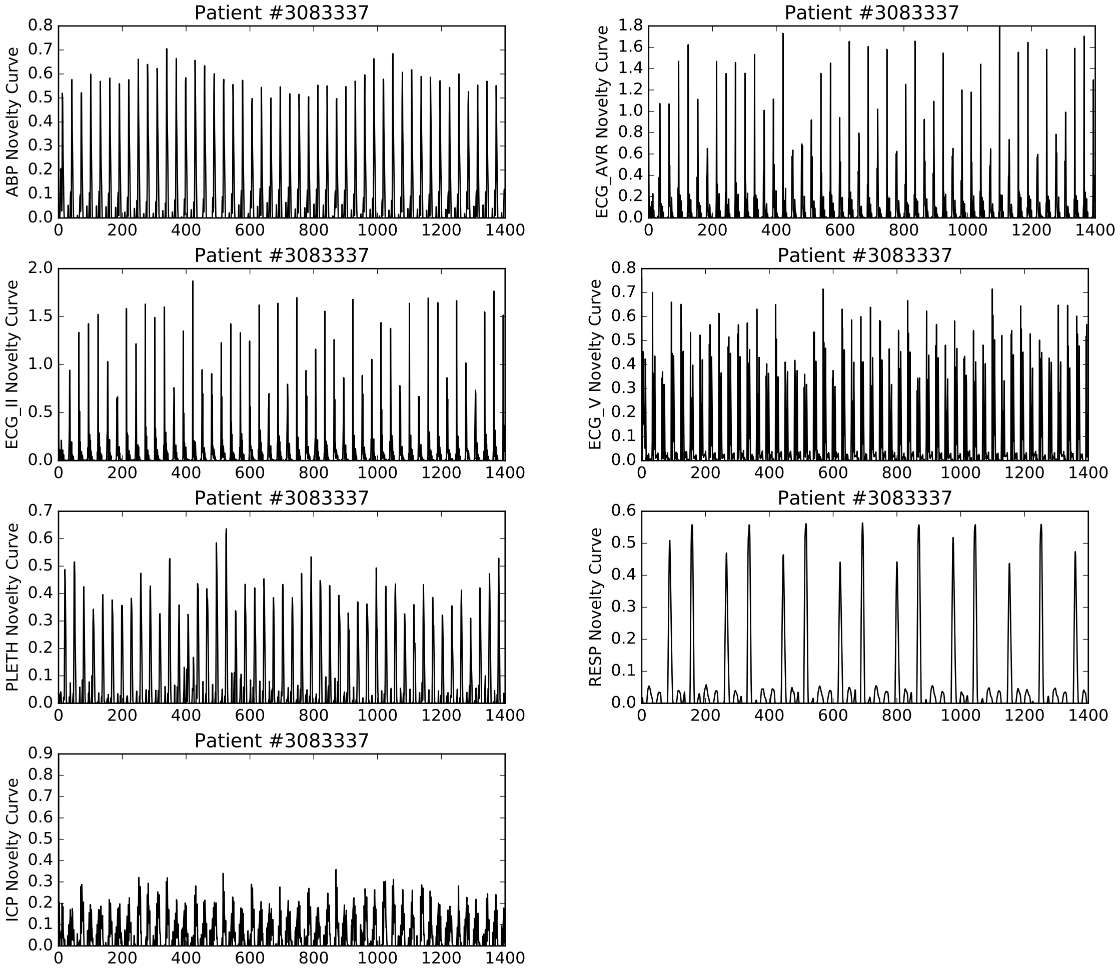

Figure A.5: Novelty curves of subject 3083337

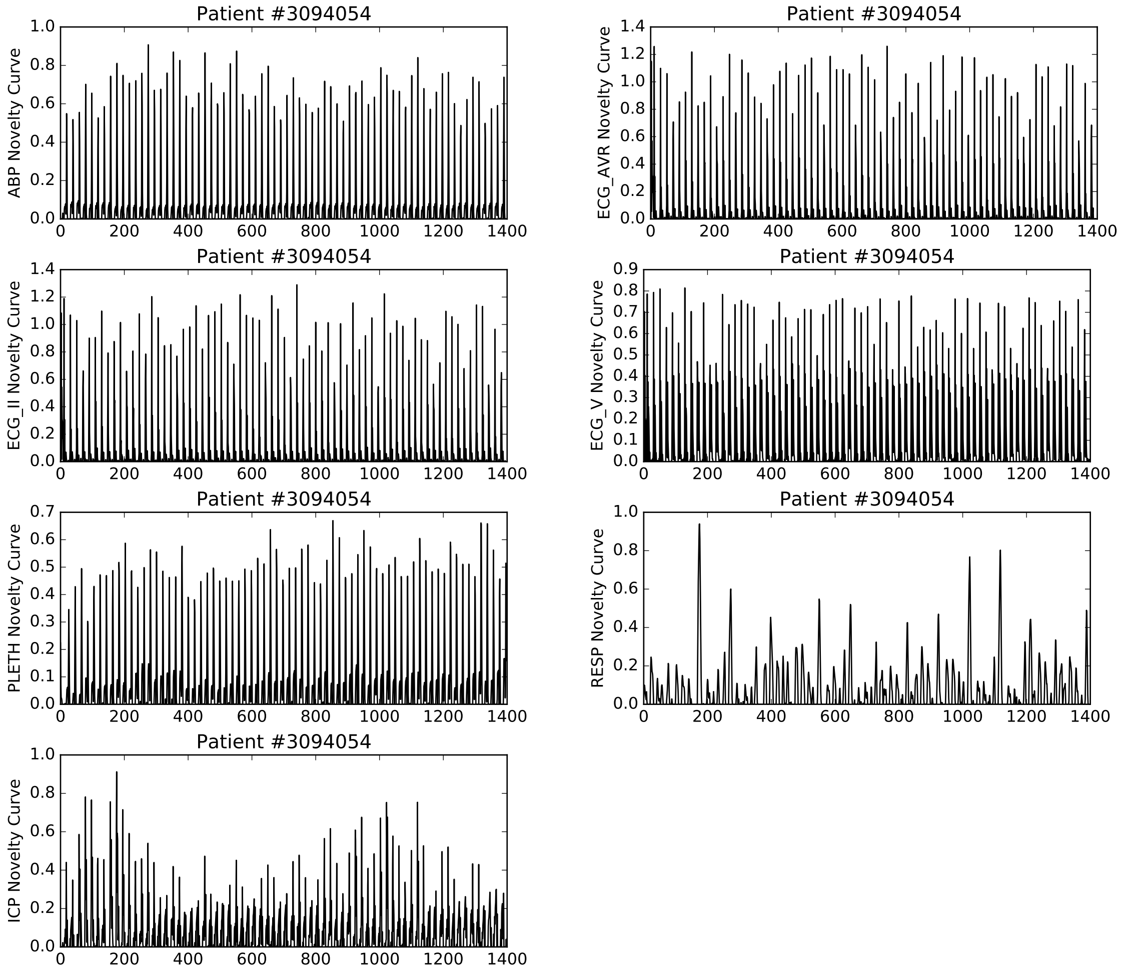

Figure A.6: Novelty curves of subject 3094054

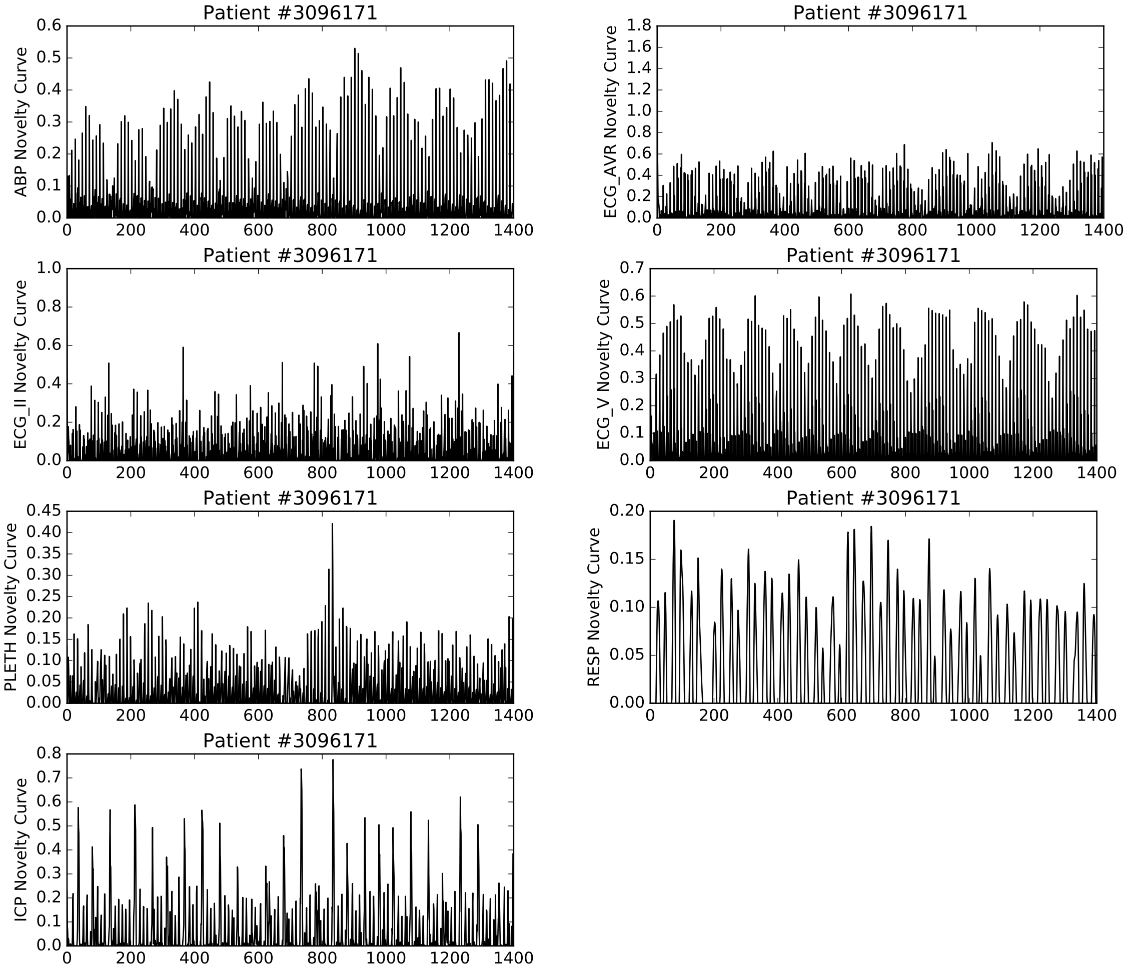

Figure A.7: Novelty curves of subject 3096171

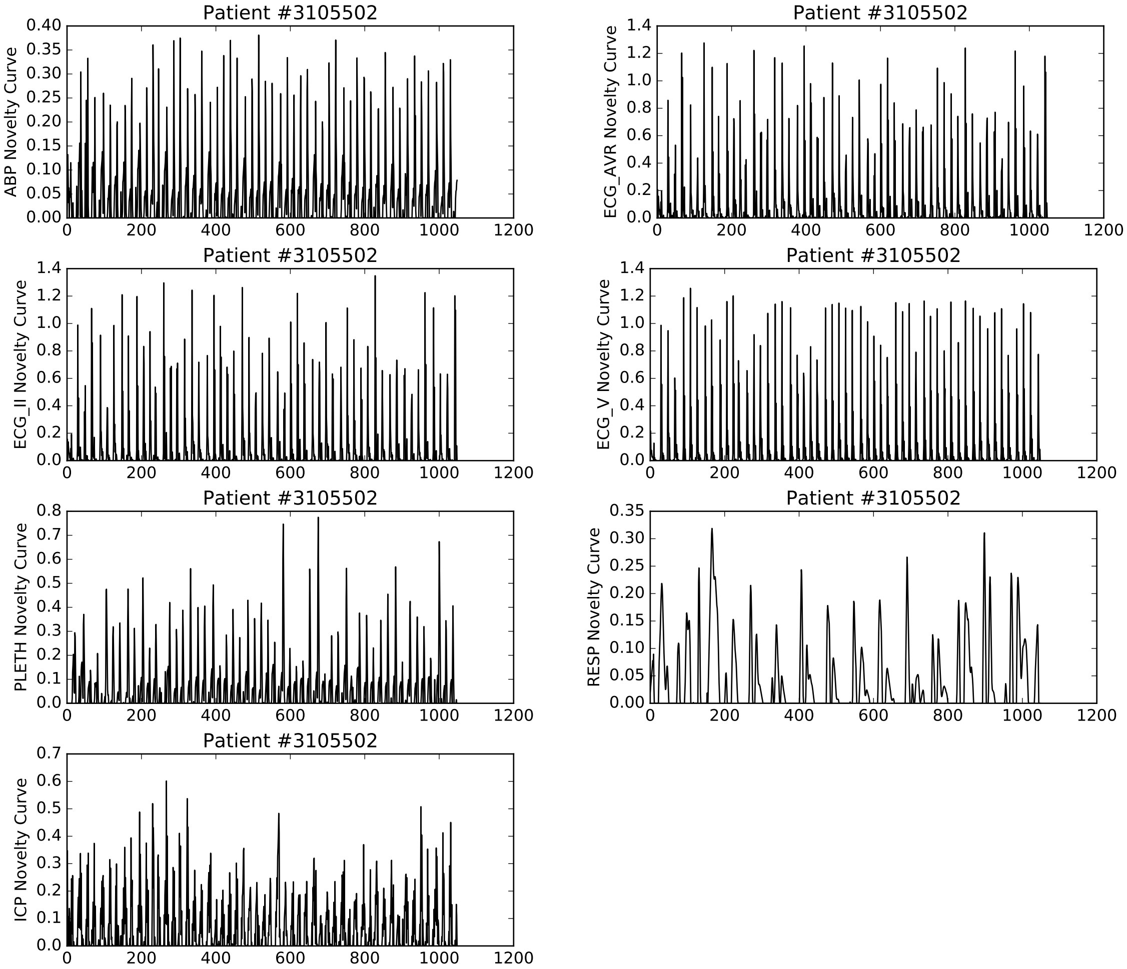

Figure A.8: Novelty curves of subject 3105502

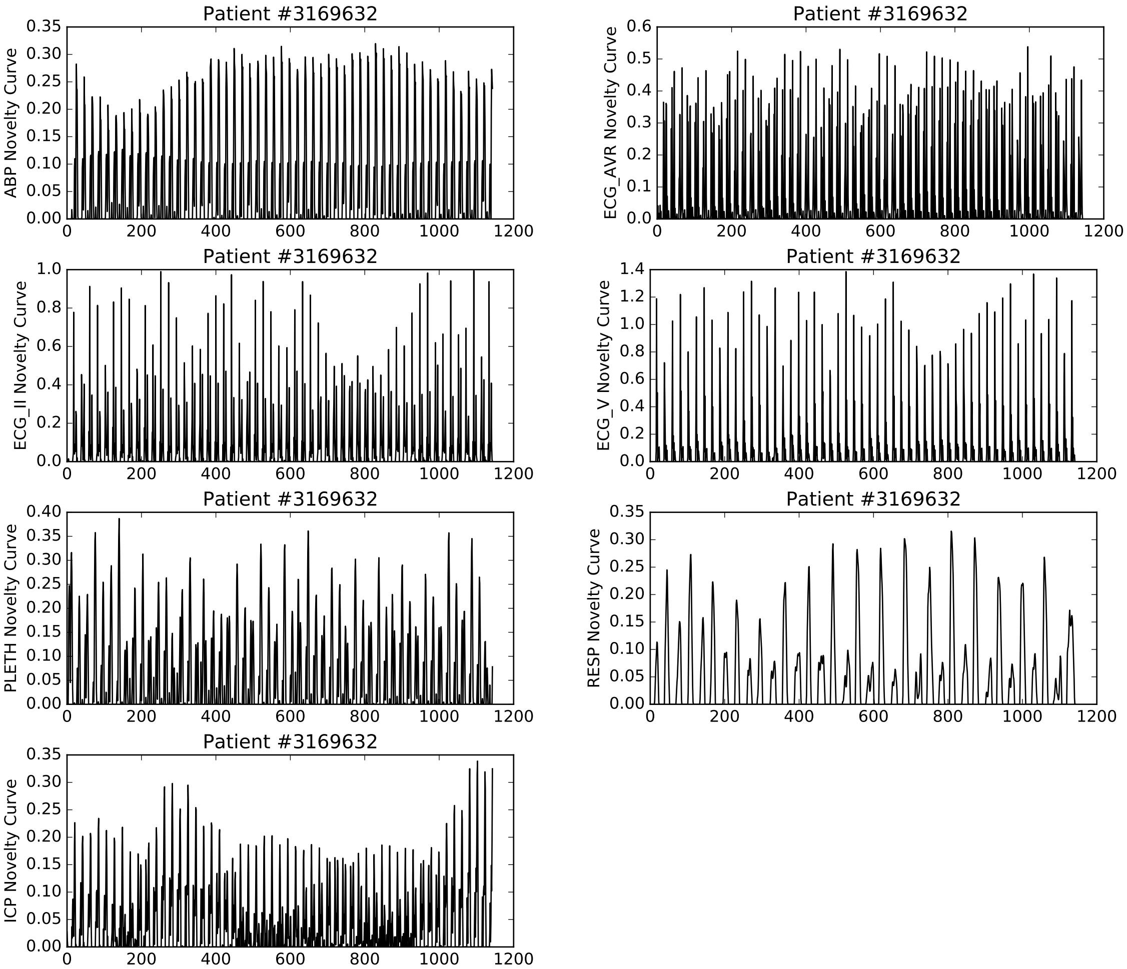

Figure A.9: Novelty curves of subject 3169632

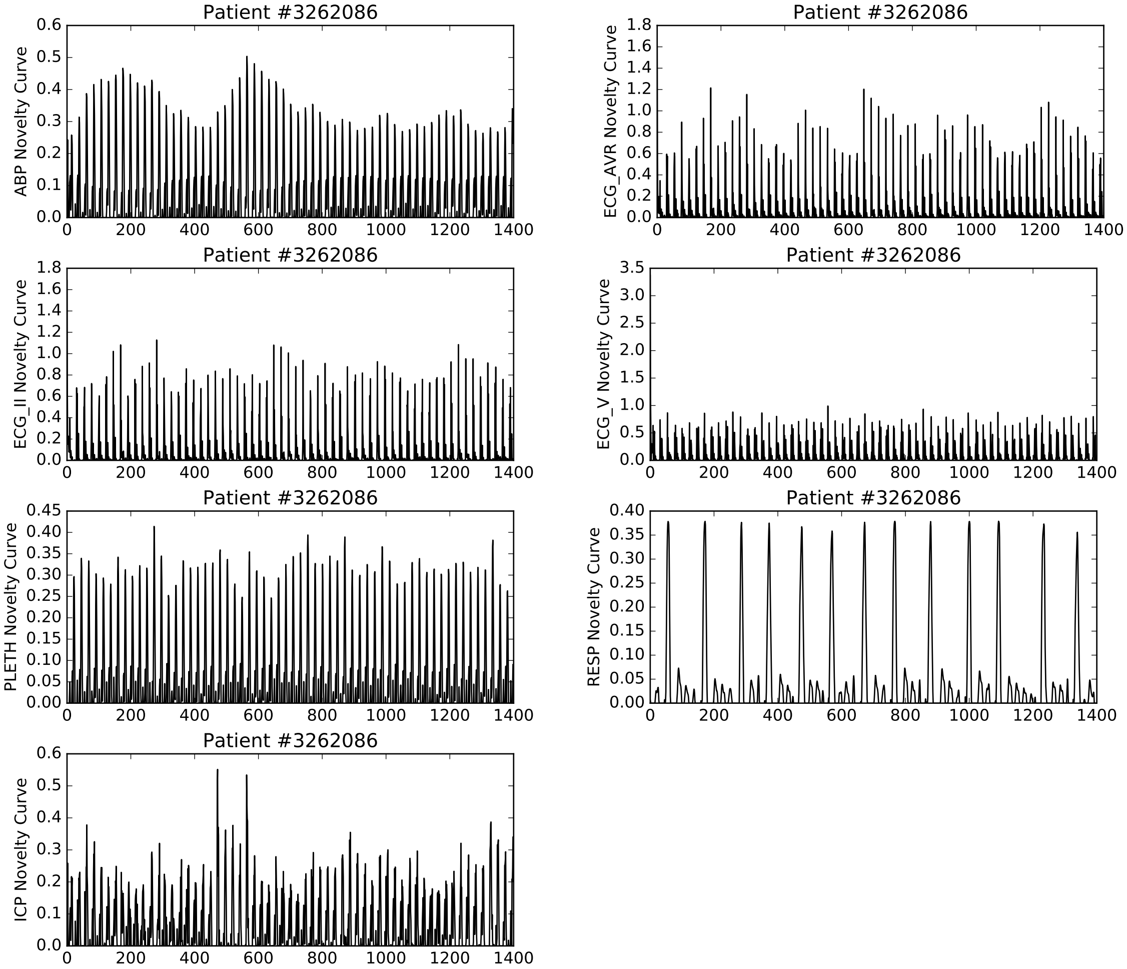

Figure A.10: Novelty curves of subject 3262086

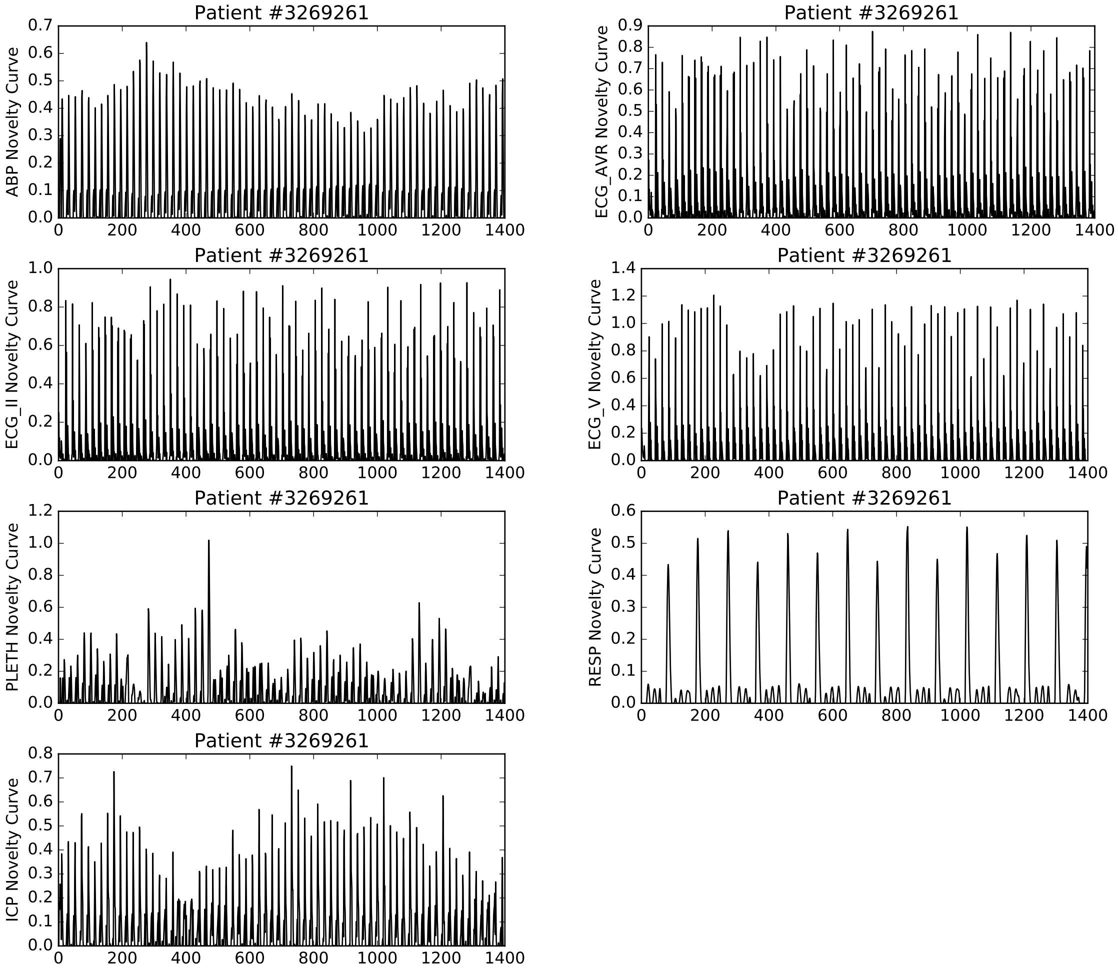

Figure A.11: Novelty curves of subject 3269261

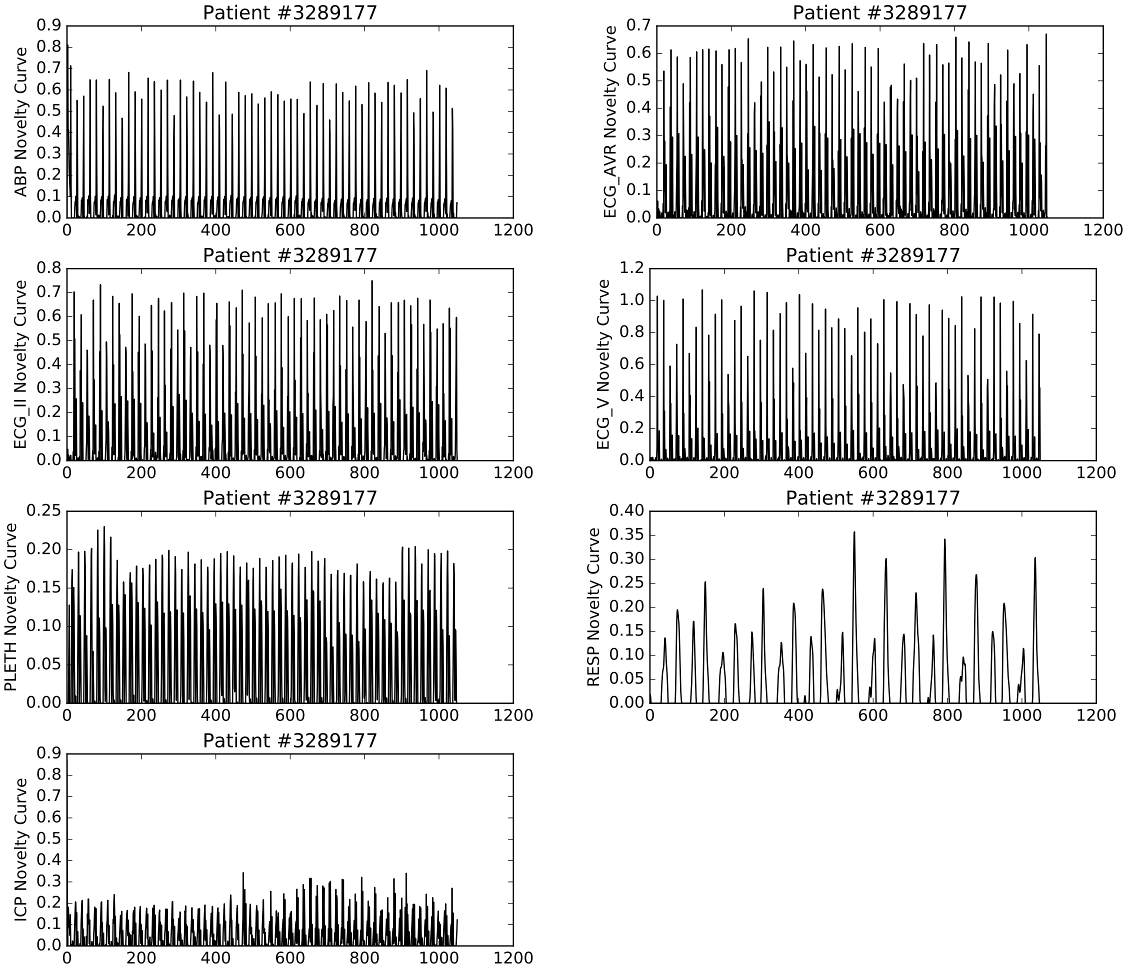

Figure A.12: Novelty curves of subject 3289177

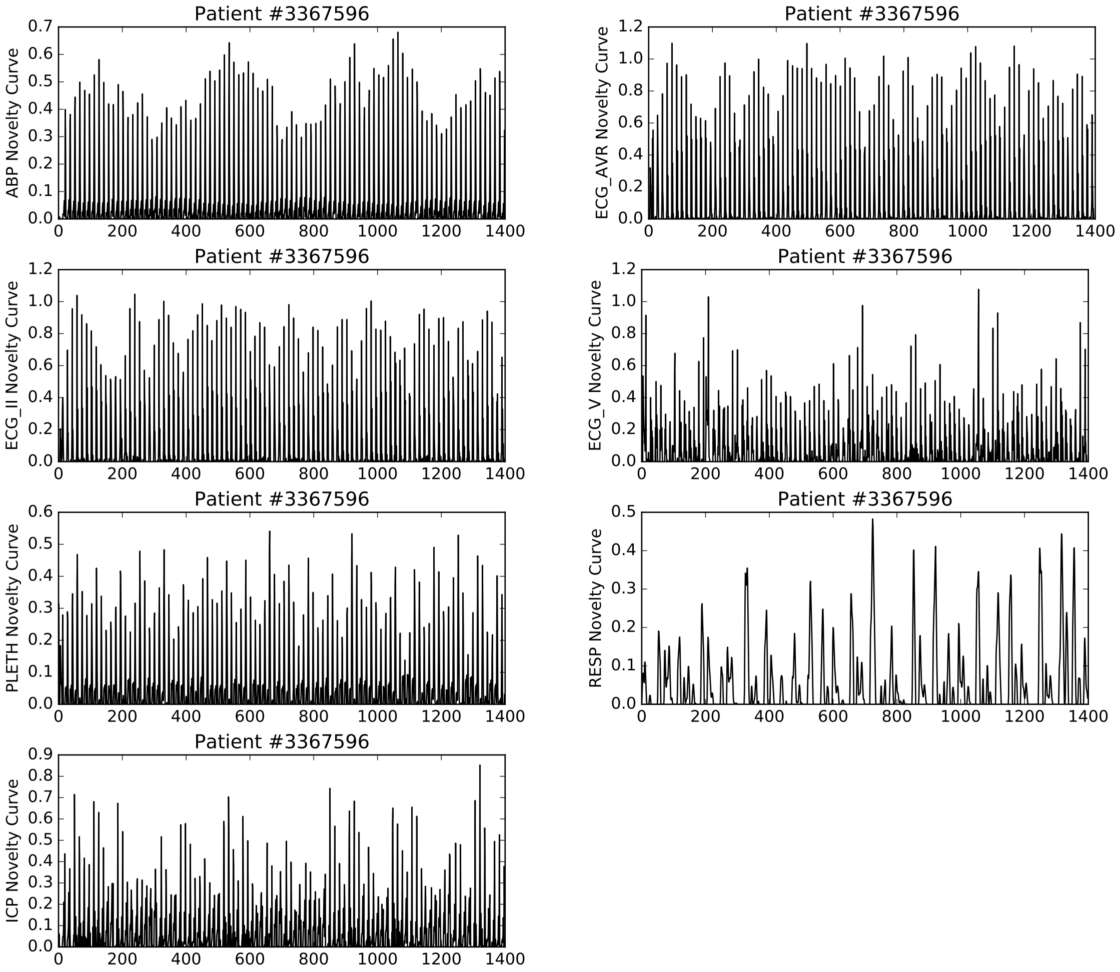

Figure A.13: Novelty curves of subject 3367596

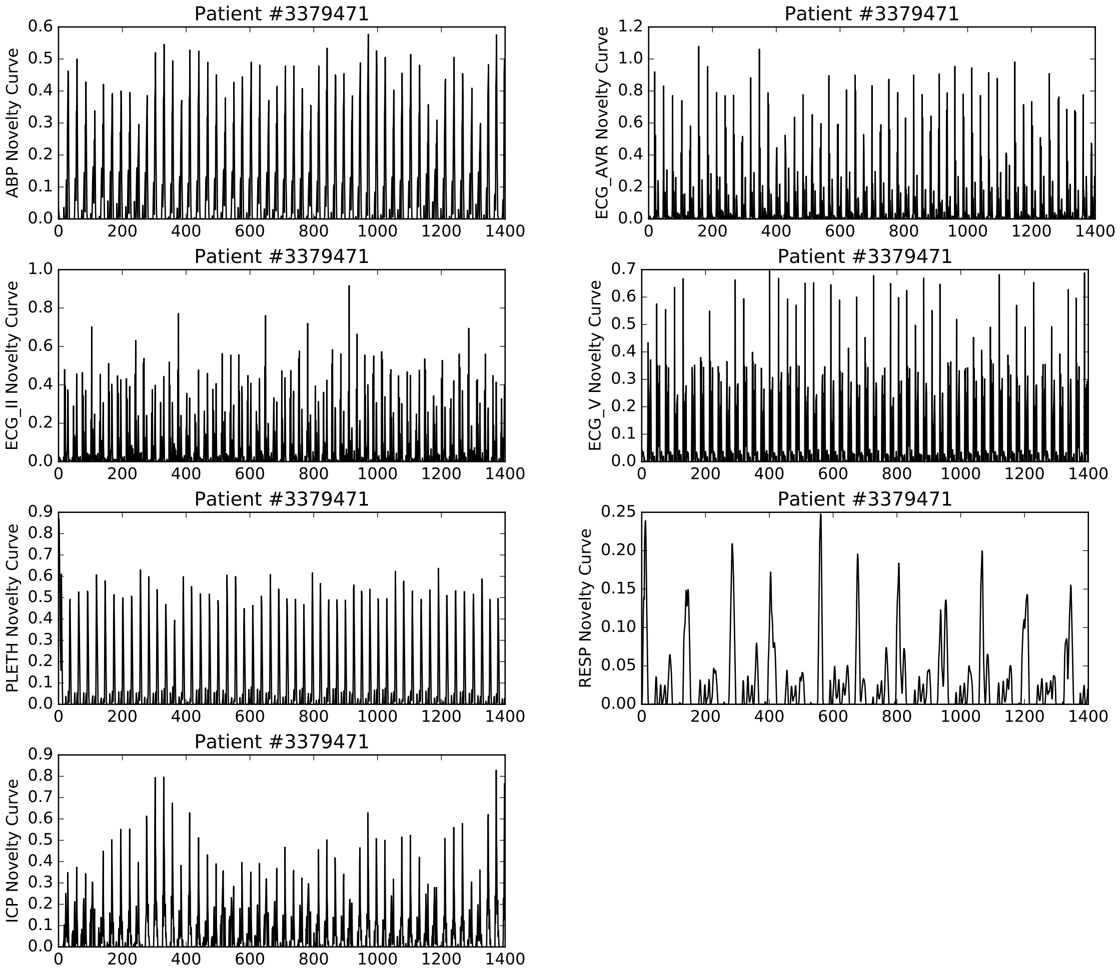

Figure A.14: Novelty curves of subject 3379471

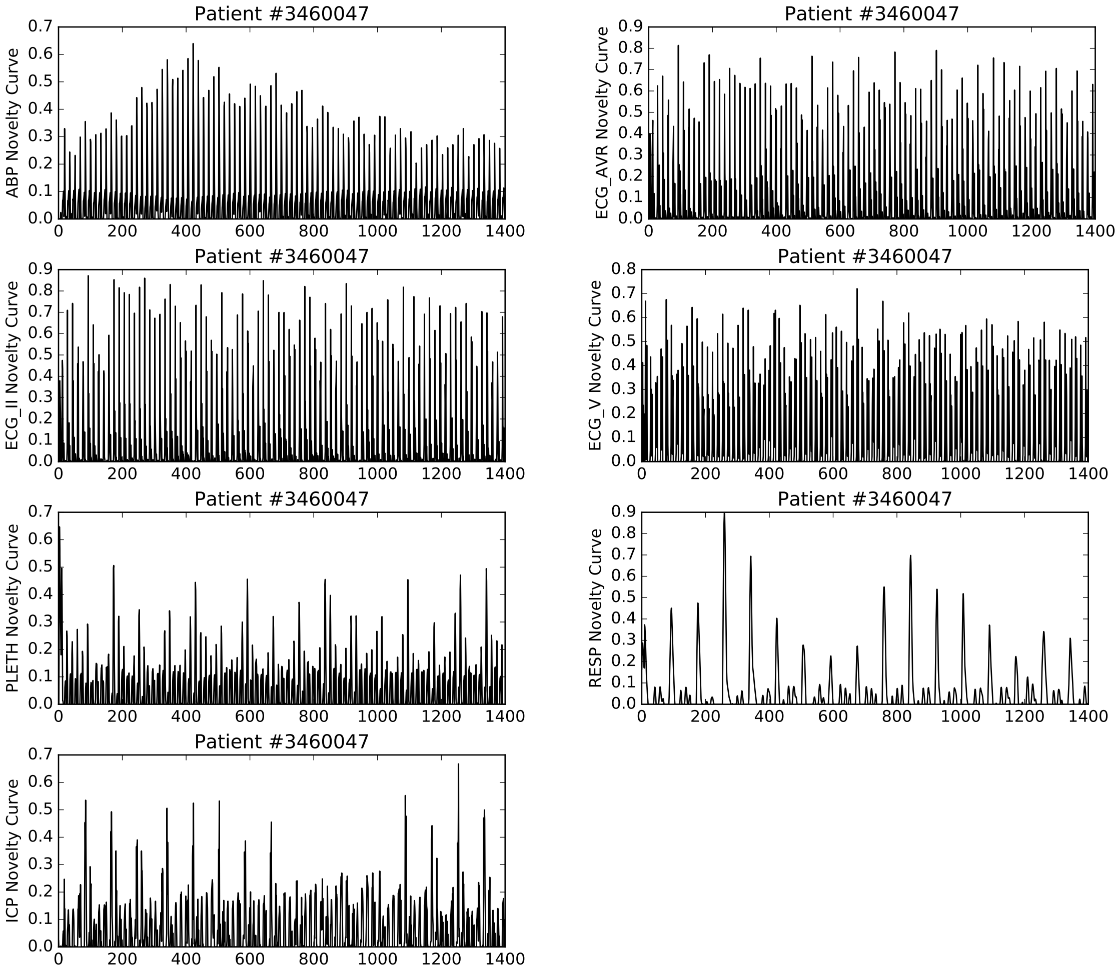

Figure A.15: Novelty curves of subject 3460047

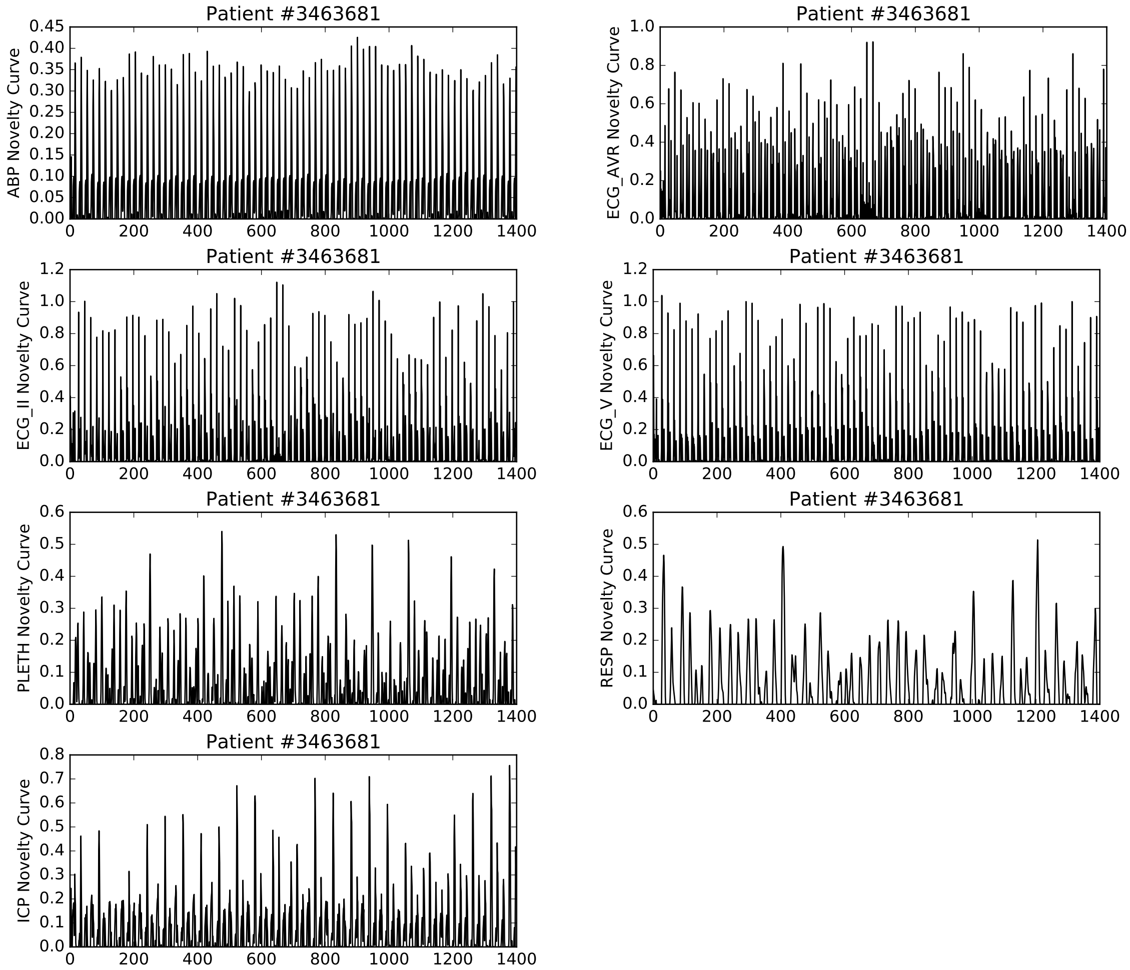

Figure A.16: Novelty curves of subject 3463681

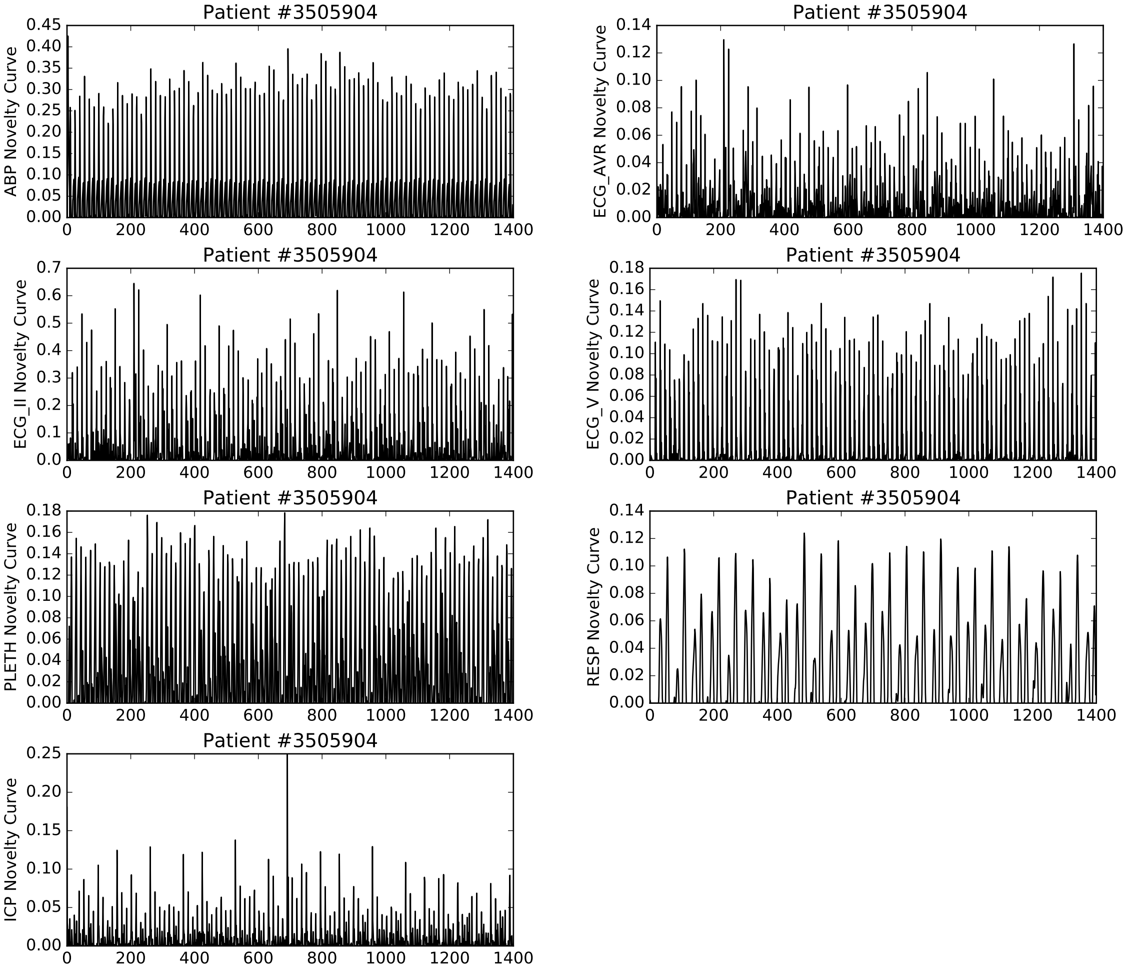

Figure A.17: Novelty curves of subject 3505904

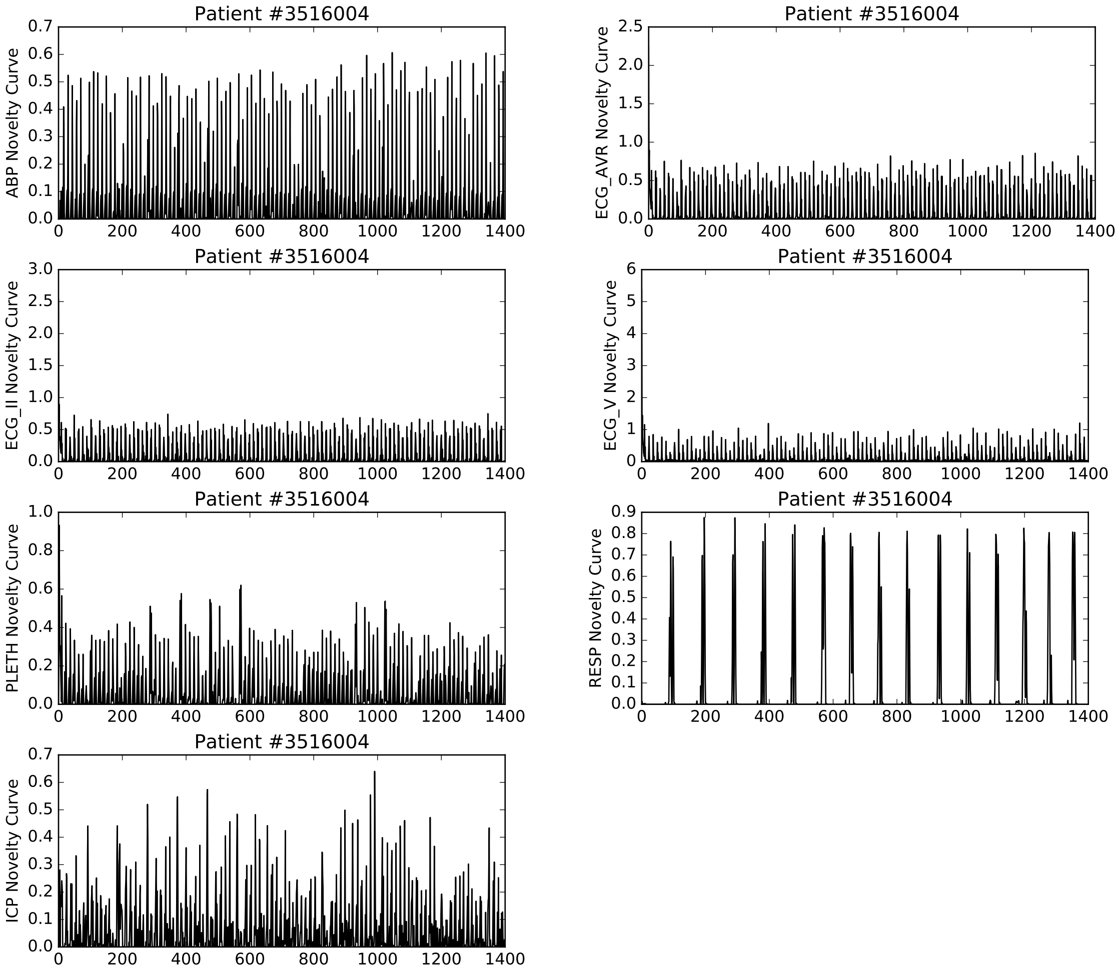

Figure A.18: Novelty curves of subject 3516004

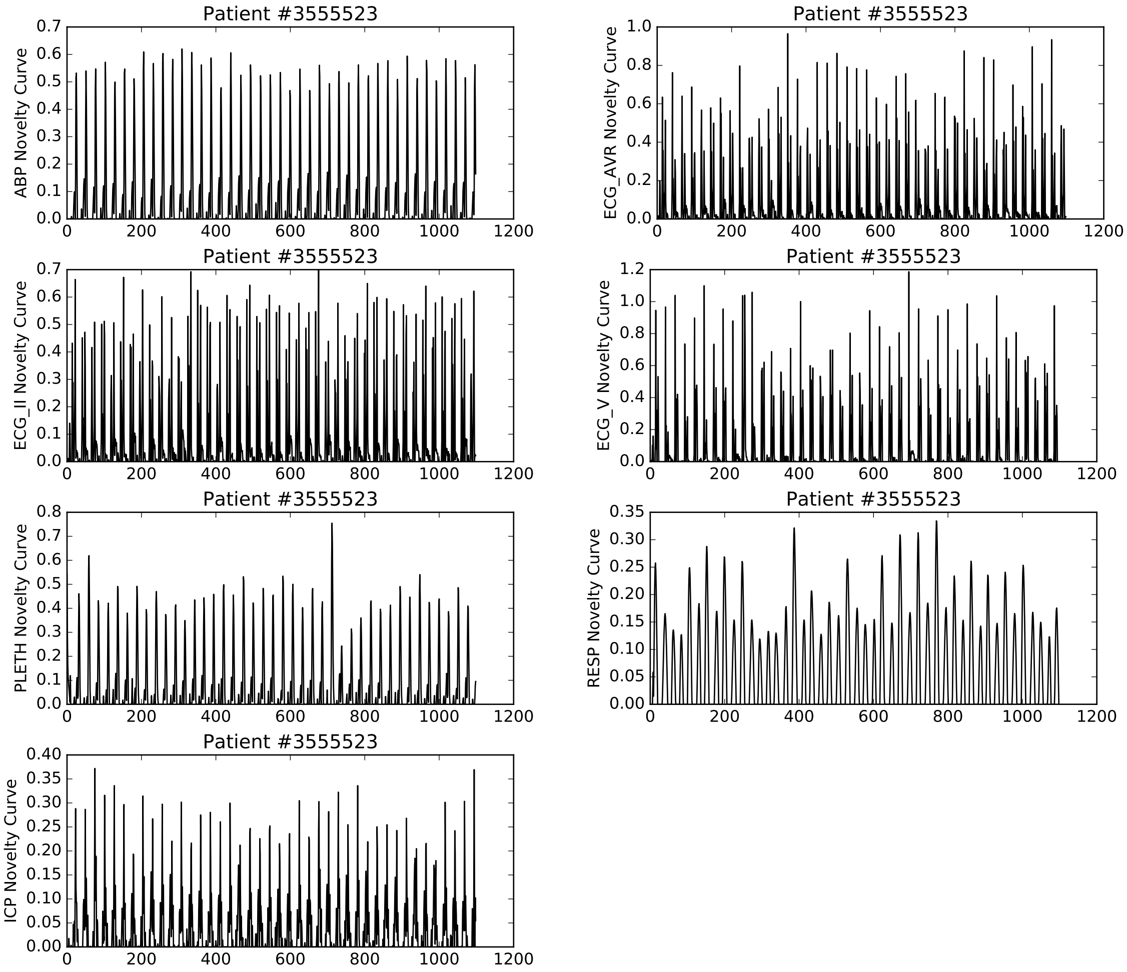

Figure A.19: Novelty curves of subject 3555523

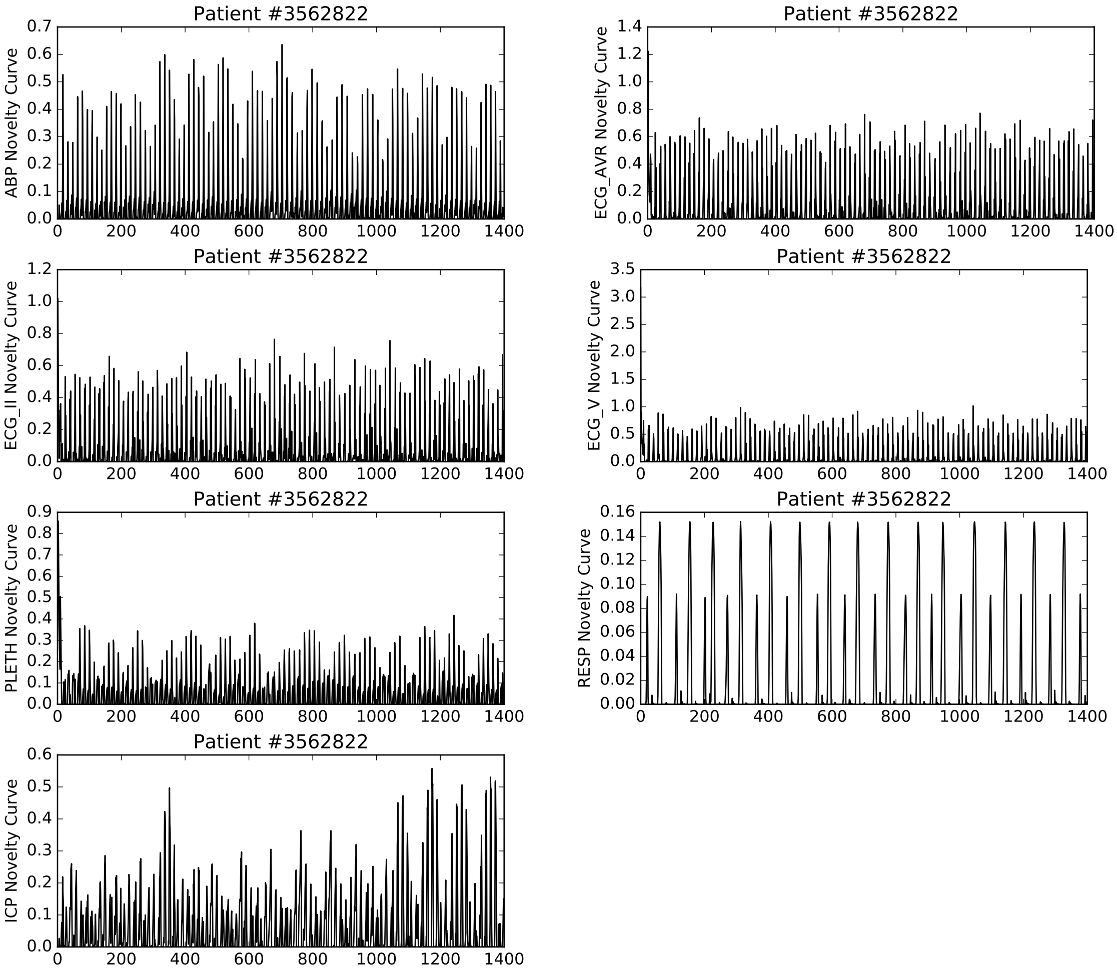
Patient #3562822

Figure A.20: Novelty curves of subject 3562822

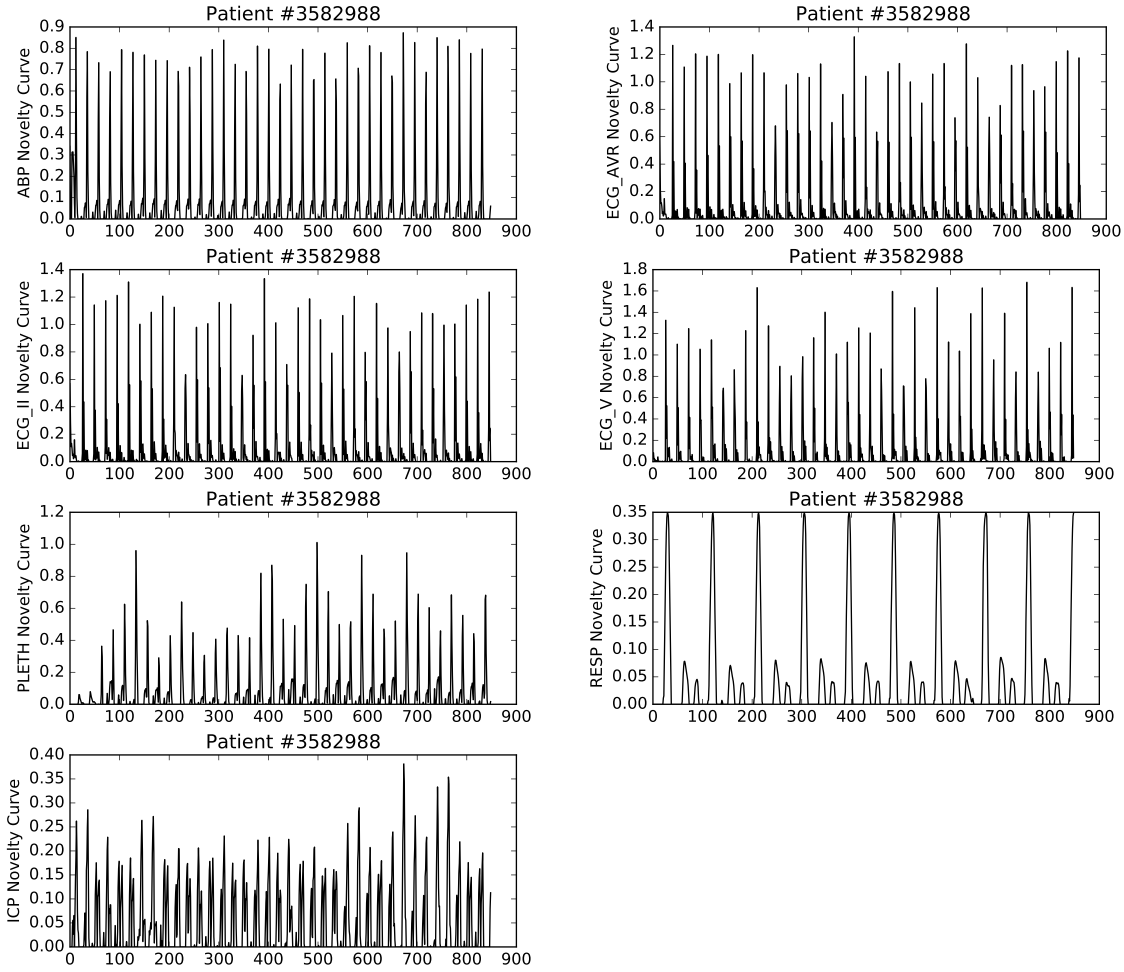

Figure A.21: Novelty curves of subject 3582988

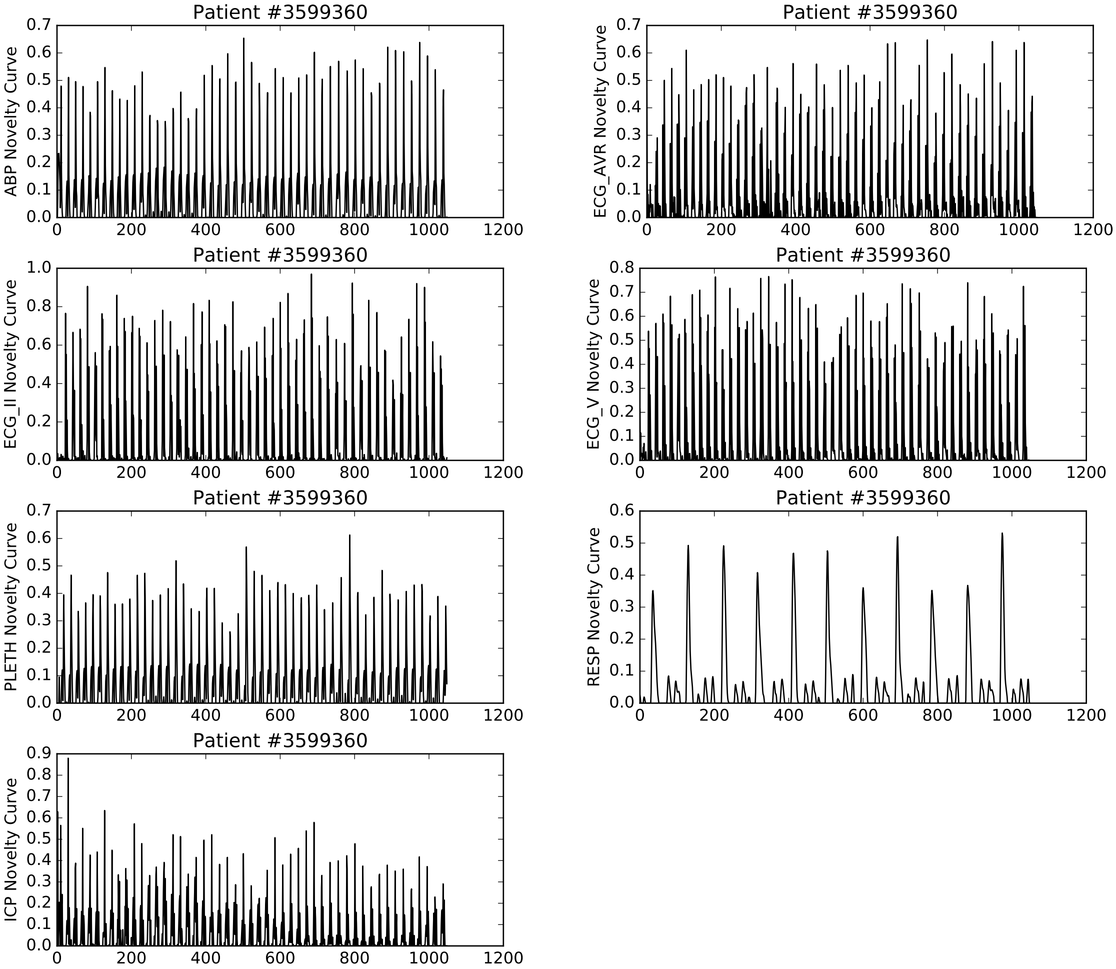

Figure A.22: Novelty curves of subject 3599360

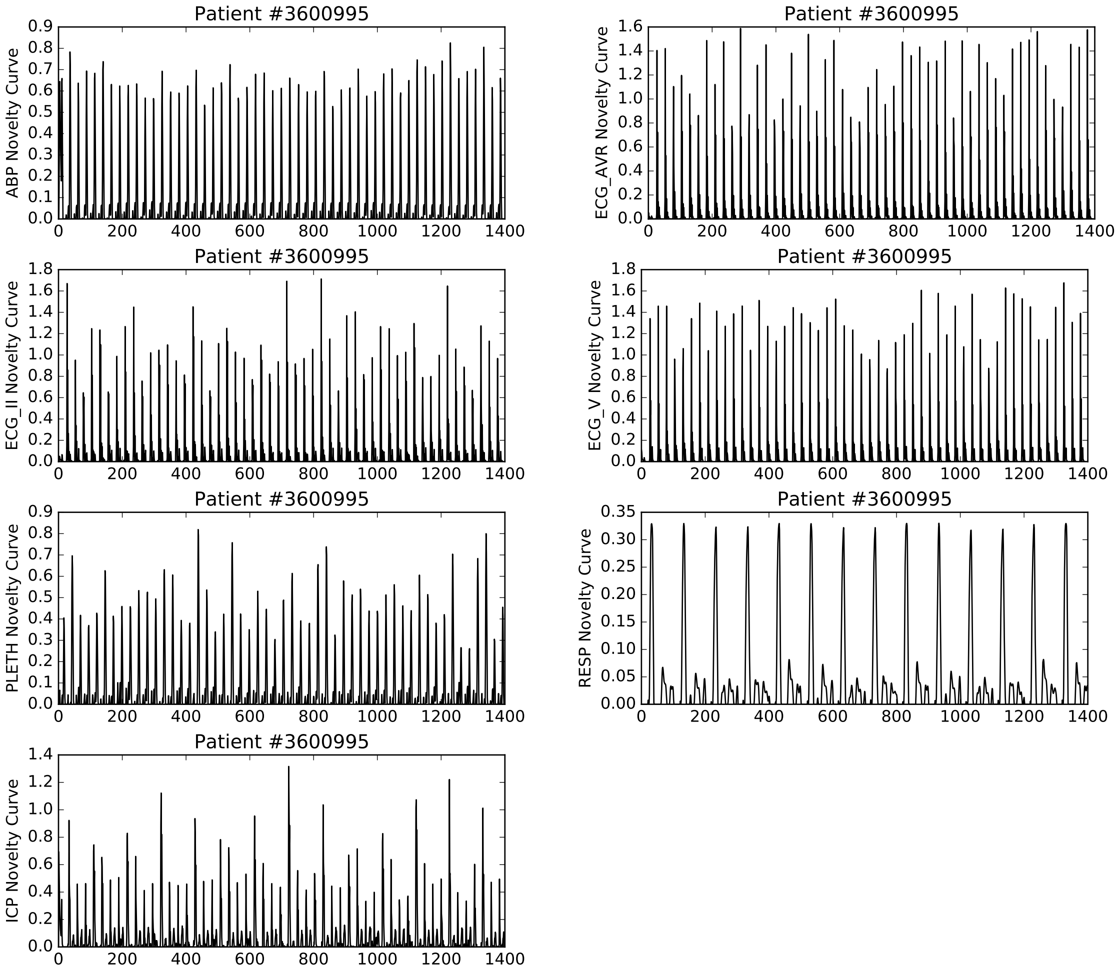

Figure A.23: Novelty curves of subject 3600995

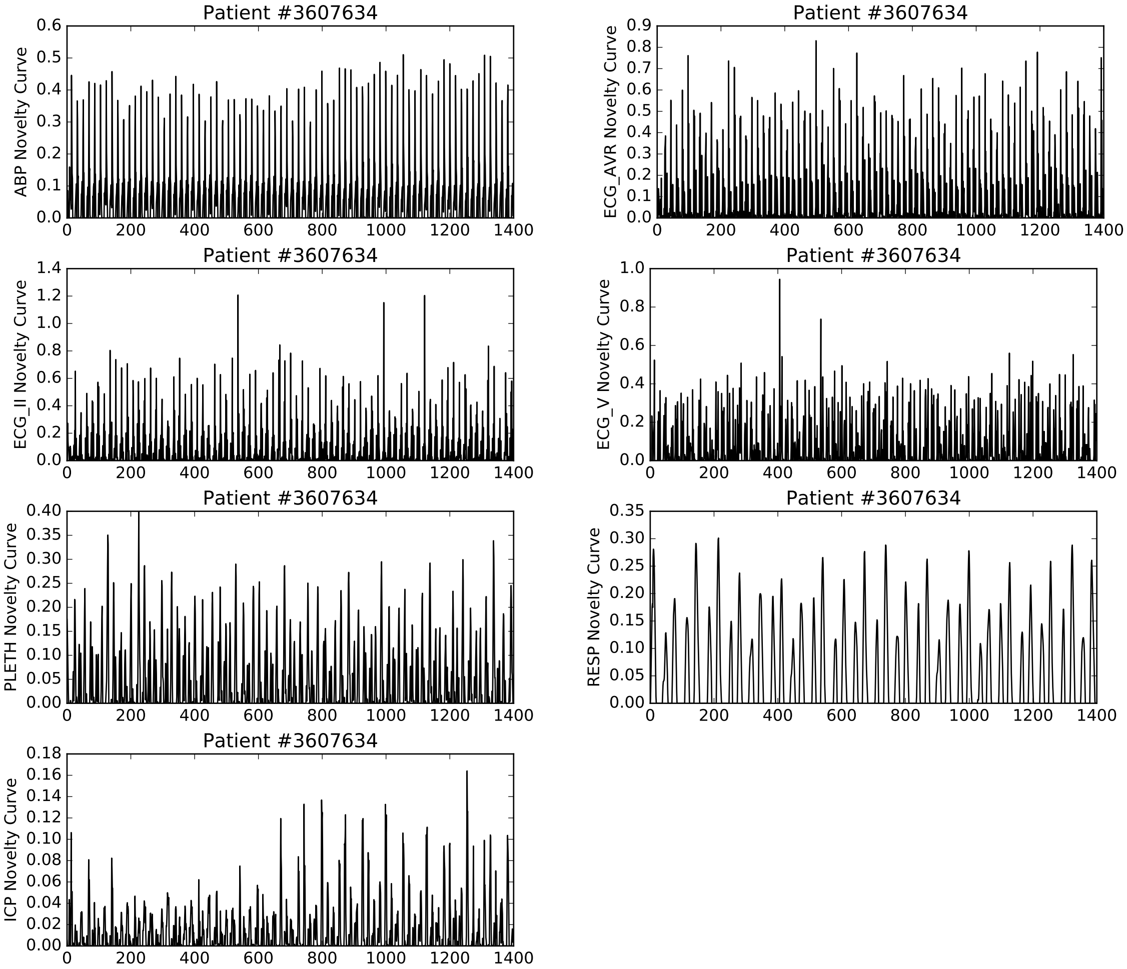

Figure A.24: Novelty curves of subject 3607634

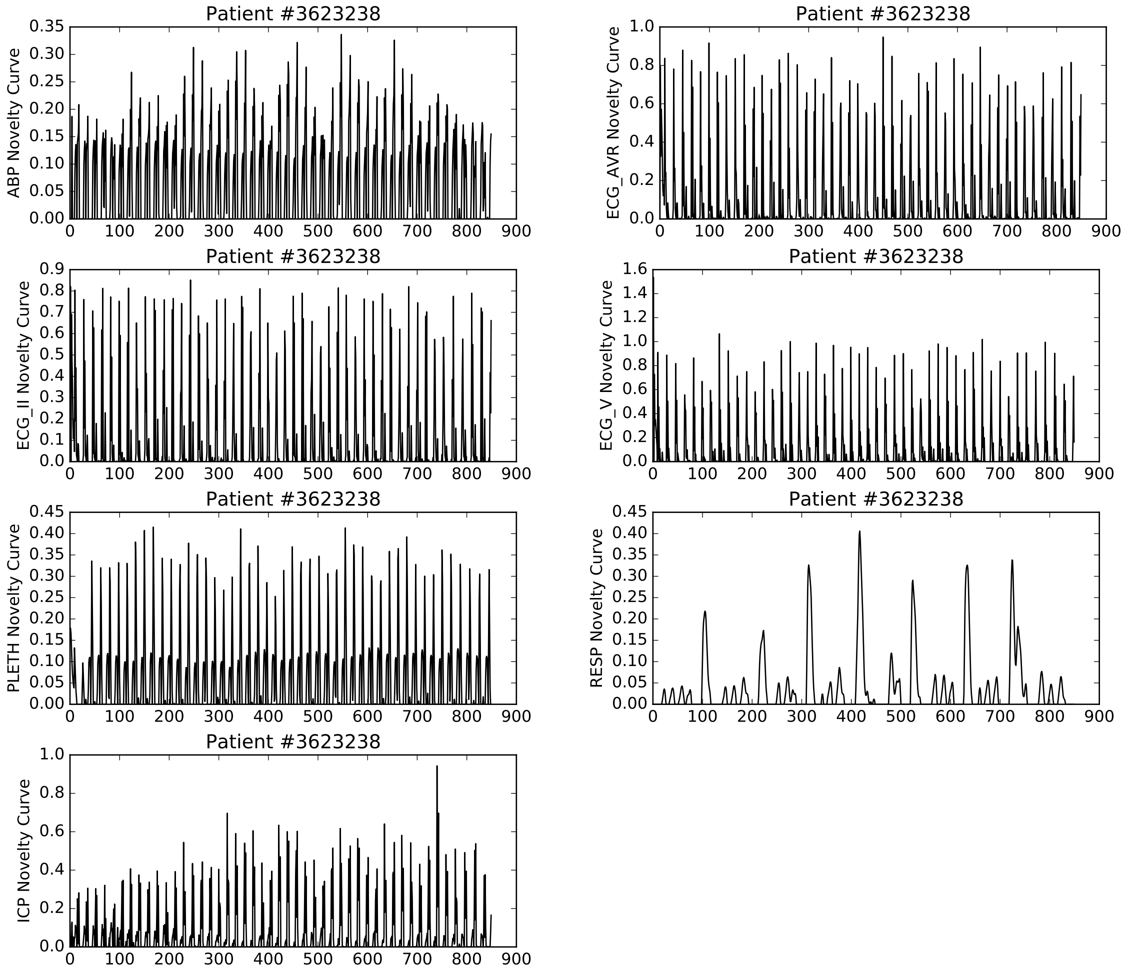

Patient #3623238

Patient #3623238

Patient #3623238

Patient #3623238

Patient #3623238

Patient #3623238

Patient #3623238

Figure A.25: Novelty curves of subject 3623238

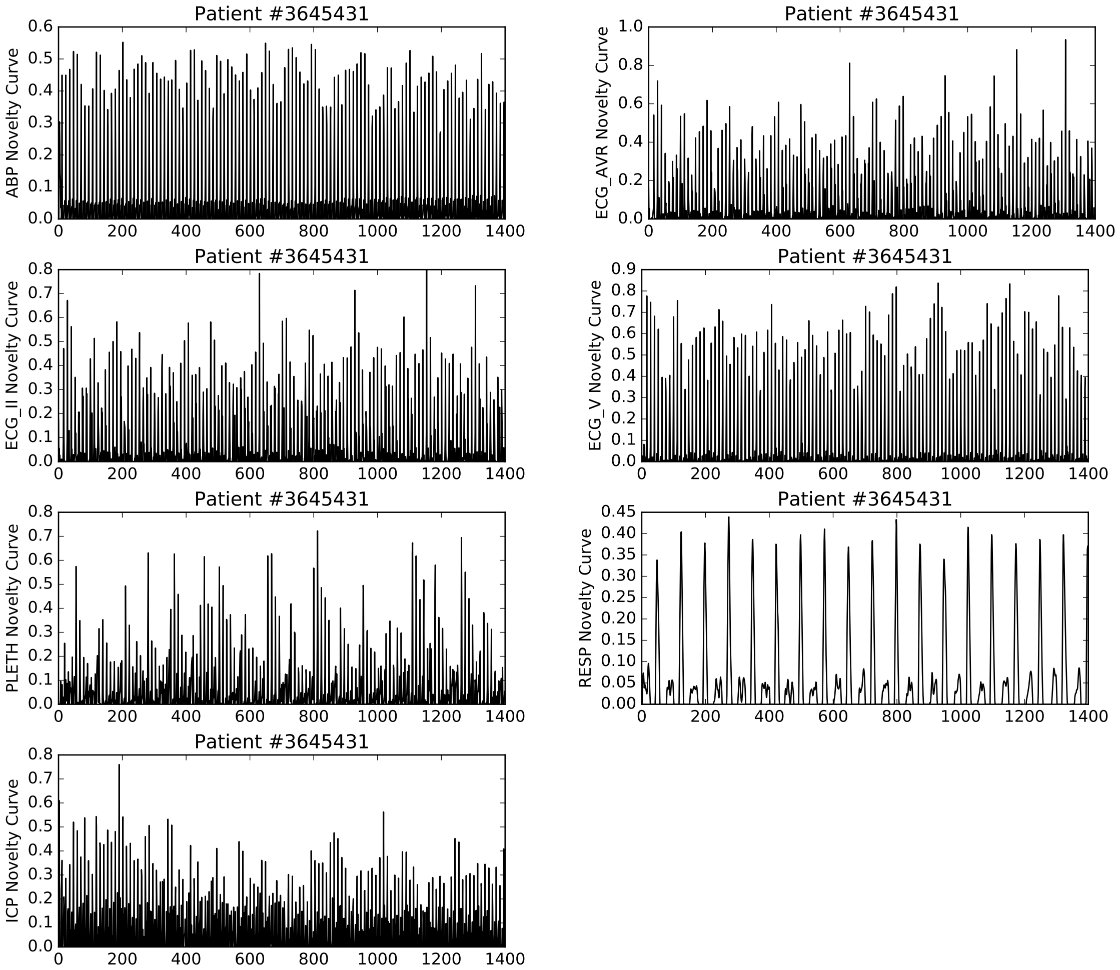

Figure A.26: Novelty curves of subject 3645431

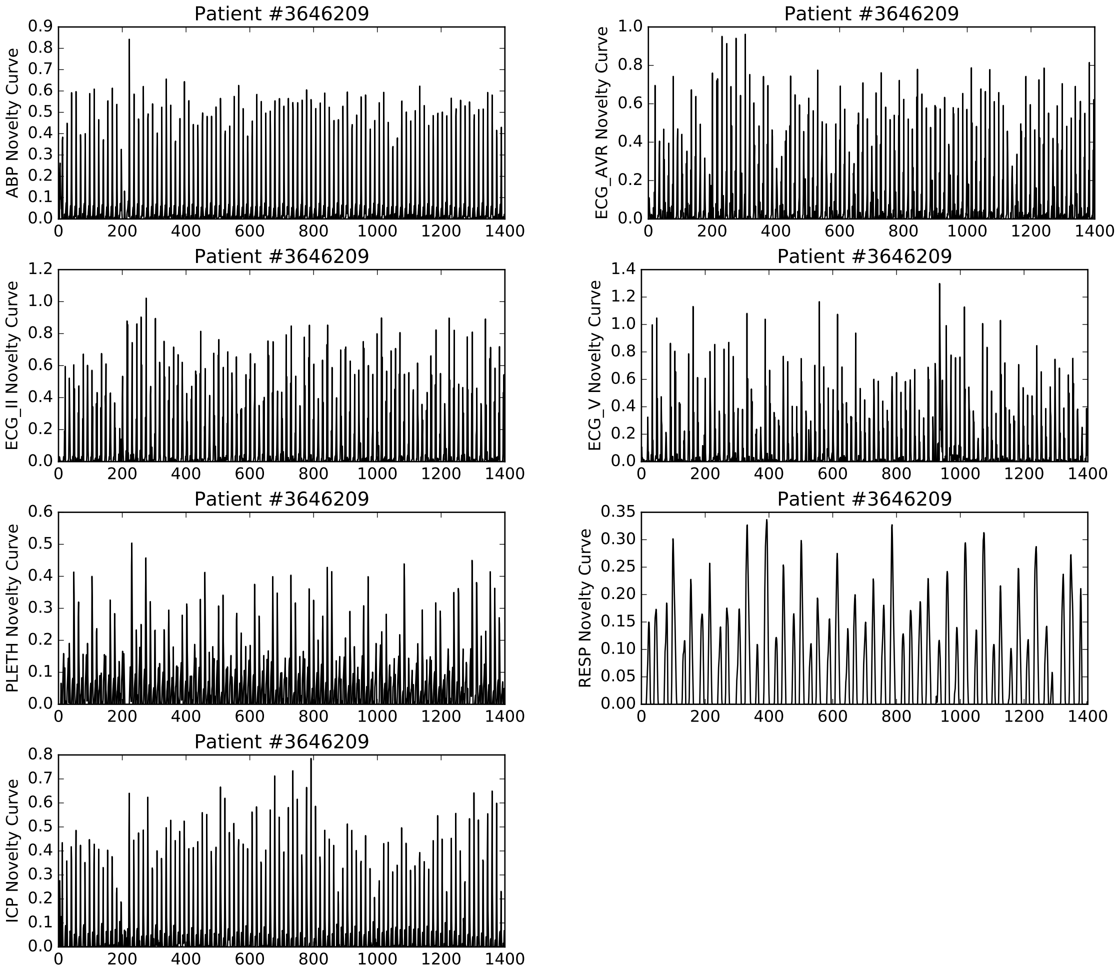

Figure A.27: Novelty curves of subject 3646209

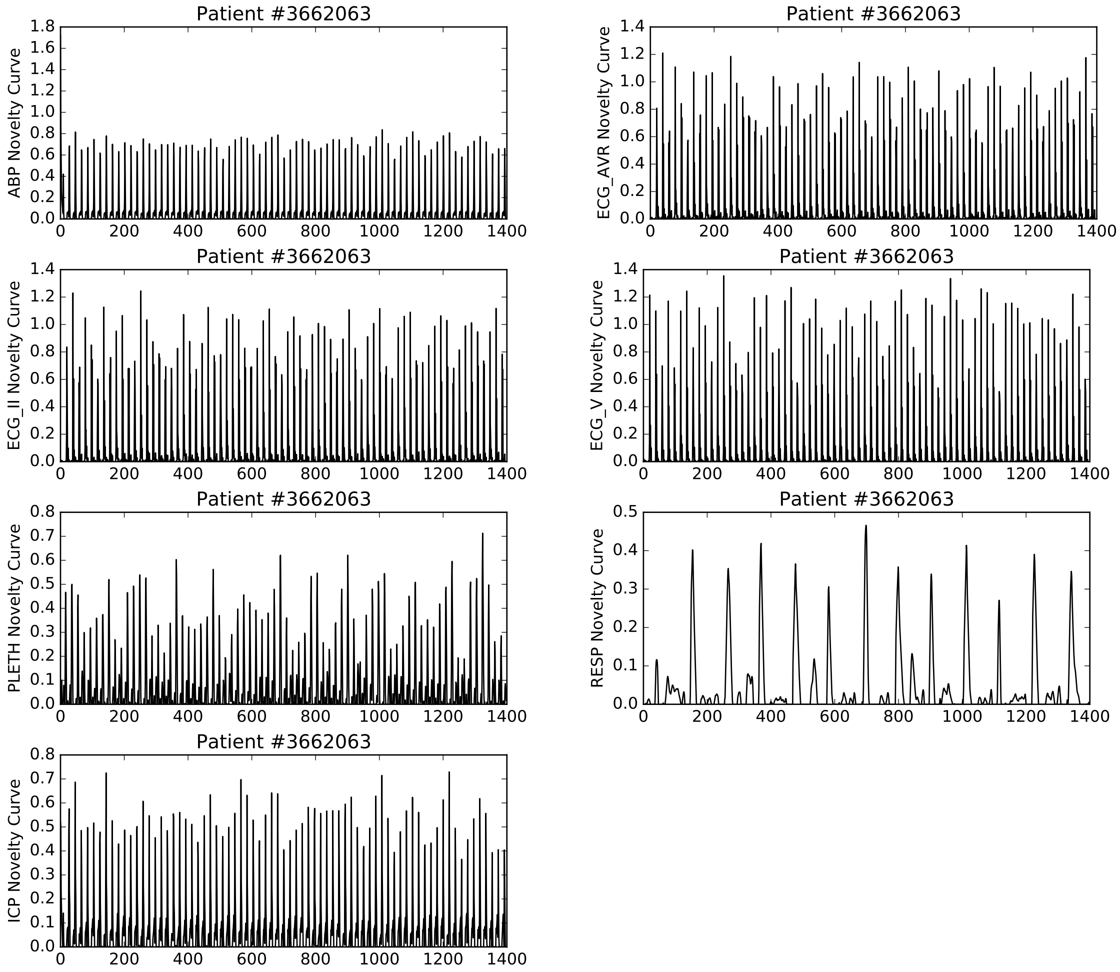

Figure A.28: Novelty curves of subject 3662063

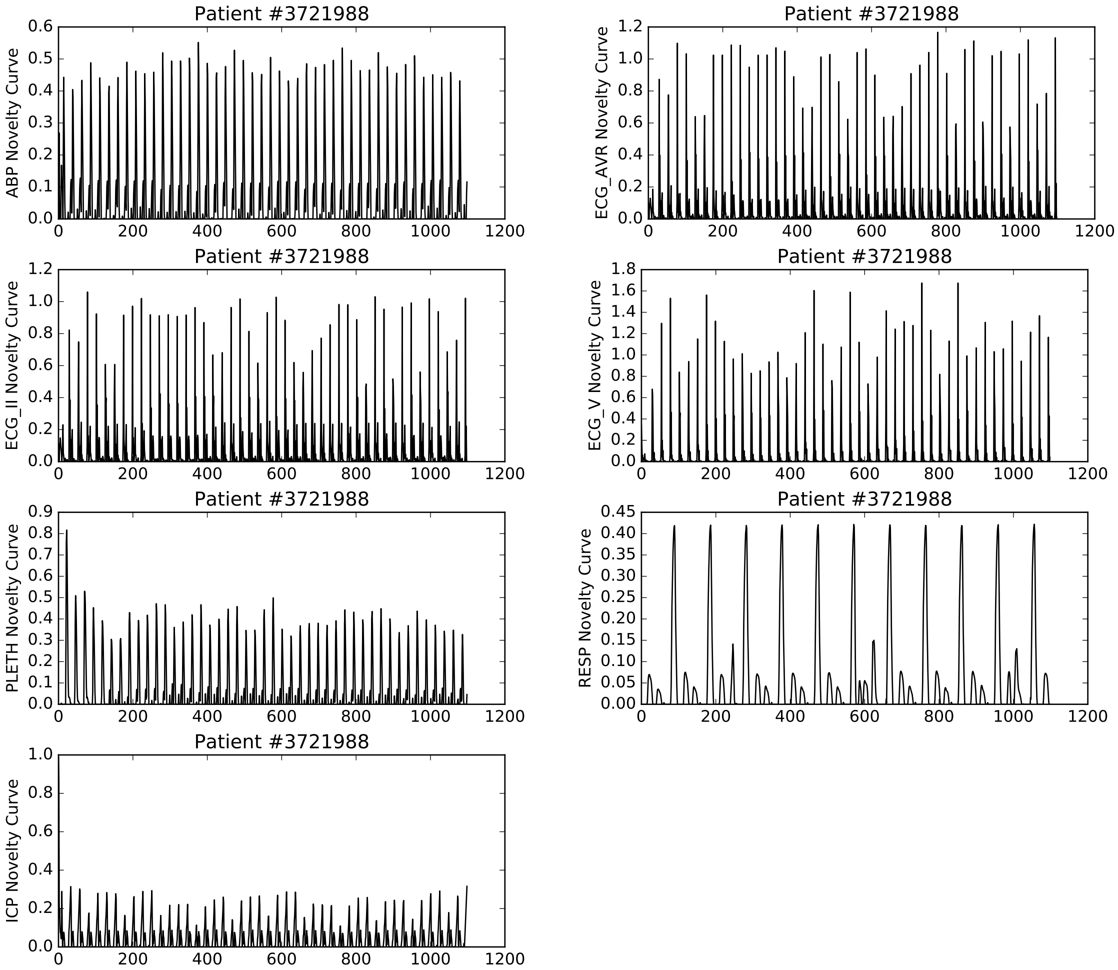

Figure A.29: Novelty curves of subject 3721988

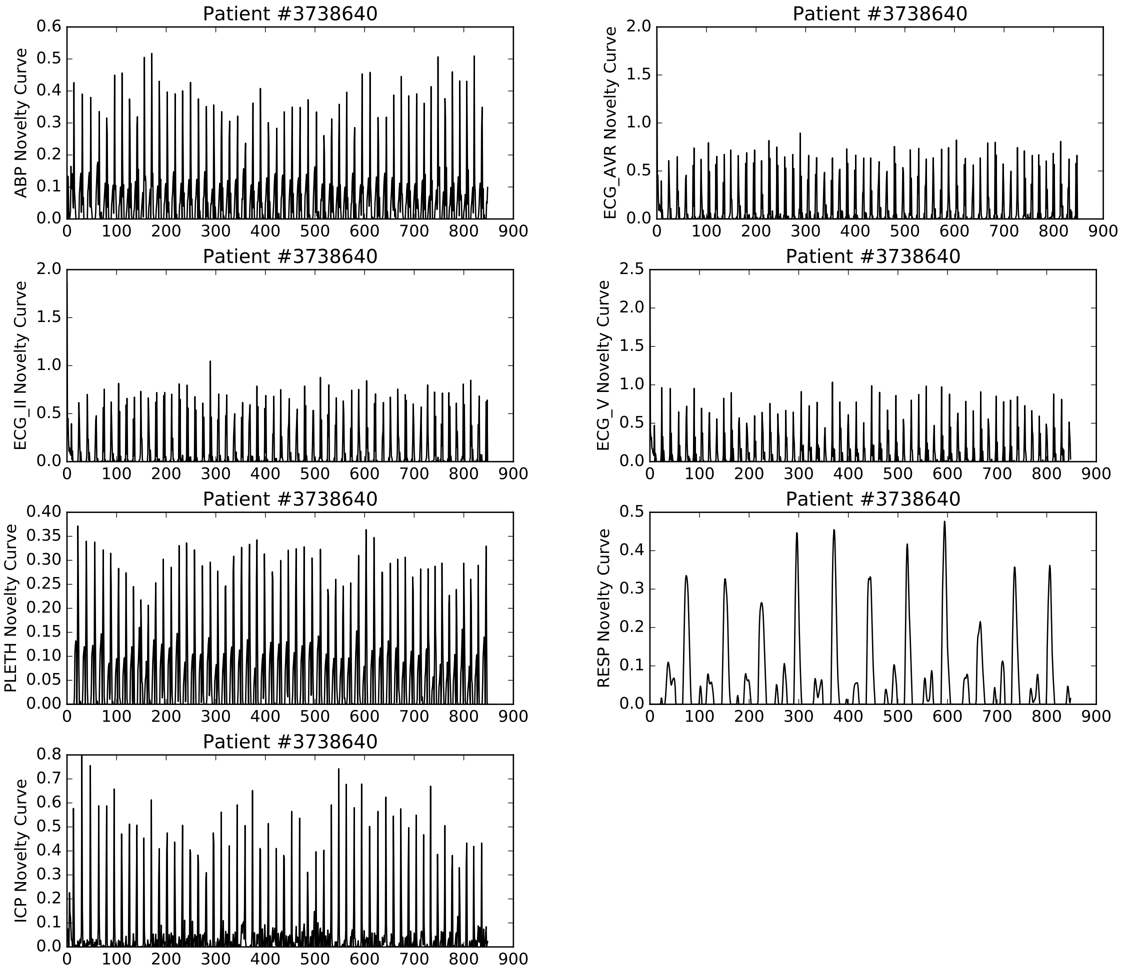

Figure A.30: Novelty curves of subject 3738640

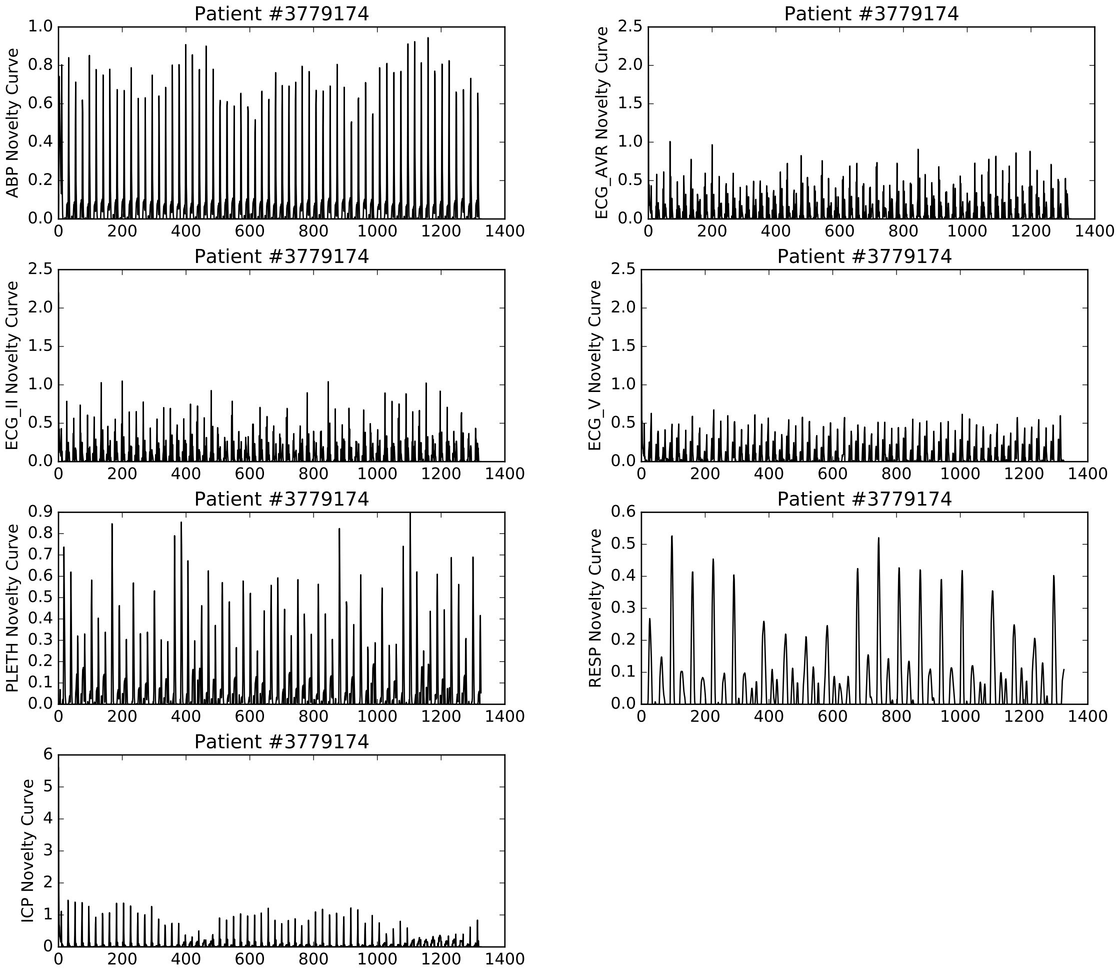

Figure A.31: Novelty curves of subject 3779174

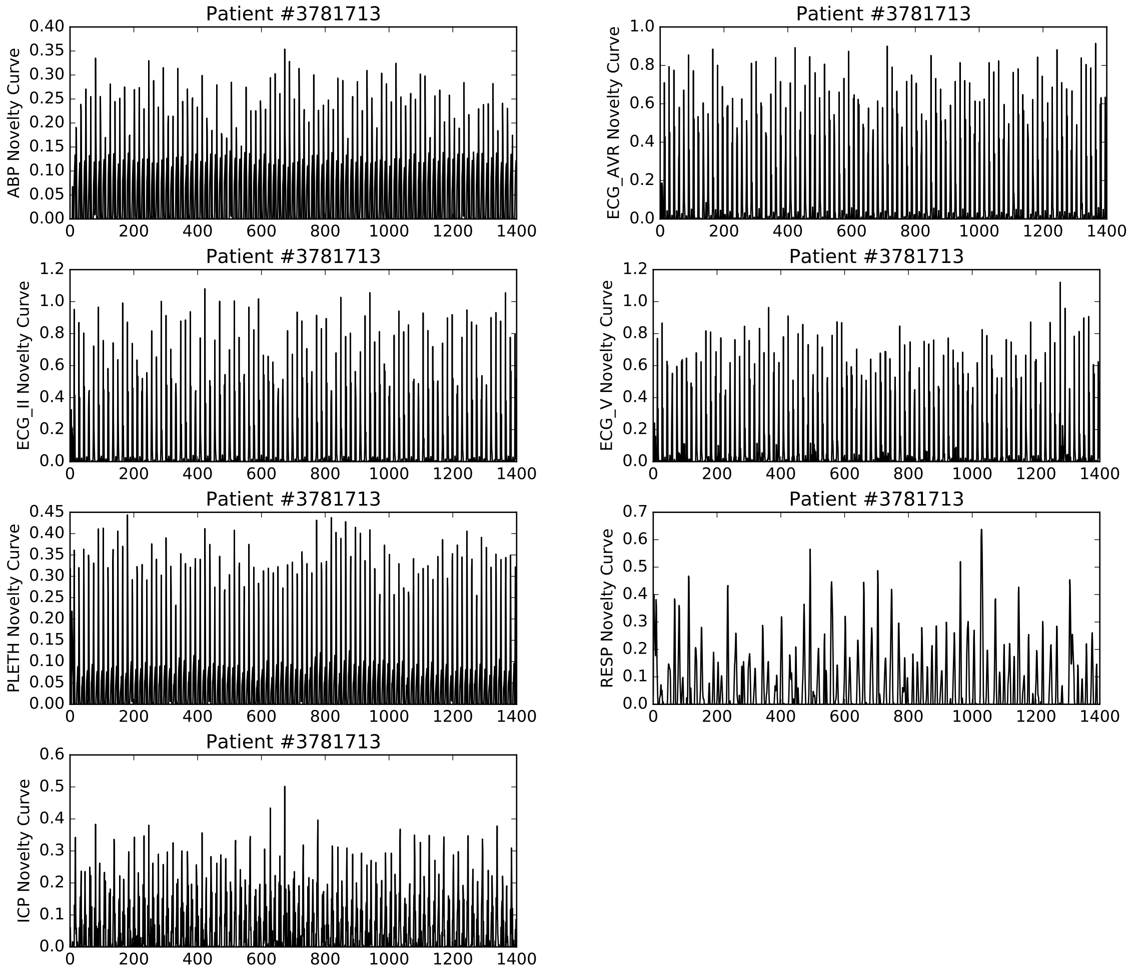

Figure A.32: Novelty curves of subject 3781713

A.3 Distance and RP Matrices of All Patients

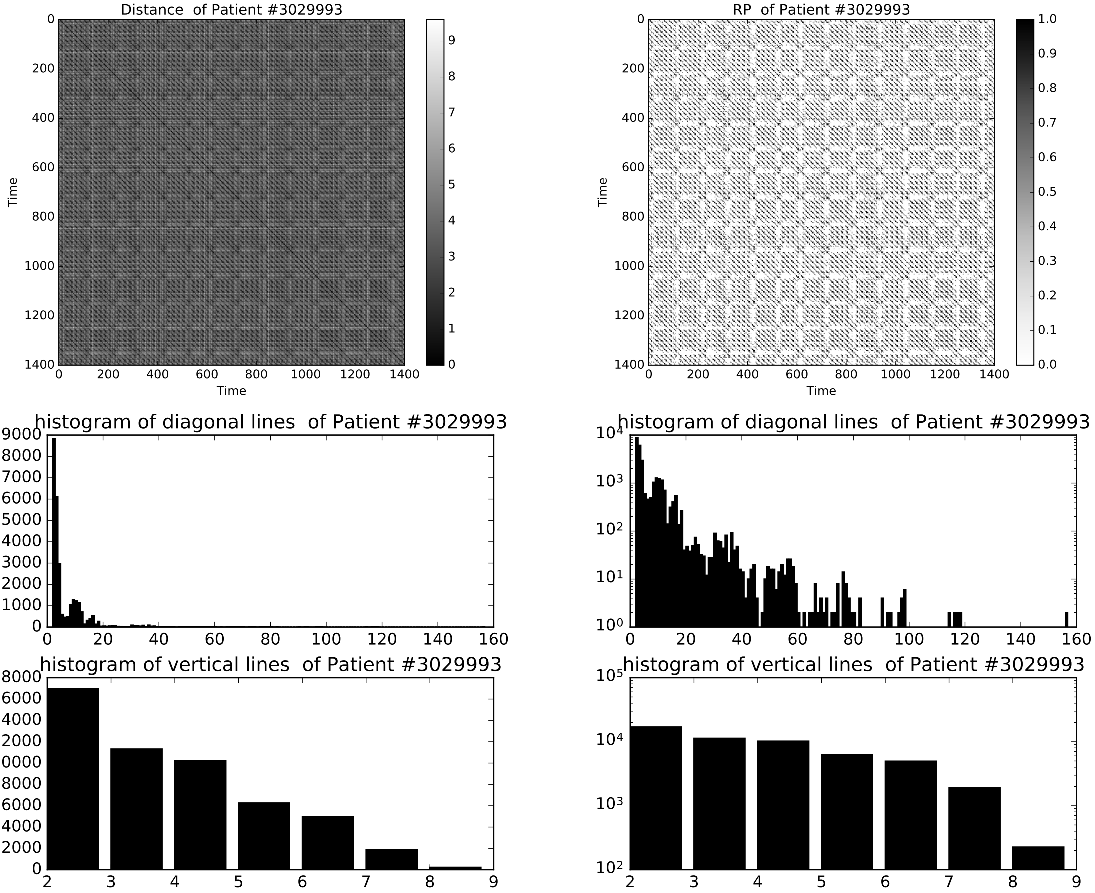

Figure A.33: RQA results of subject 3029993

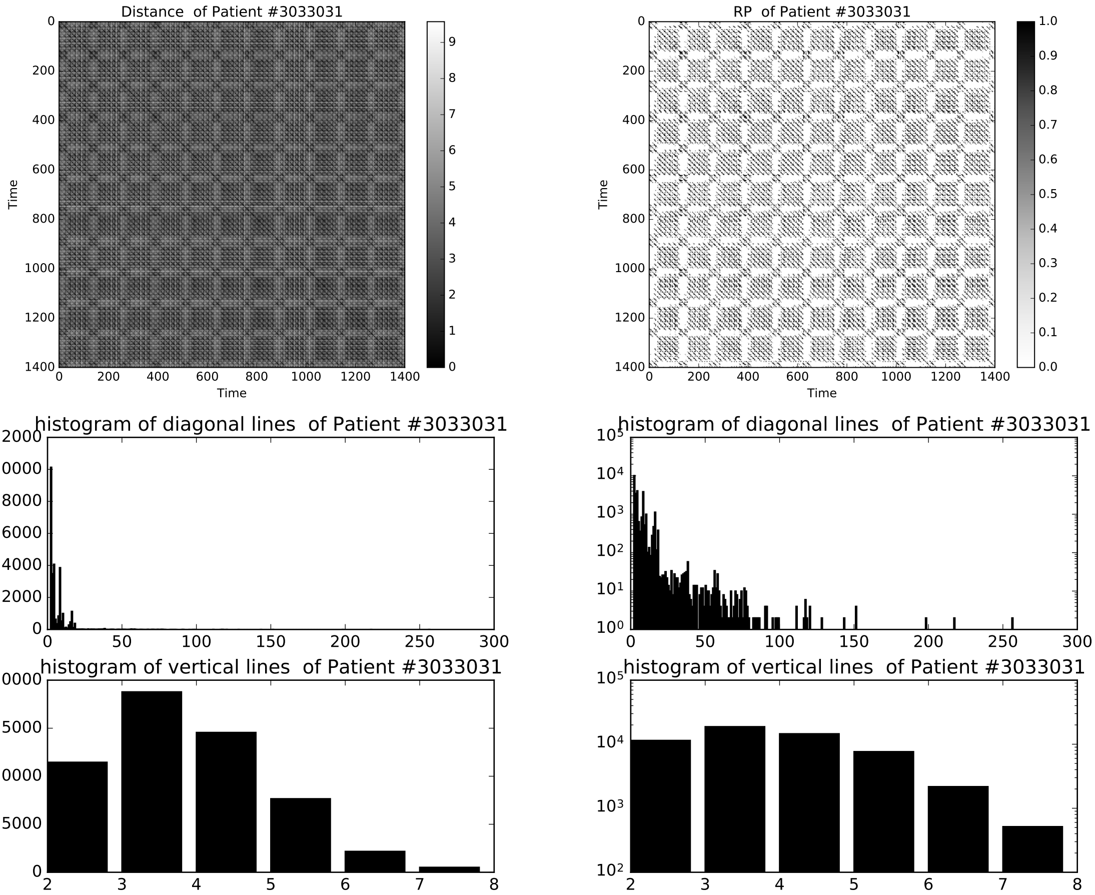

Figure A.34: RQA results of subject 3033031

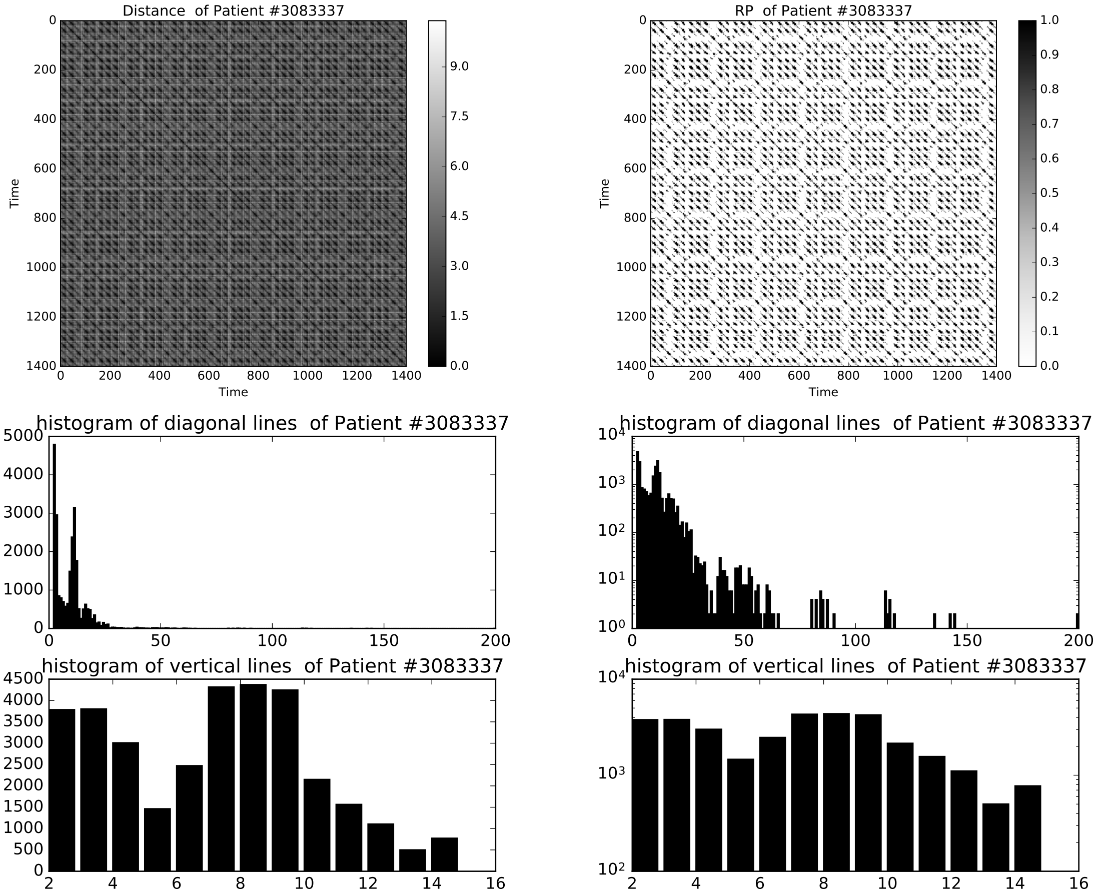

Figure A.35: RQA results of subject 3083337

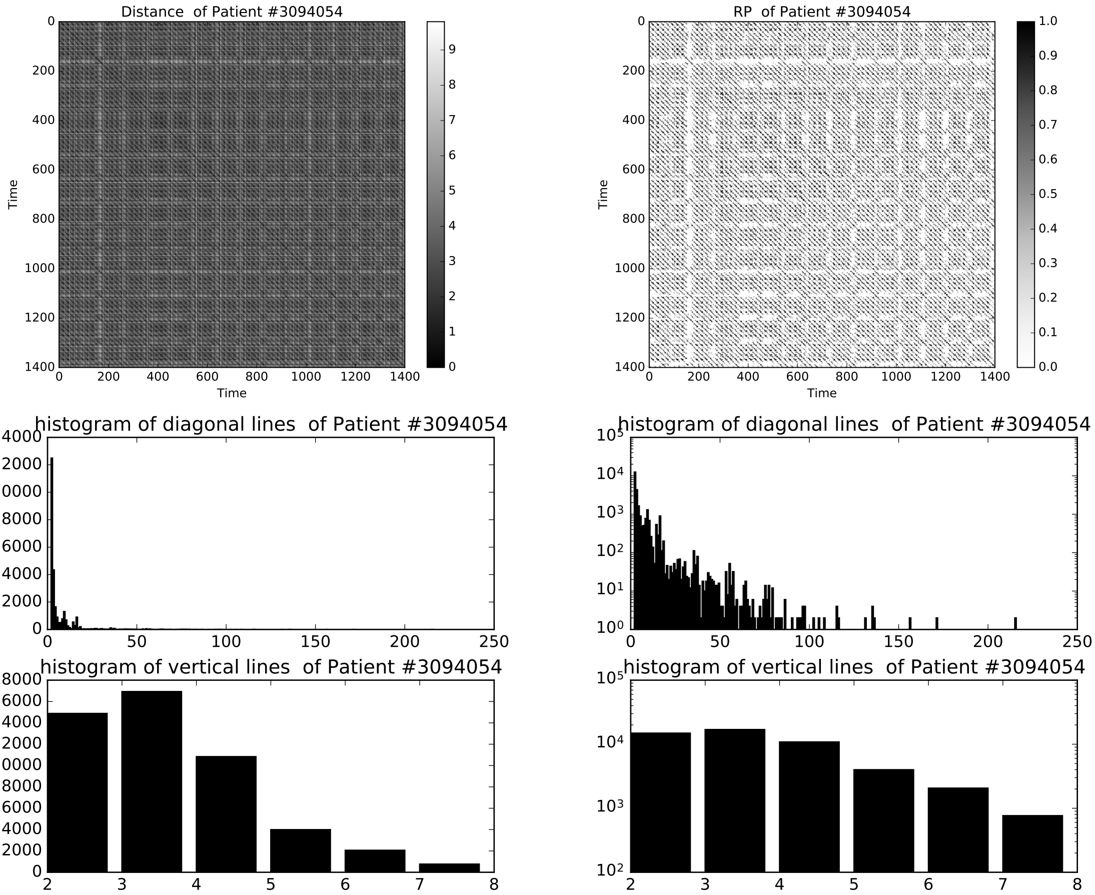

Figure A.36: RQA results of subject 3094054

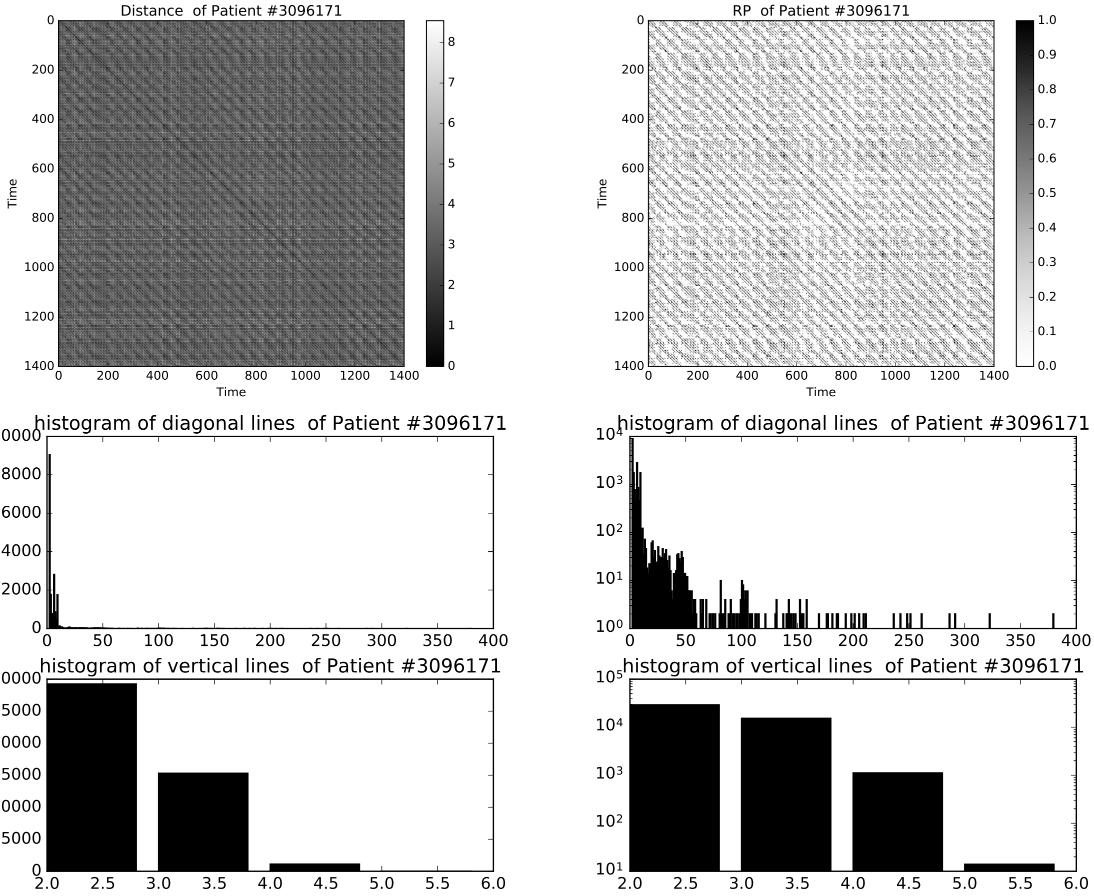

Figure A.37: RQA results of subject 3096171

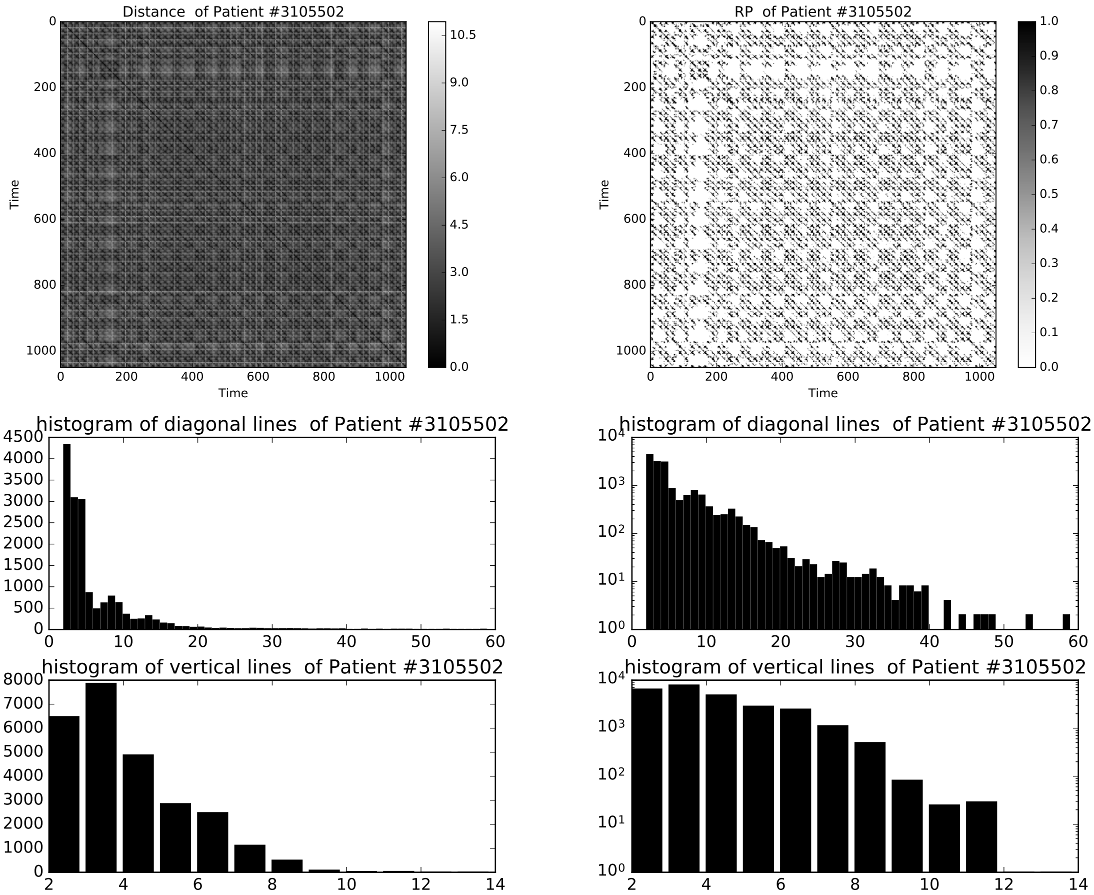

Figure A.38: RQA results of subject 3105502

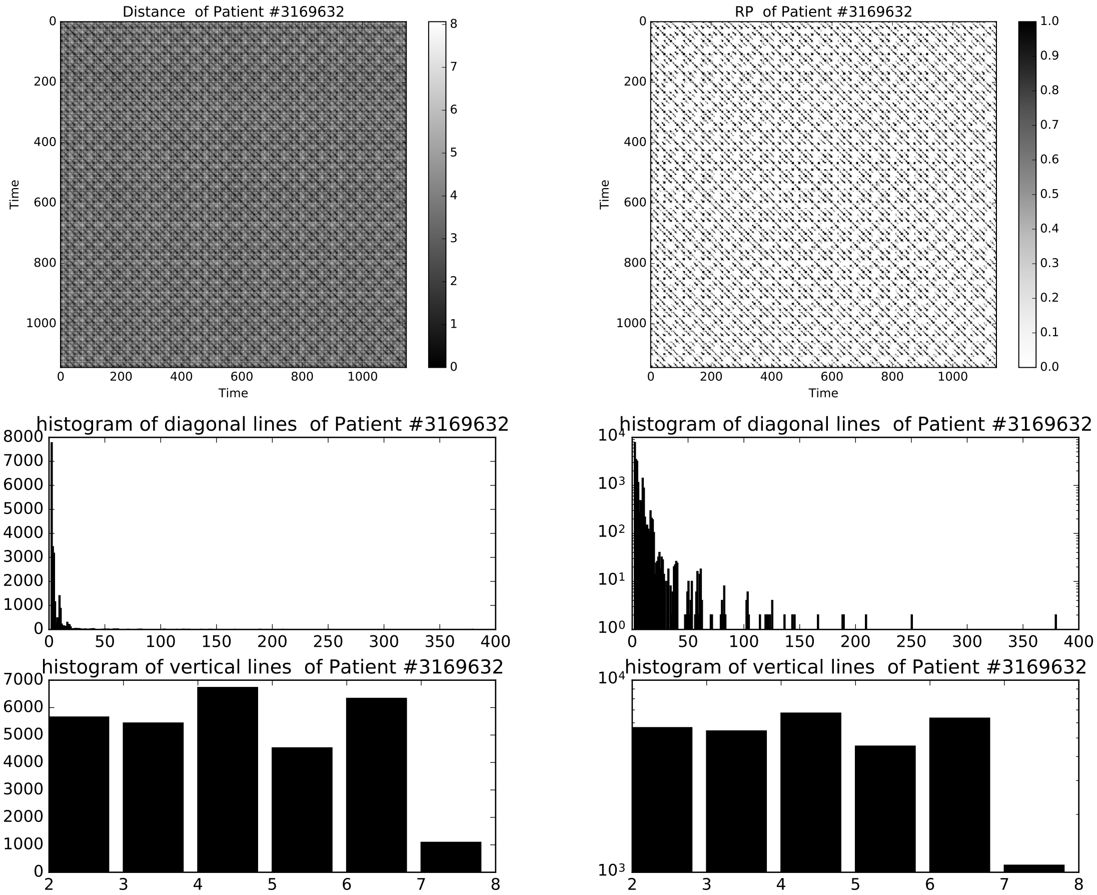

Figure A.39: RQA results of subject 3169632

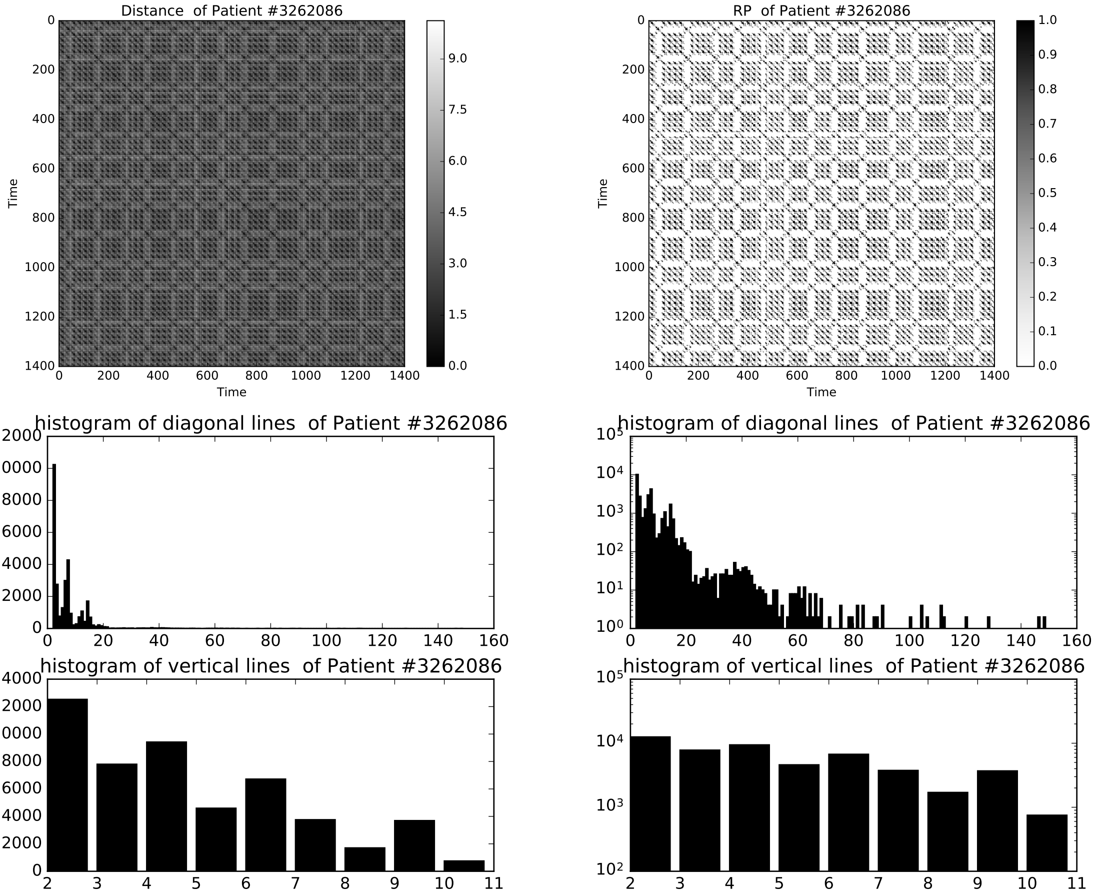

Figure A.40: RQA results of subject 3262086

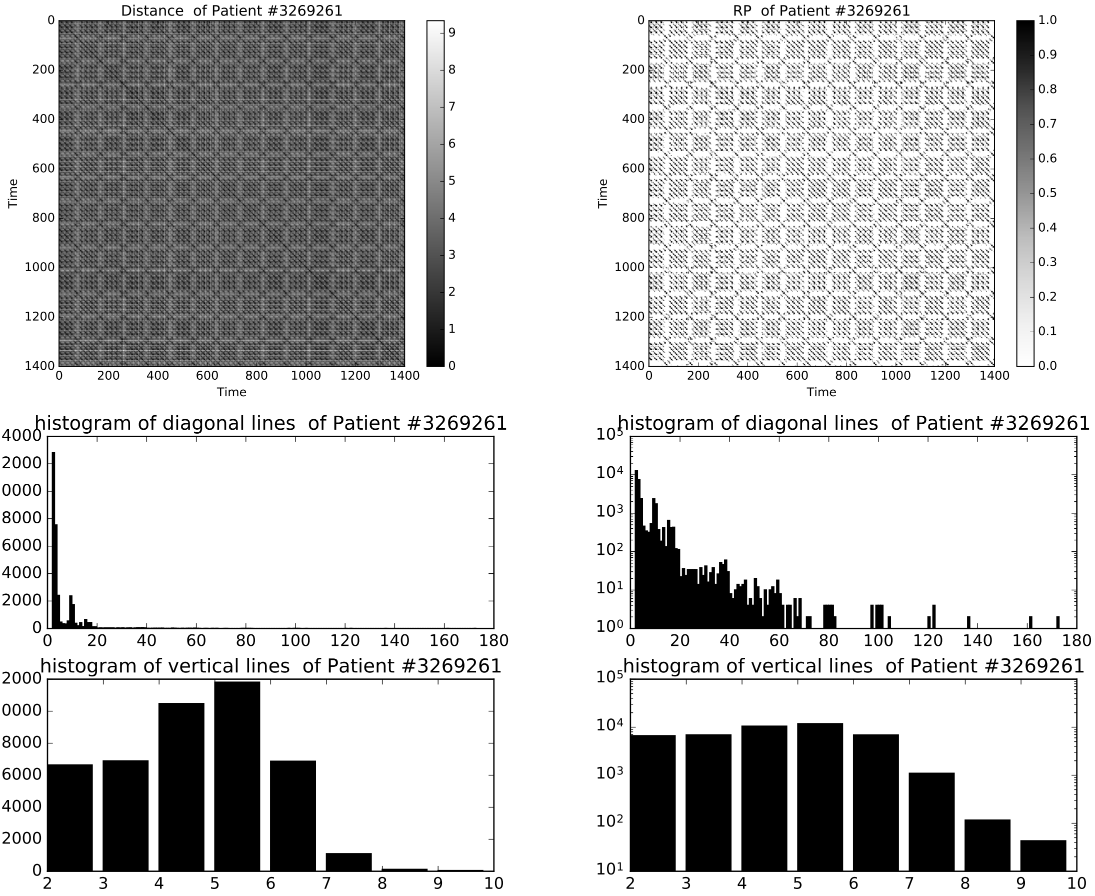

Figure A.41: RQA results of subject 3269261

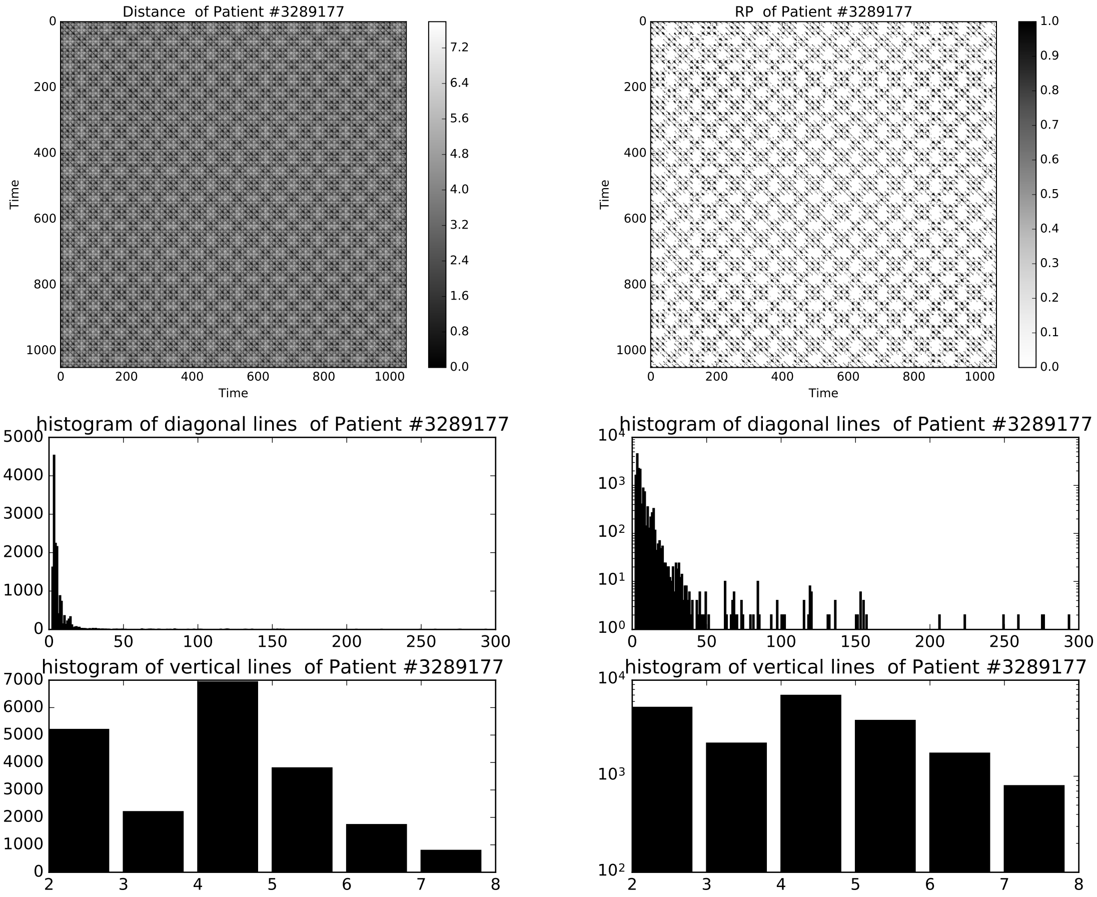

Figure A.42: RQA results of subject 3289177

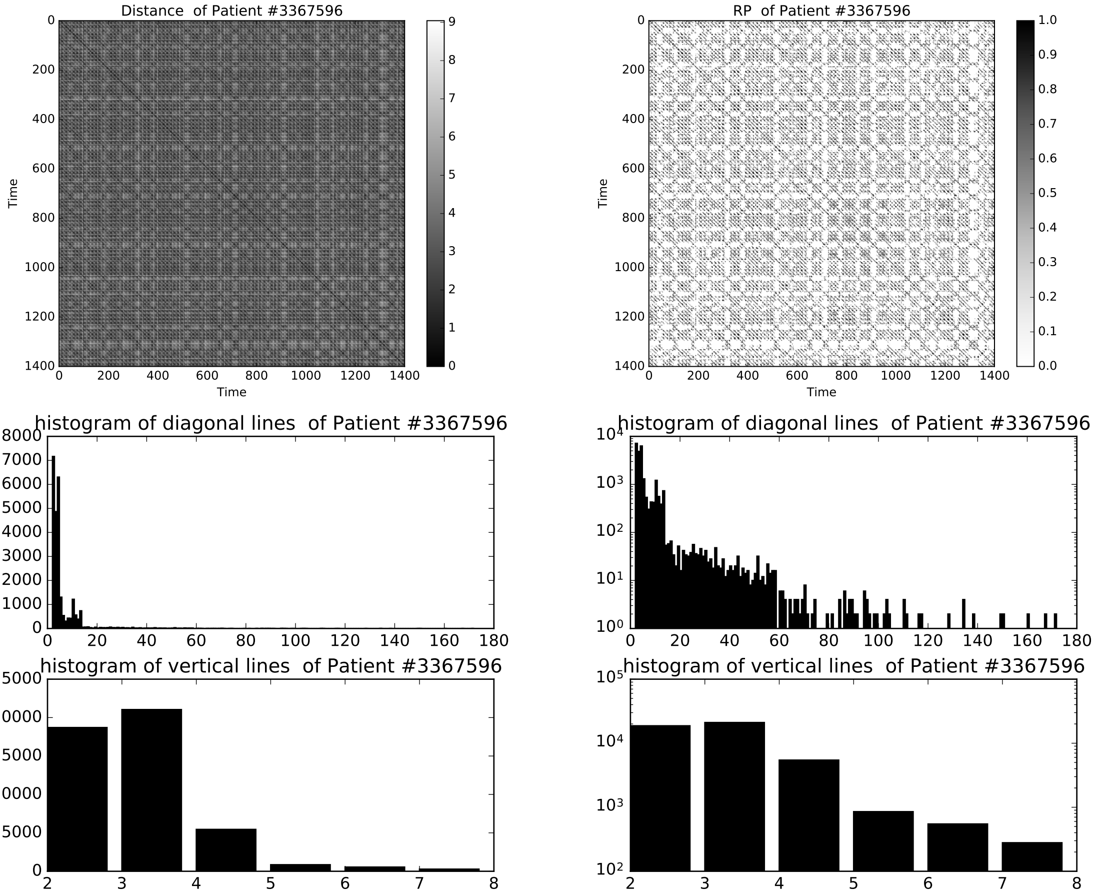

Figure A.43: RQA results of subject 3367596

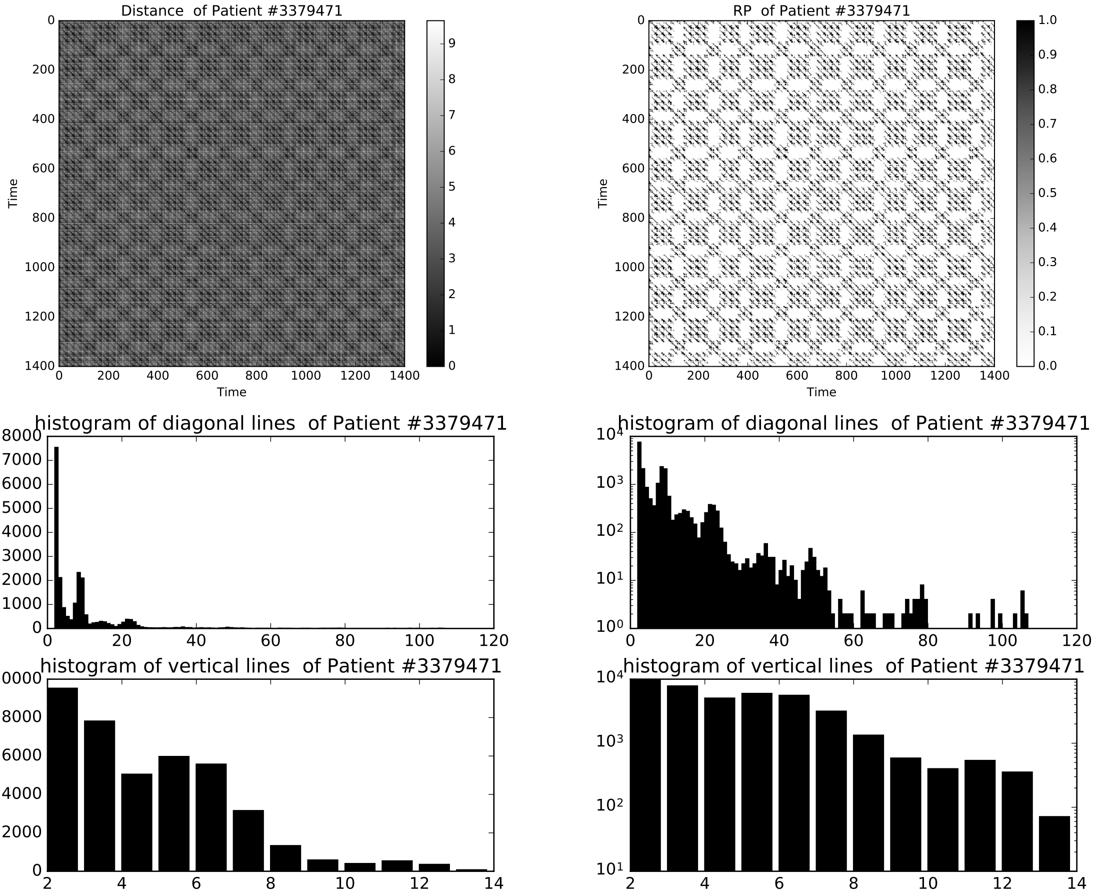

Figure A.44: RQA results of subject 3379471

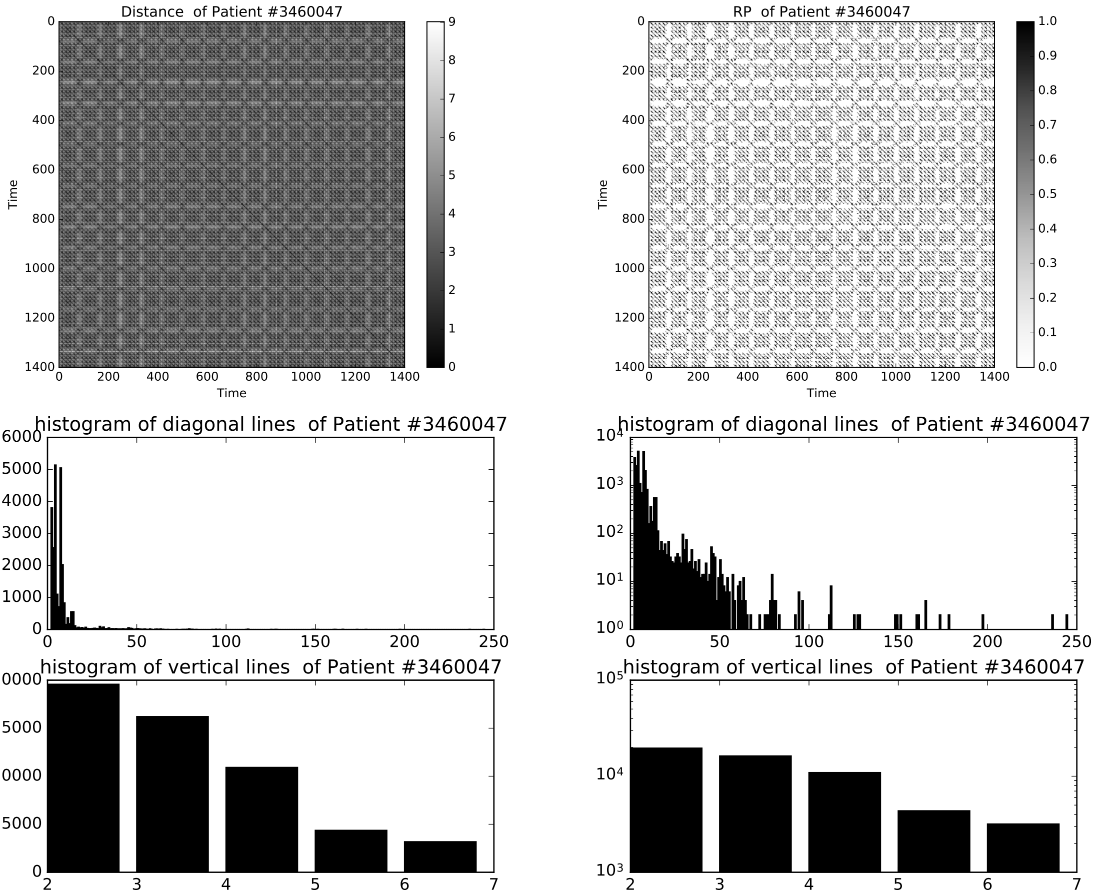

Figure A.45: RQA results of subject 3460047

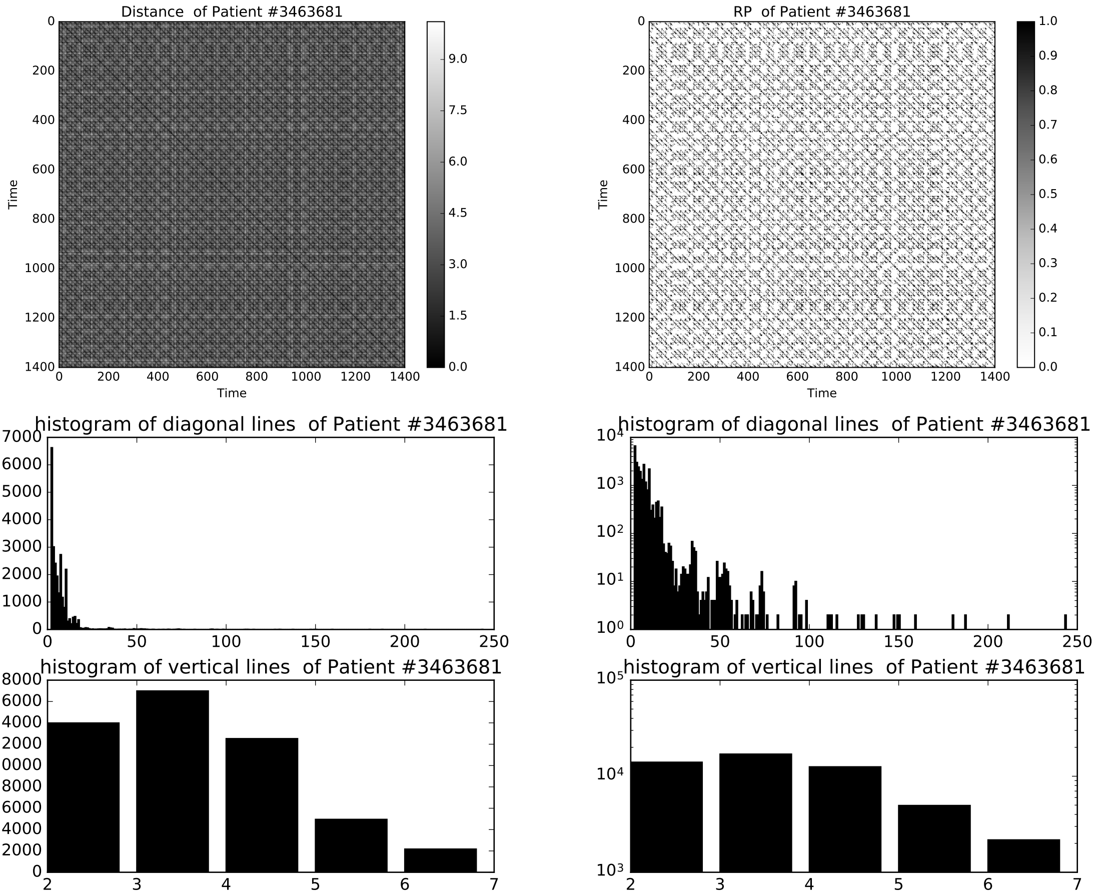

Figure A.46: RQA results of subject 3463681

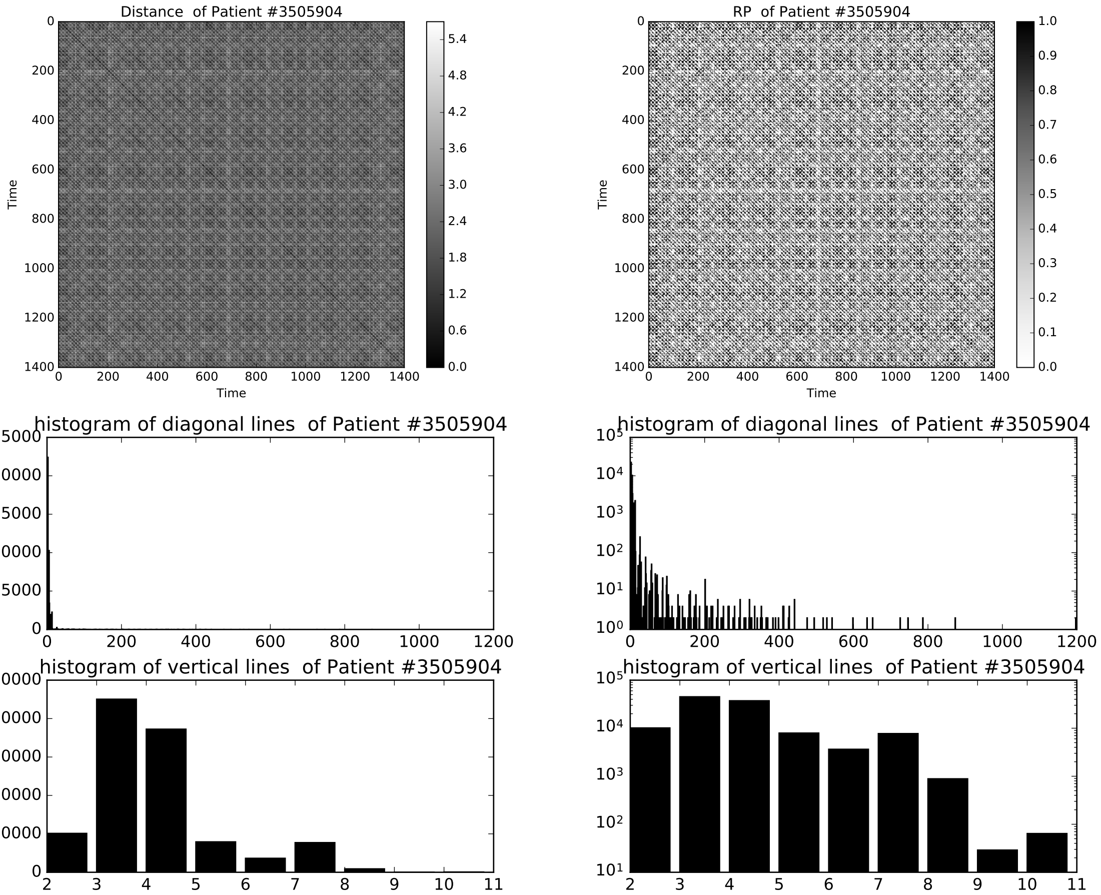

Figure A.47: RQA results of subject 3505904

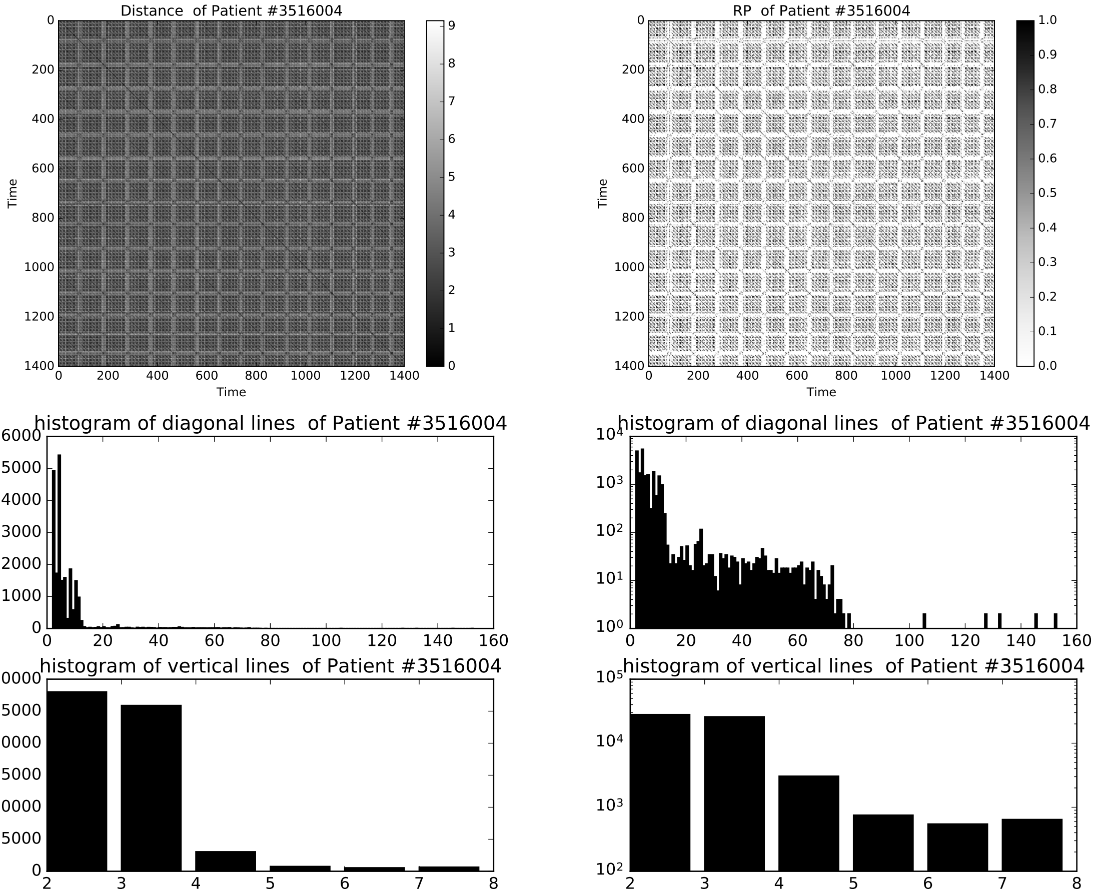

Figure A.48: RQA results of subject 3516004

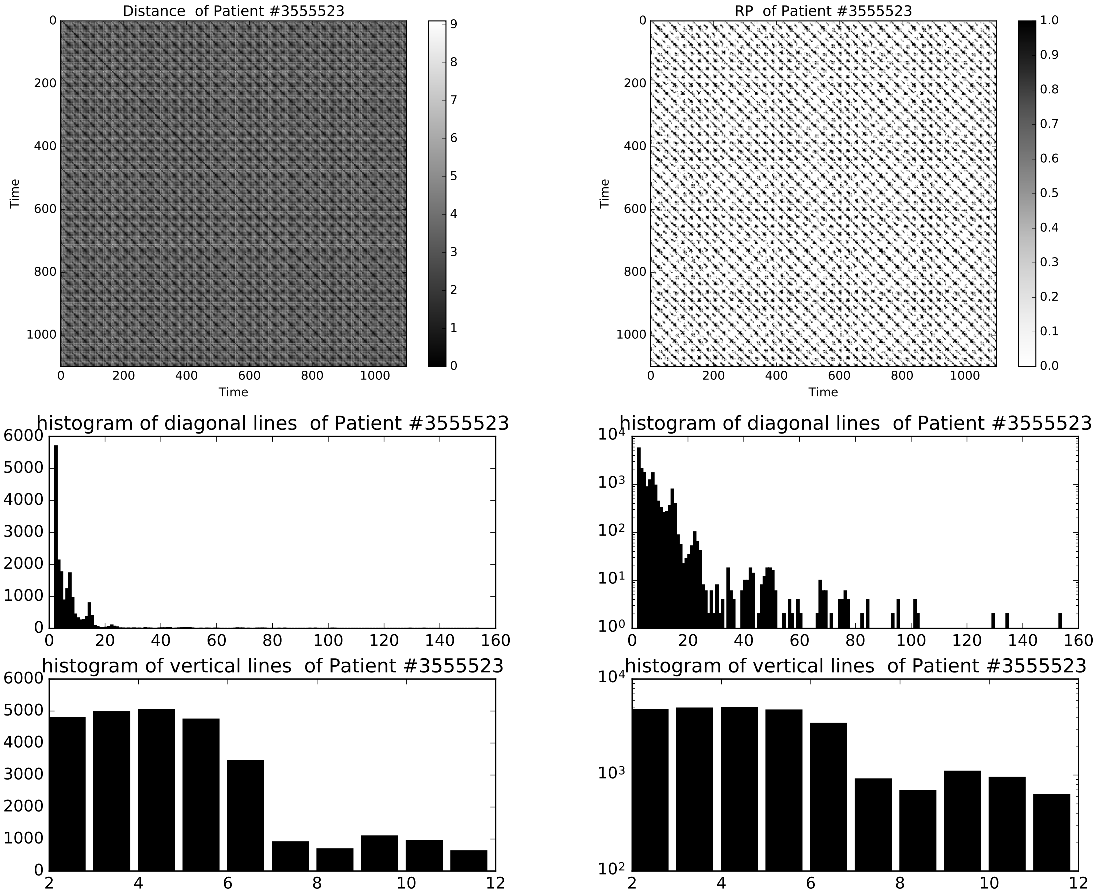

Figure A.49: RQA results of subject 3555523

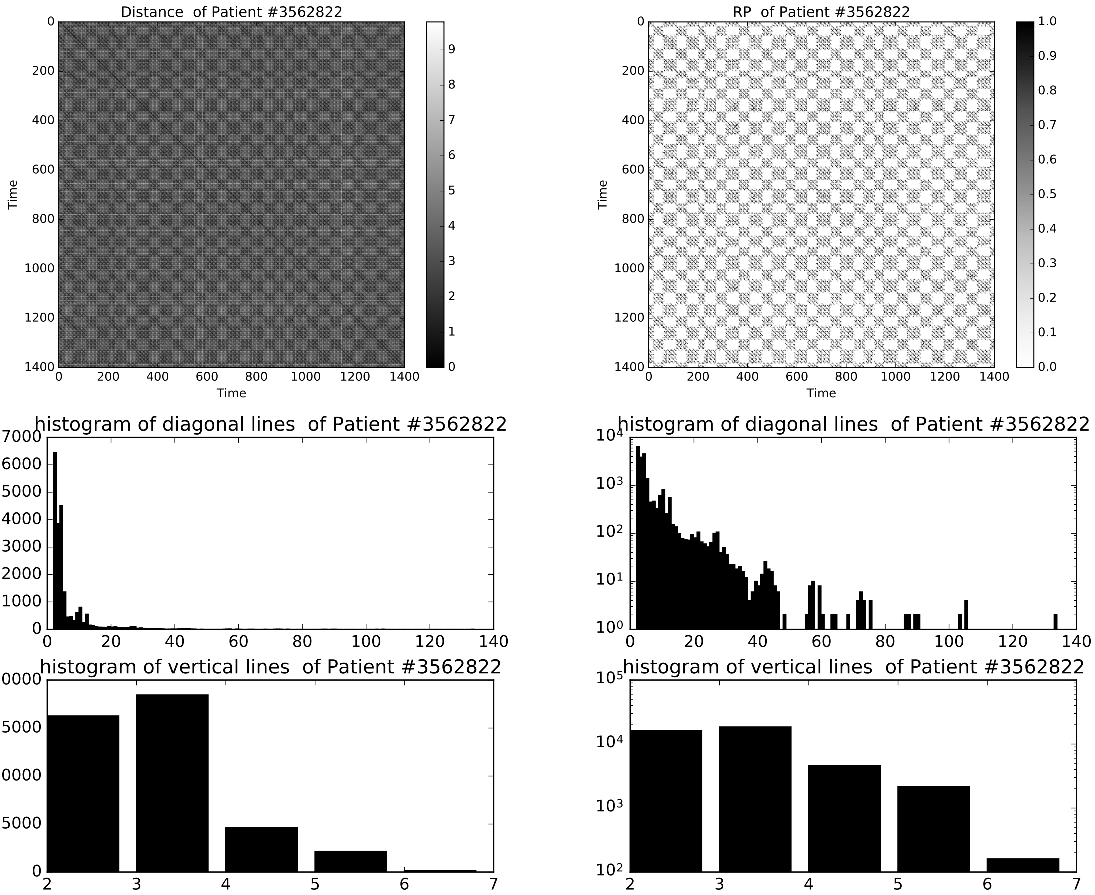

Figure A.50: RQA results of subject 3562822

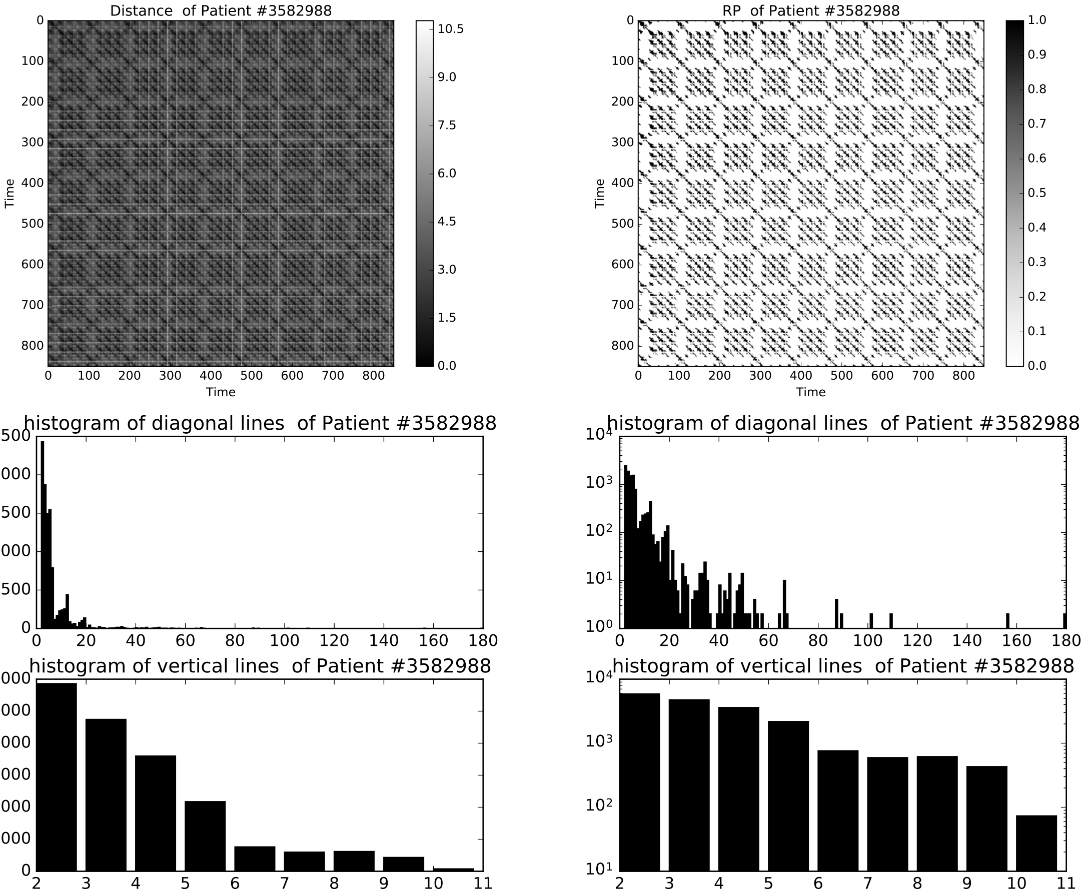

Figure A.51: RQA results of subject 3582988

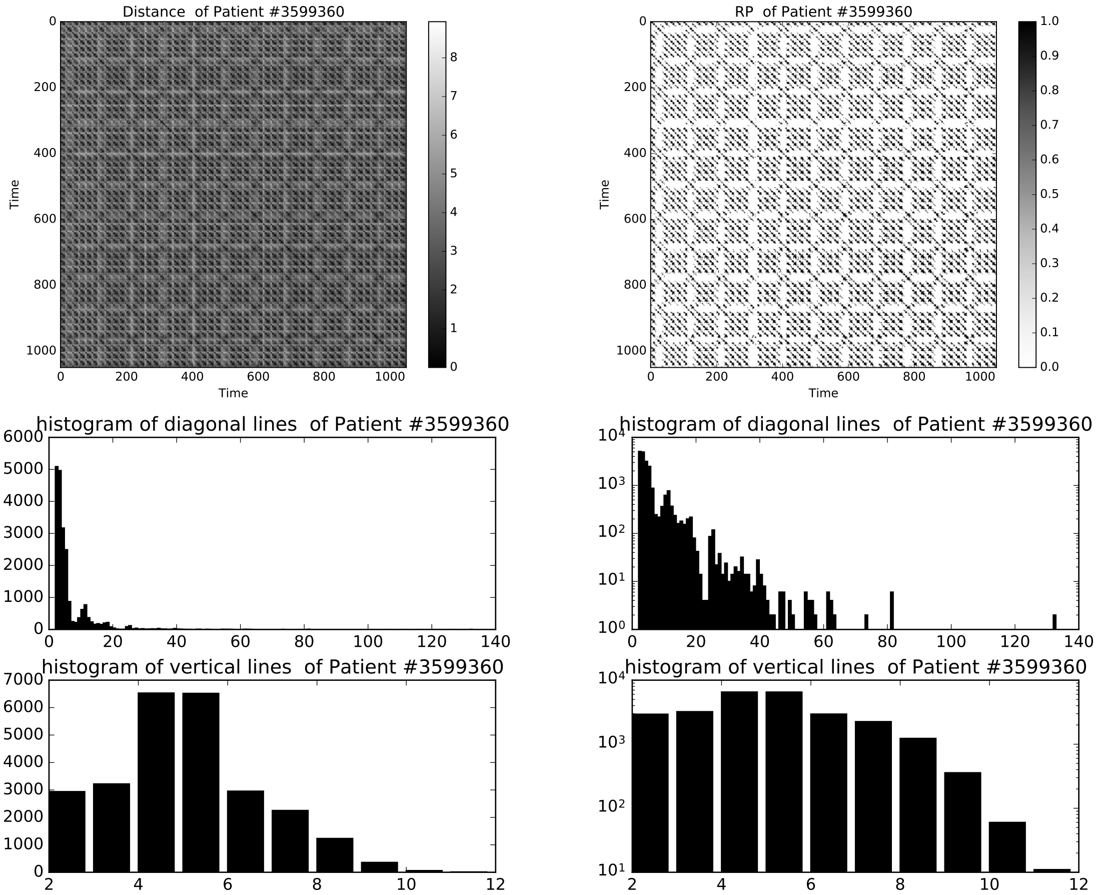

Figure A.52: RQA results of subject 3599360

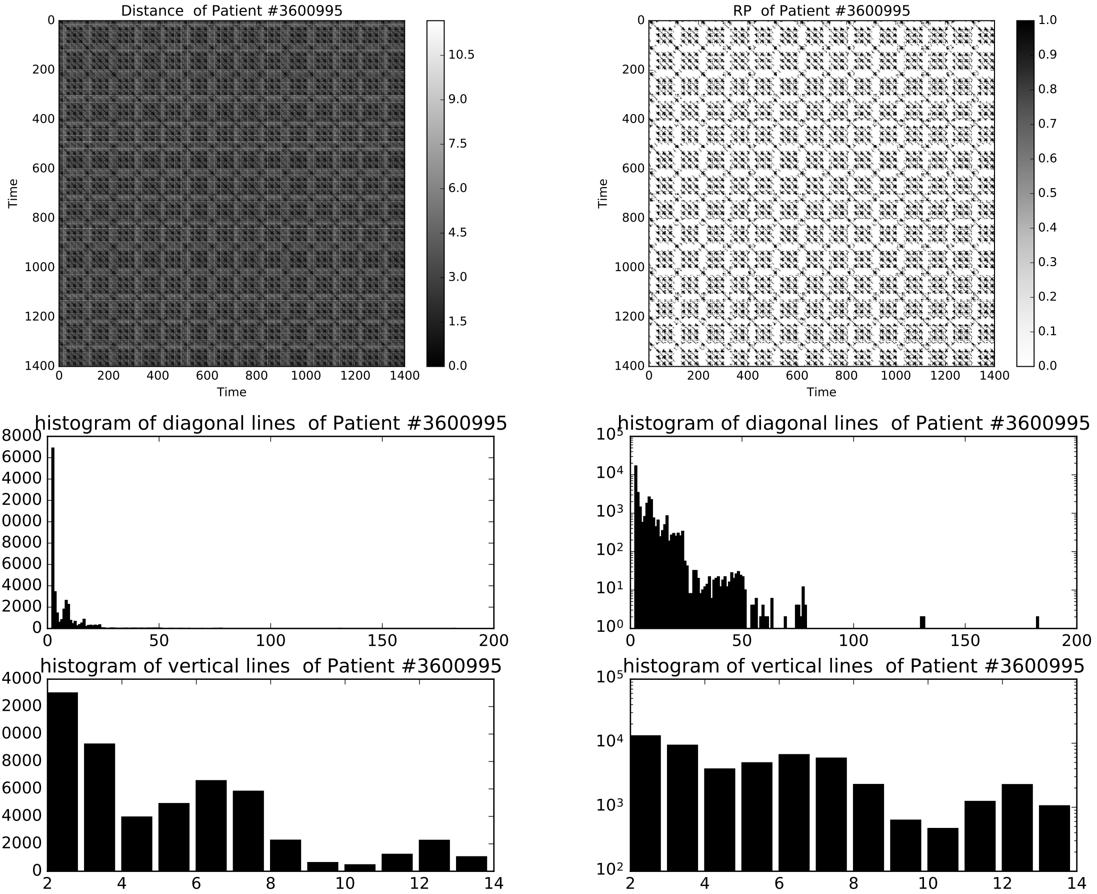

Figure A.53: RQA results of subject 3600995

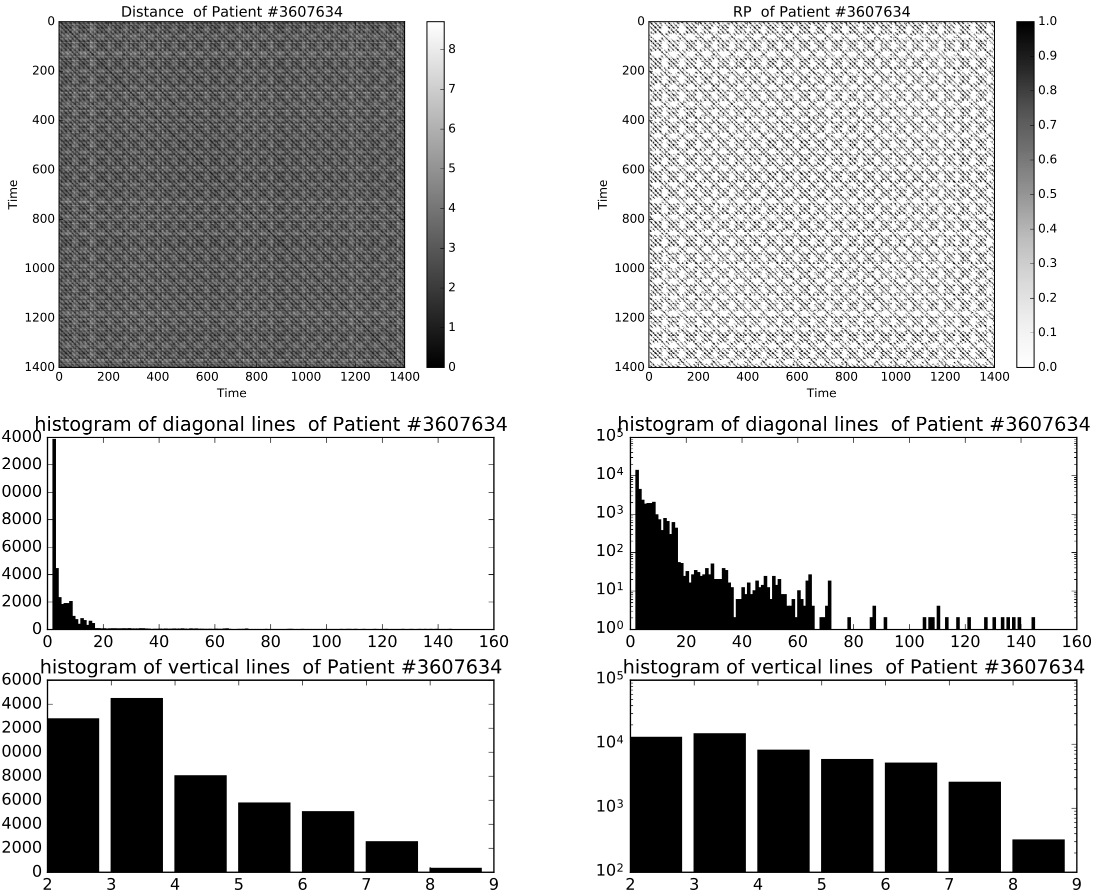

Figure A.54: RQA results of subject 3607634

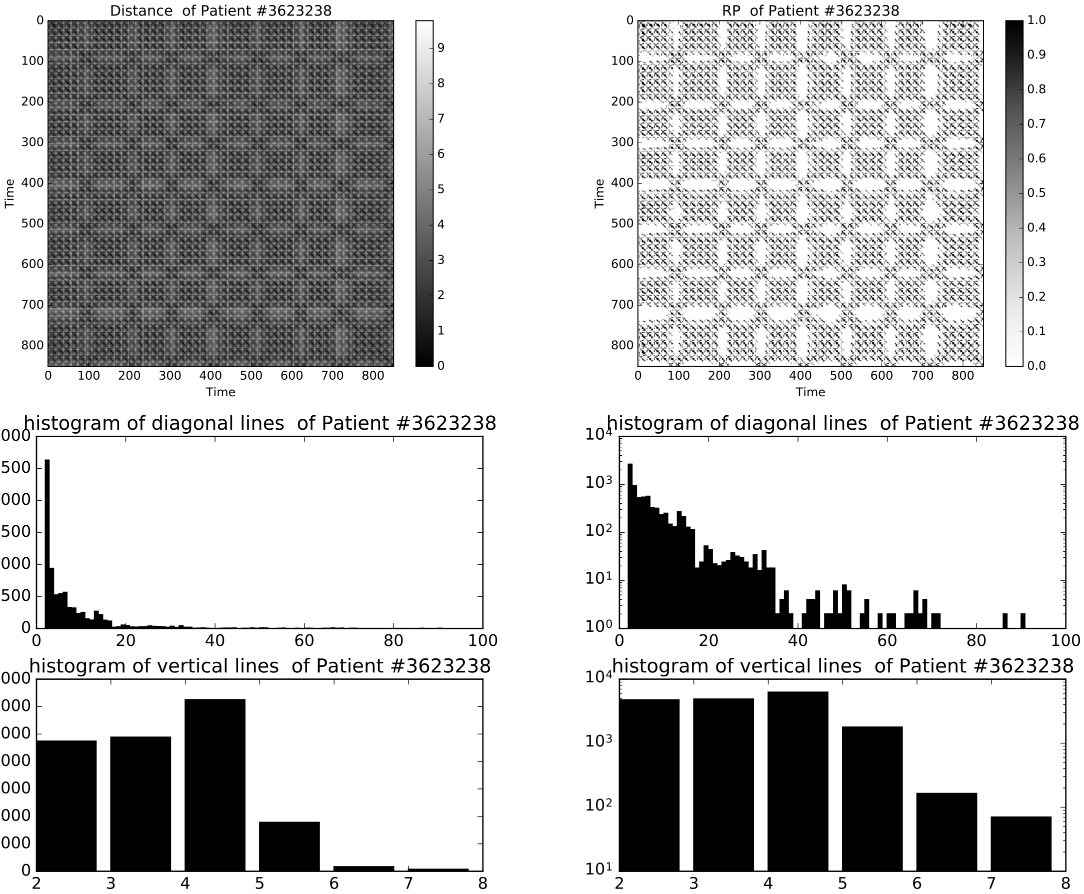

Figure A.55: RQA results of subject 3623238

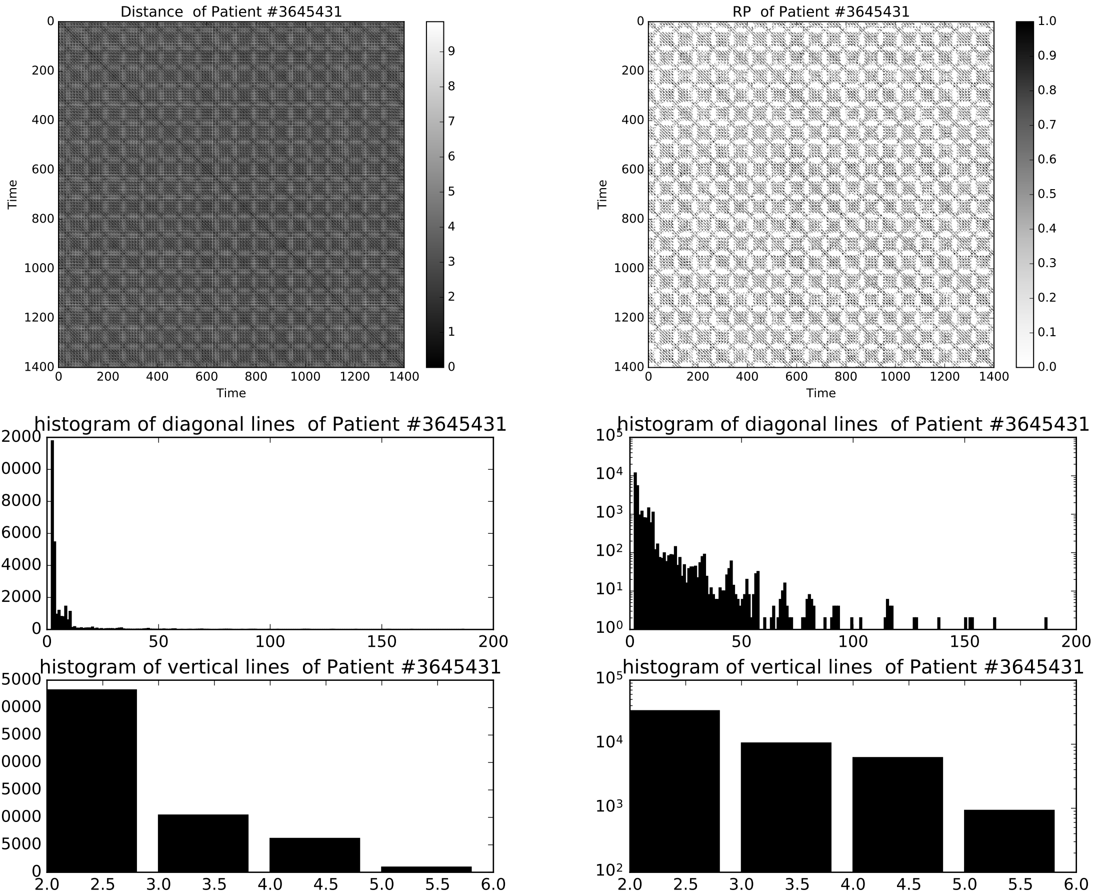

Figure A.56: RQA results of subject 3645431

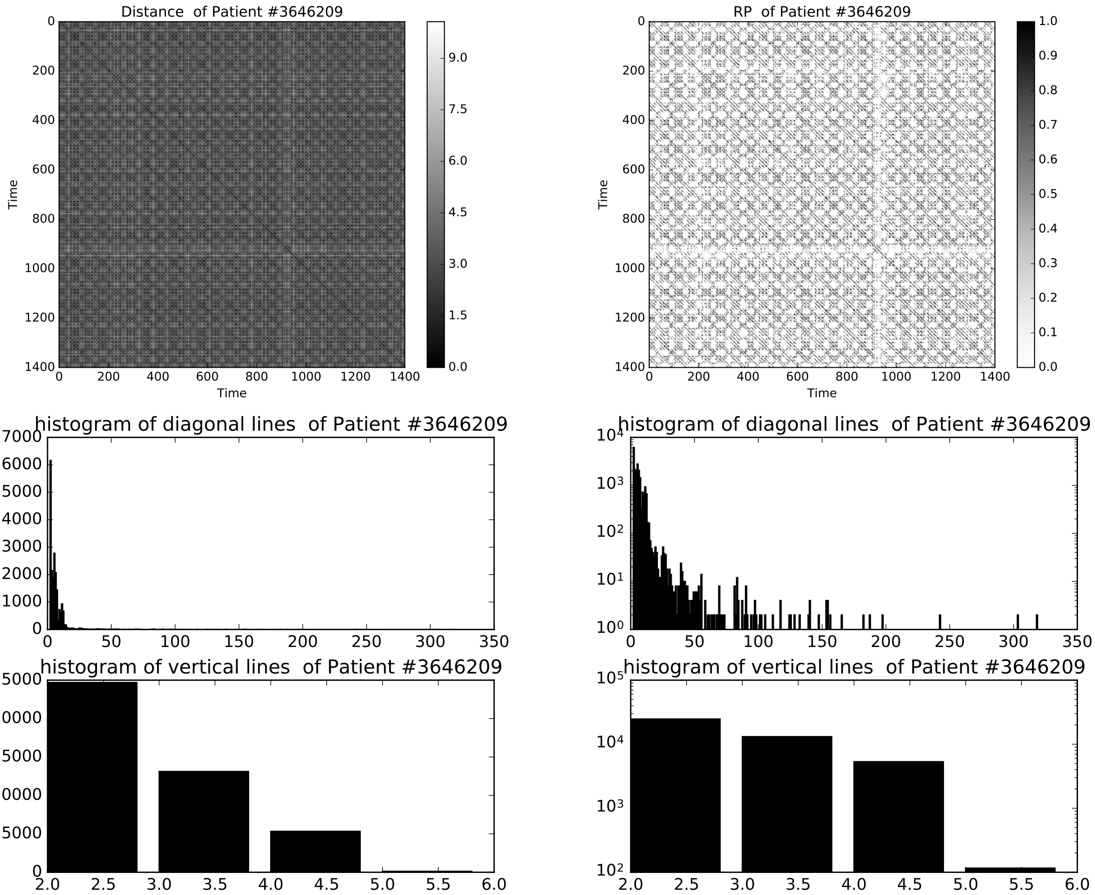

Figure A.57: RQA results of subject 3646209

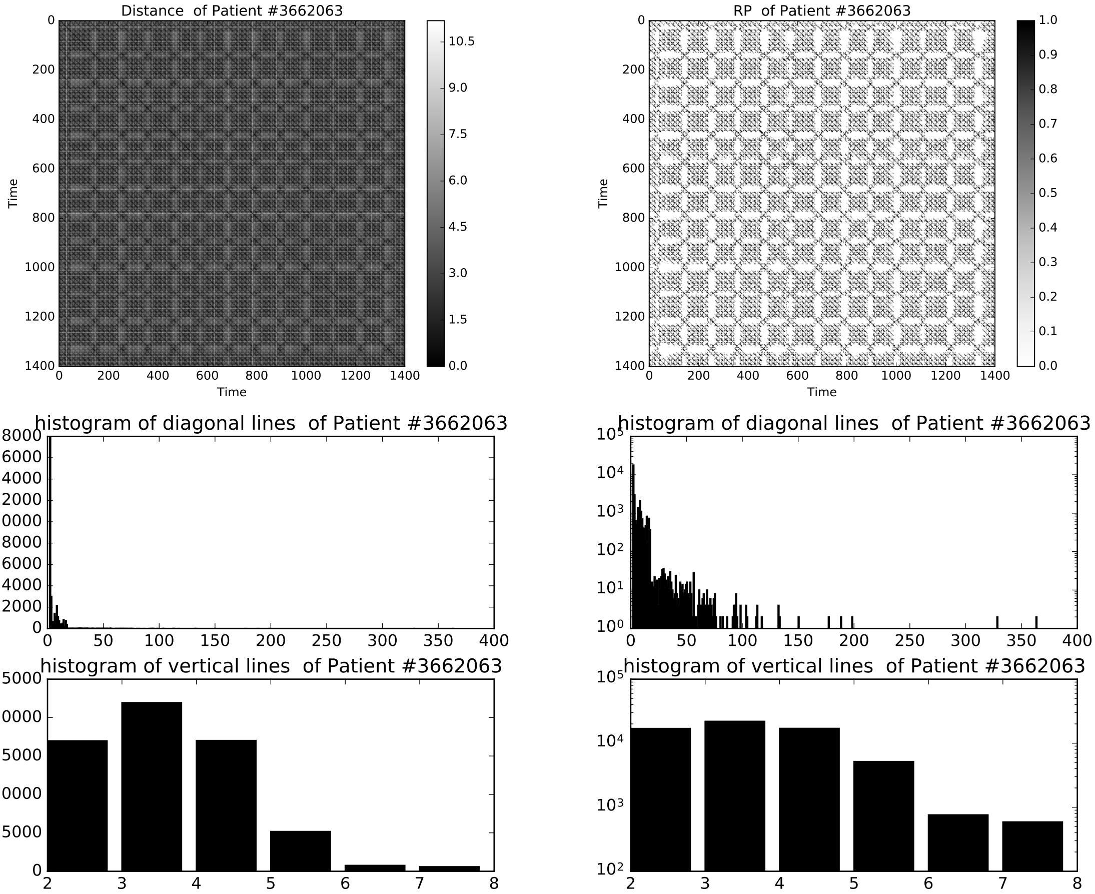

Figure A.58: RQA results of subject 3662063

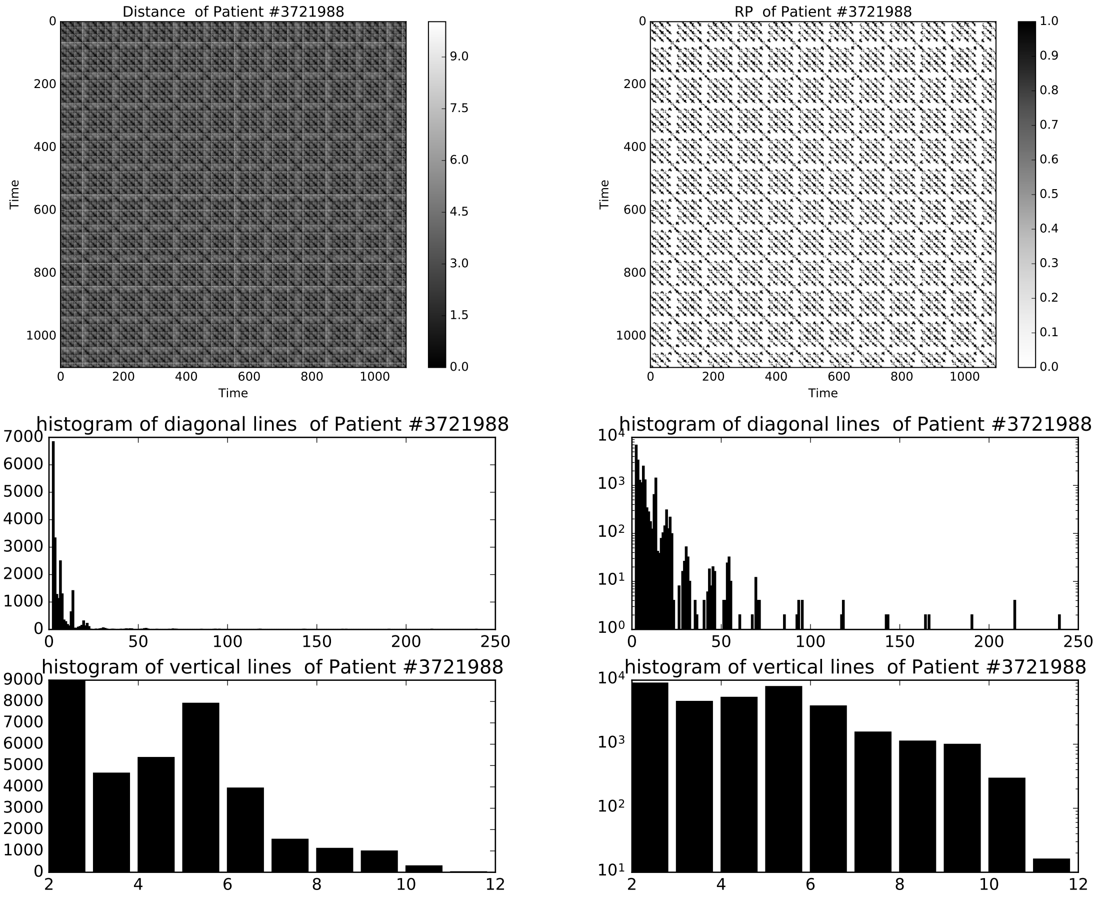

Figure A.59: RQA results of subject 3721988

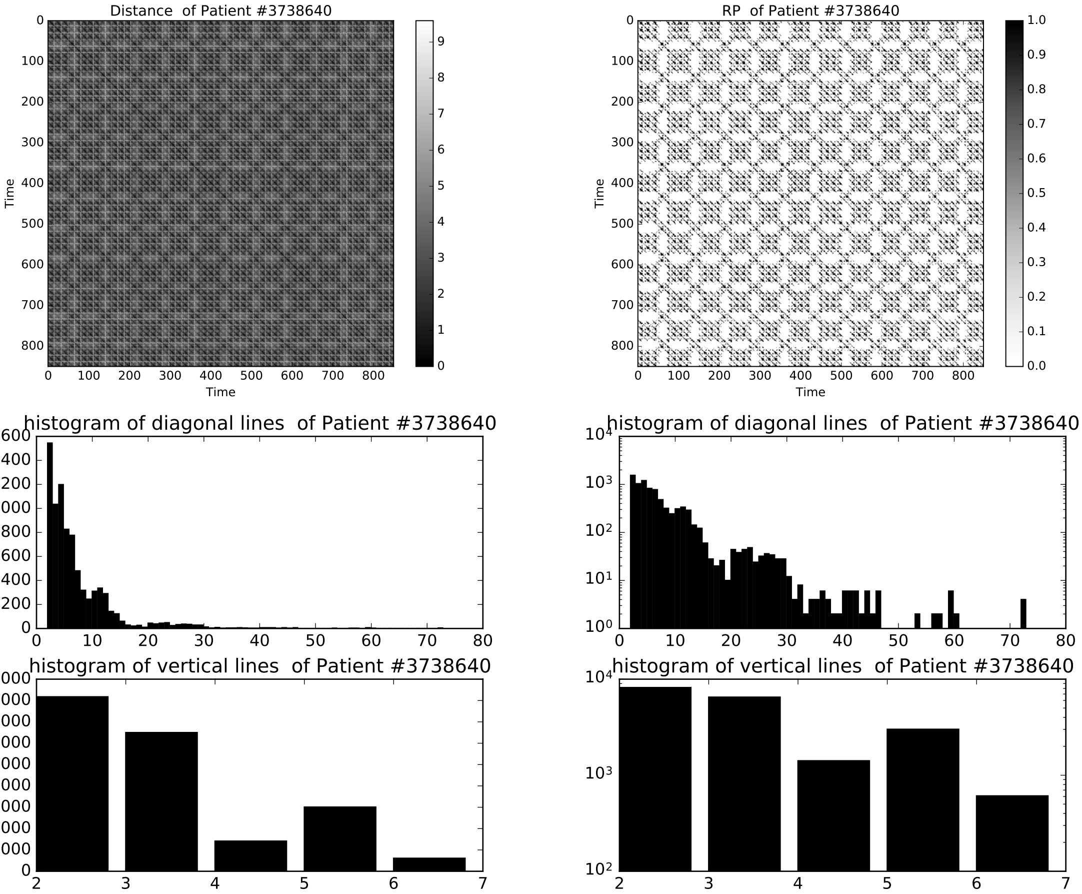

Figure A.60: RQA results of subject 3738640

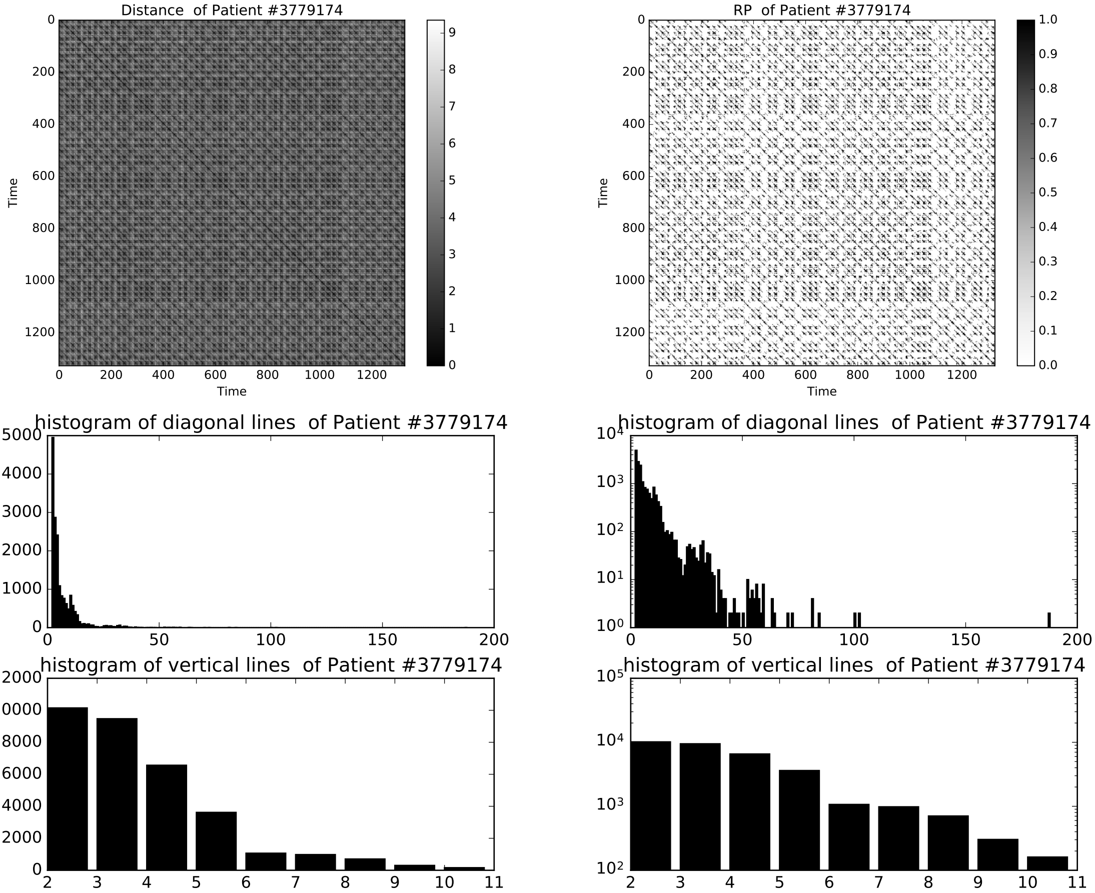

Figure A.61: RQA results of subject 3779174

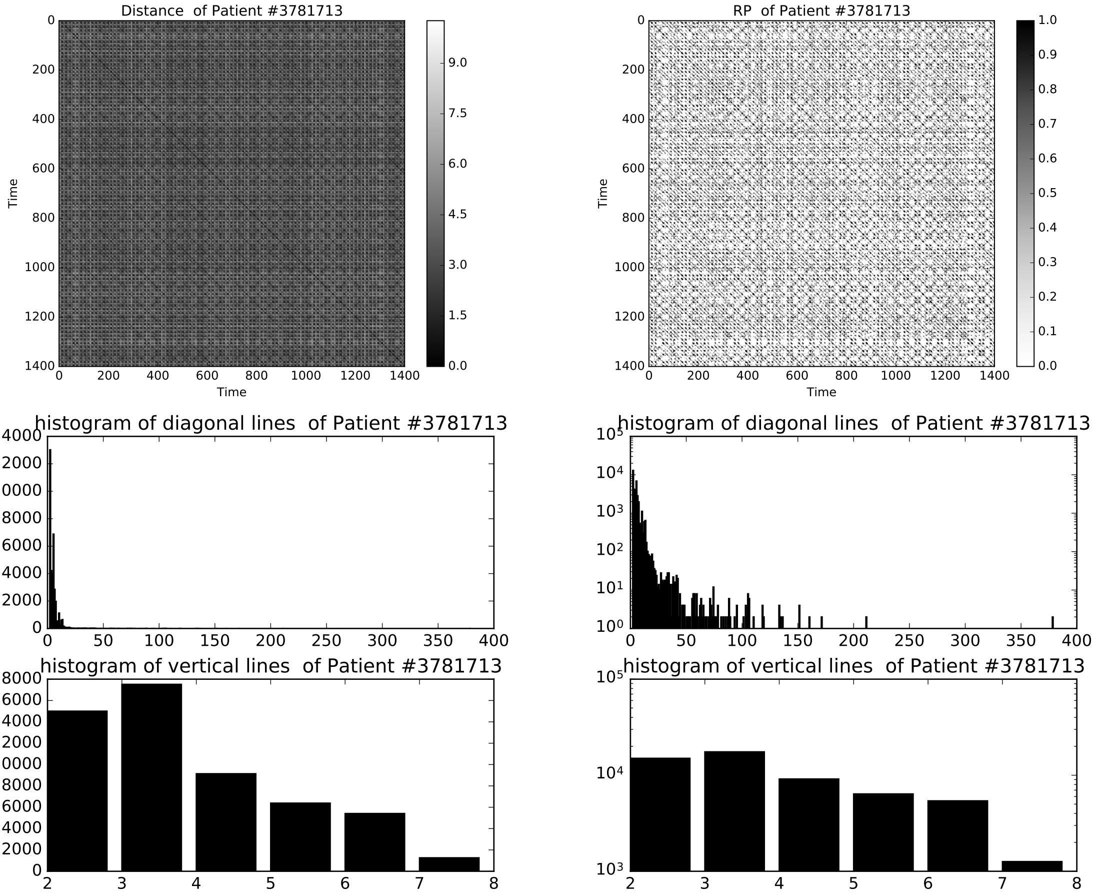

Figure A.62: RQA results of subject 3781713

A.4 RPs and Novelty Curves of All Patients

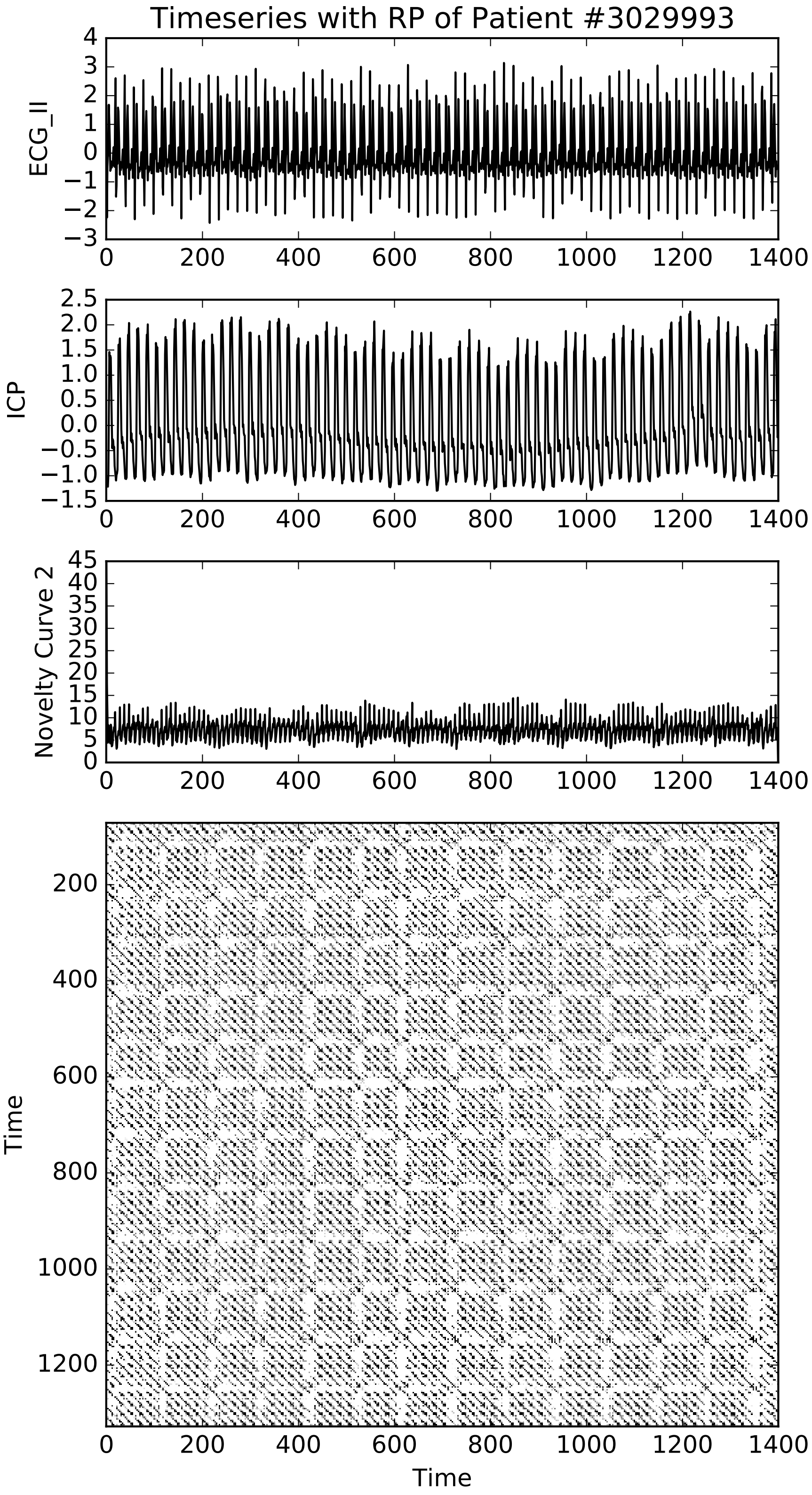

Figure A.63: RP and novelty curve of subject 3029993

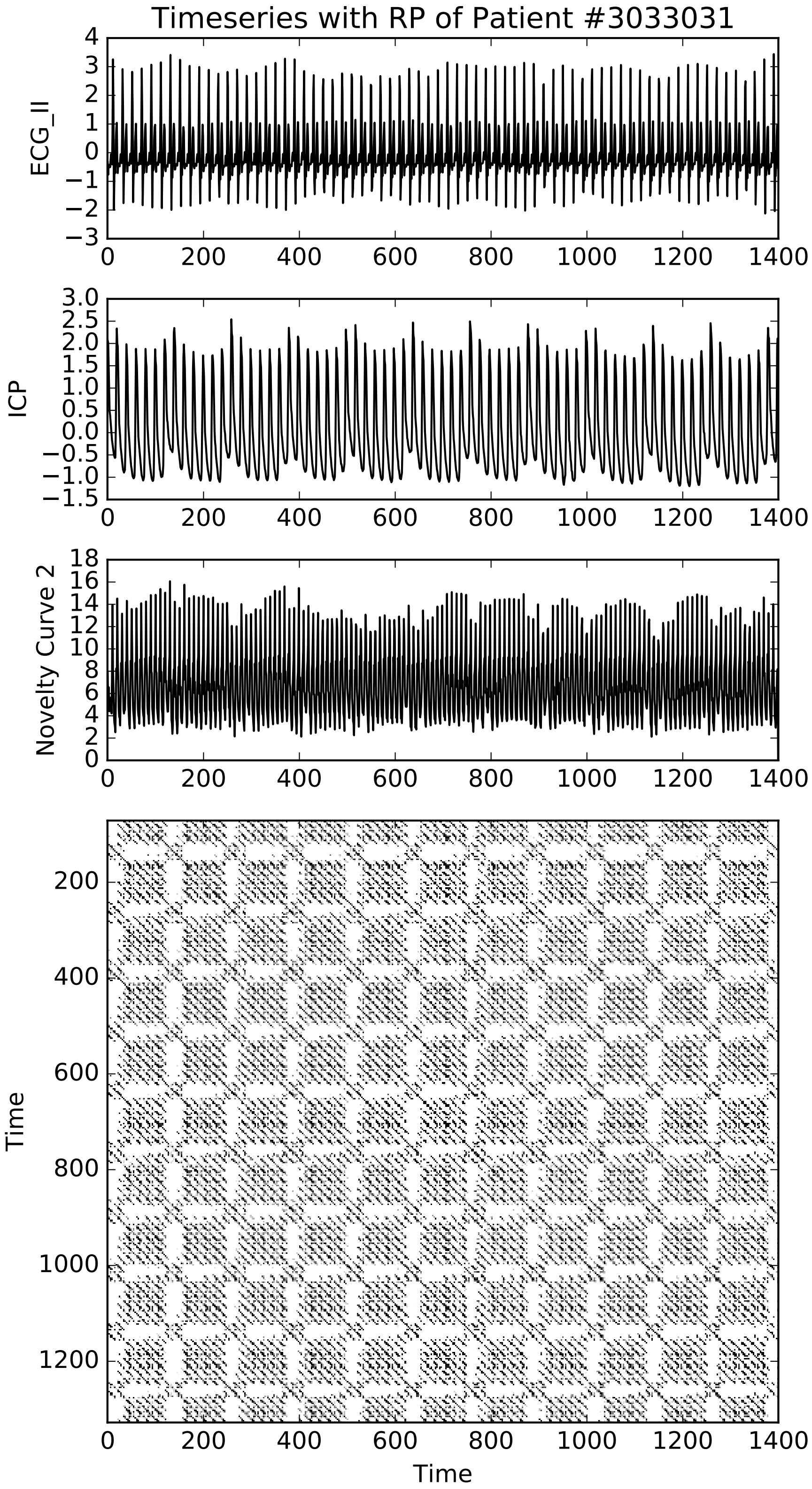

Figure A.64: RP and novelty curve of subject 3033031

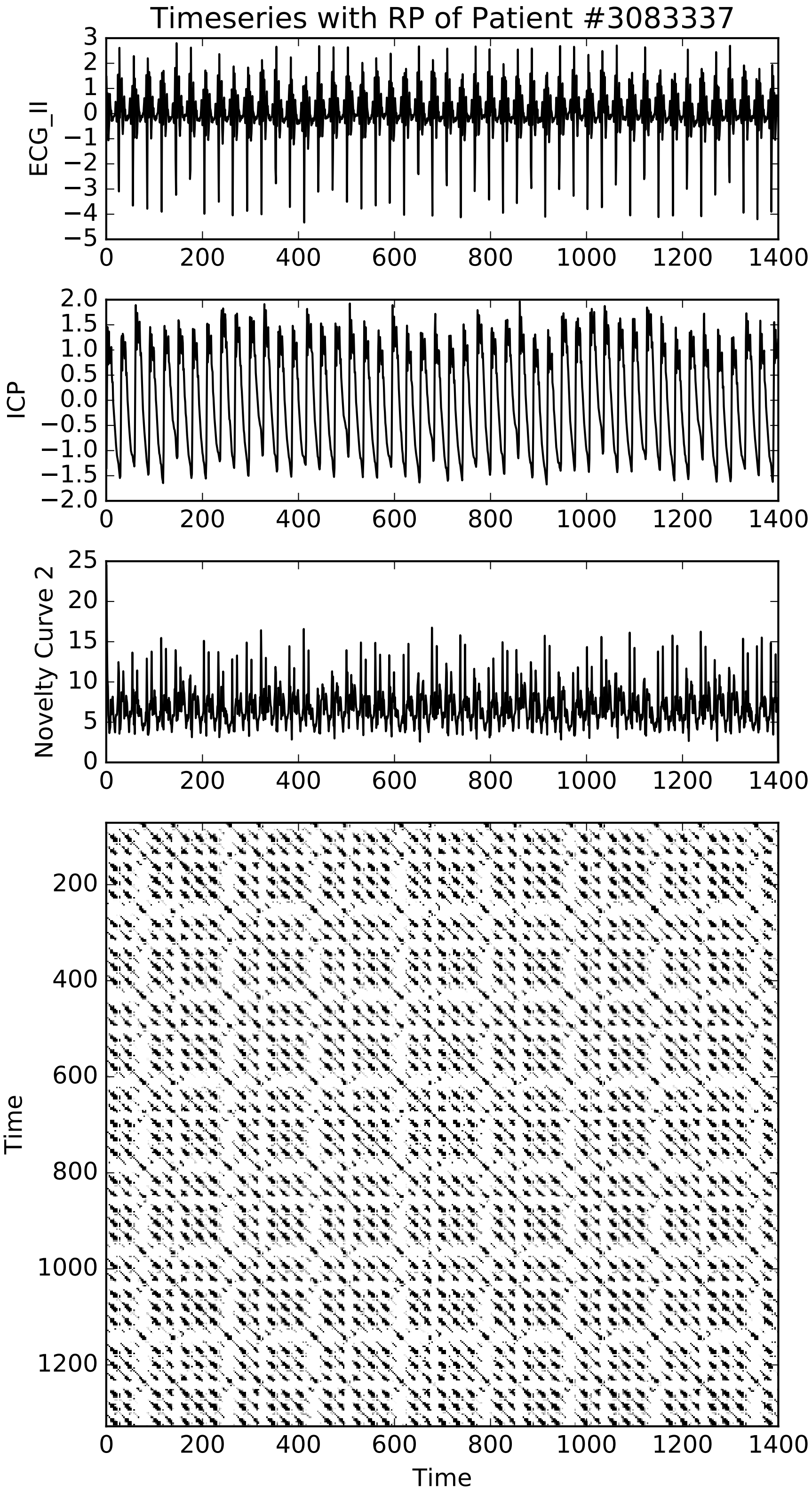

Figure A.65: RP and novelty curve of subject 3083337

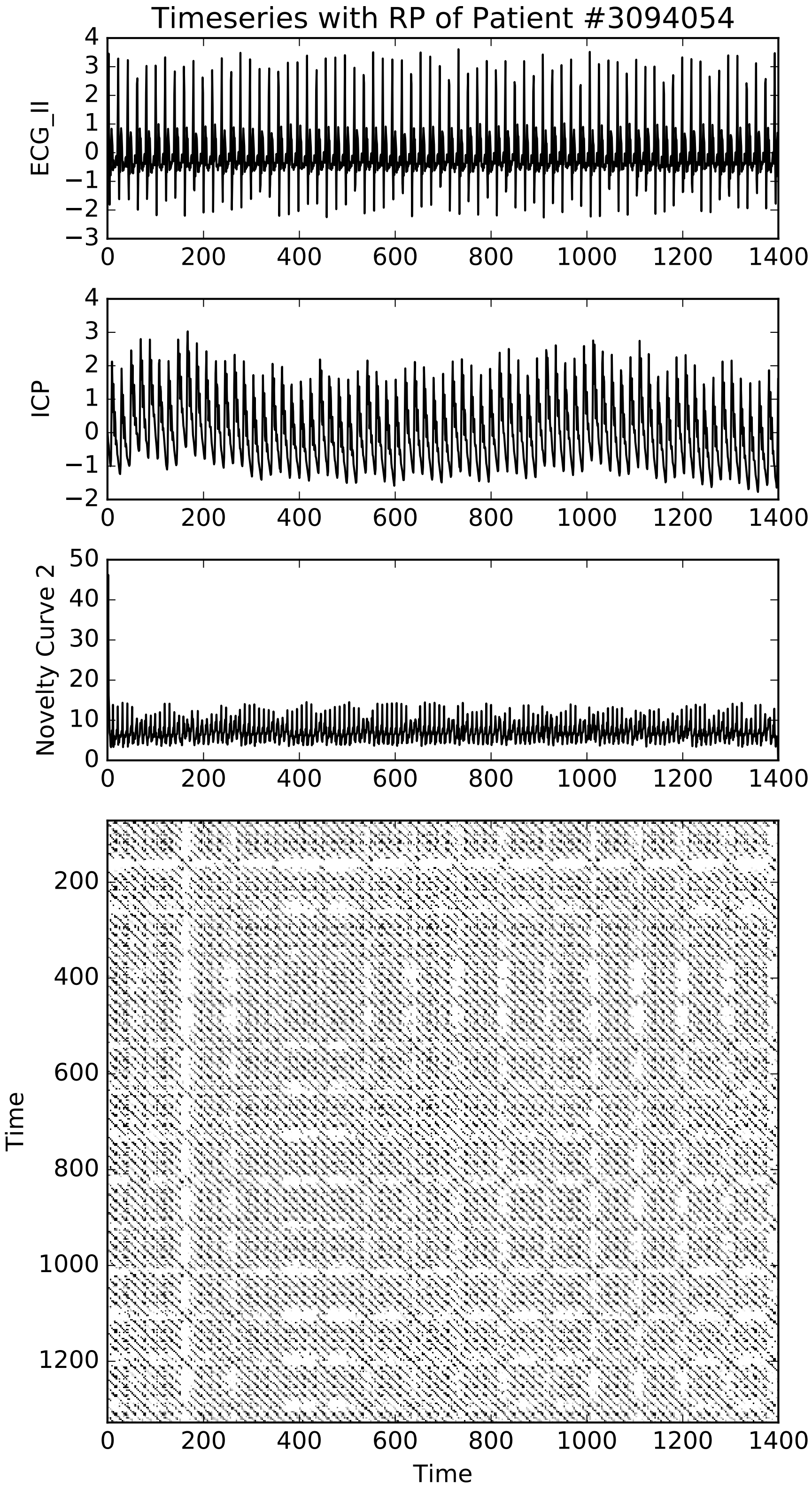

Figure A.66: RP and novelty curve of subject 3094054

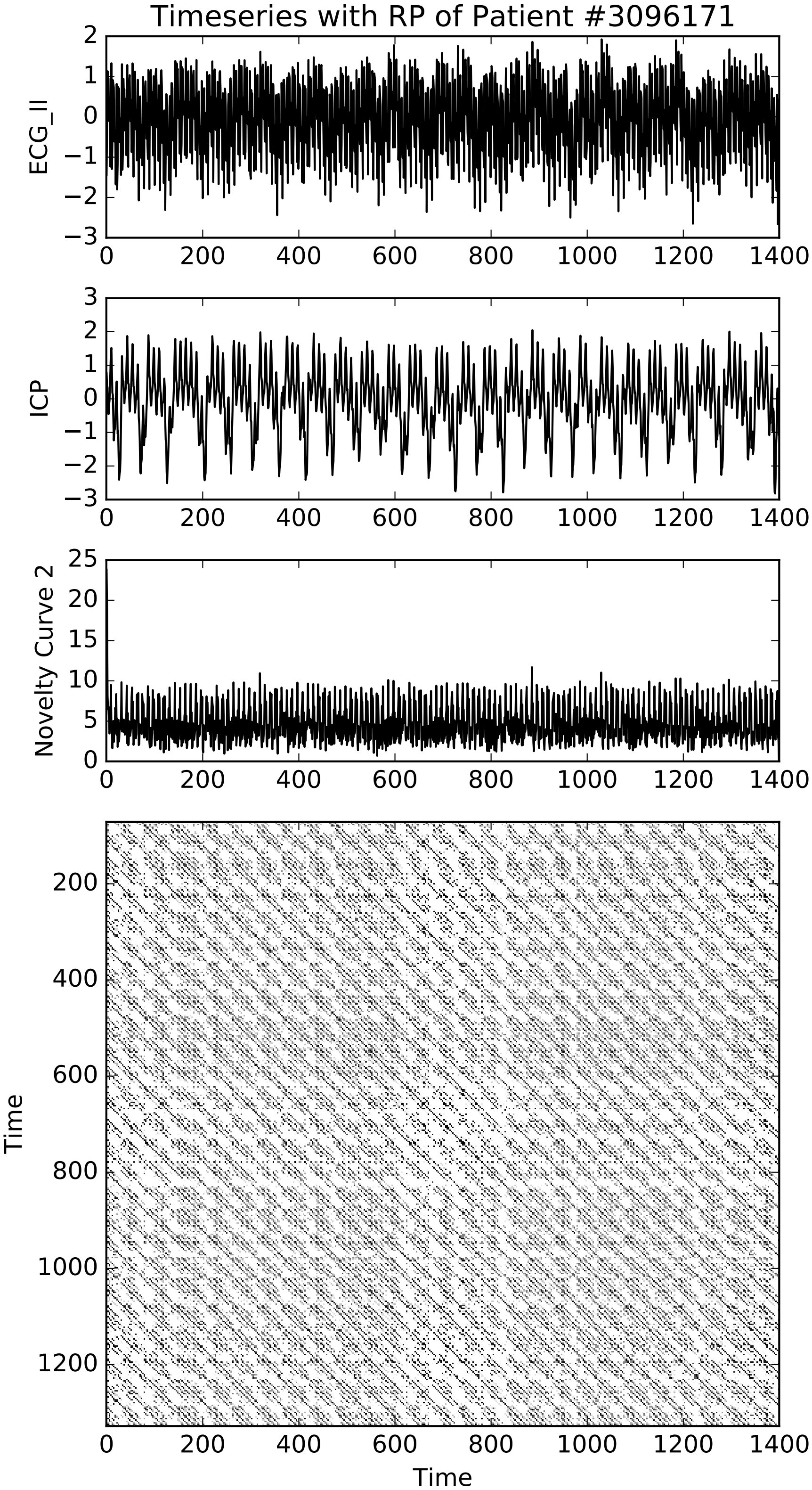

Figure A.67: RP and novelty curve of subject 3096171

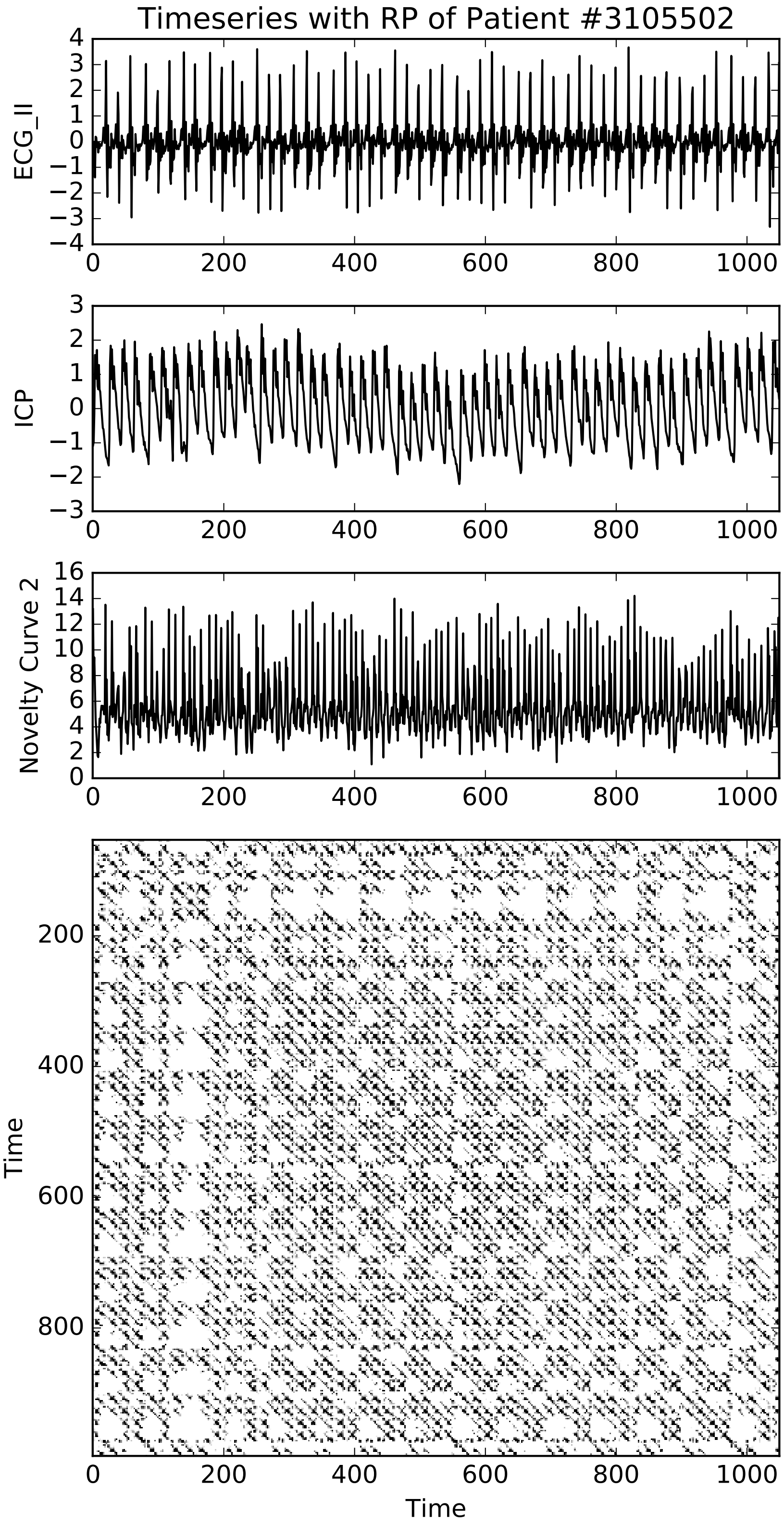

Figure A.68: RP and novelty curve of subject 3105502

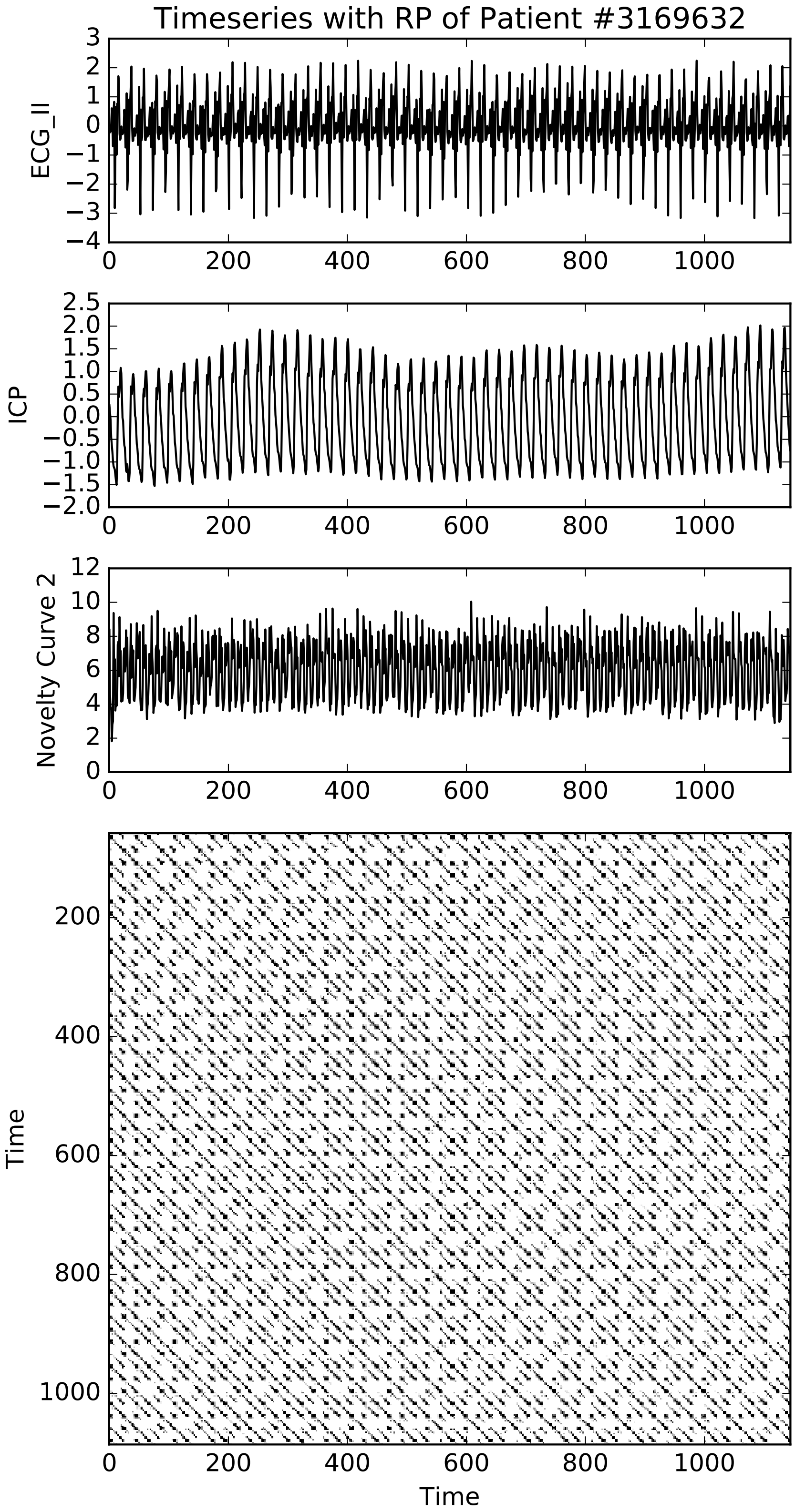

Figure A.69: RP and novelty curve of subject 3169632

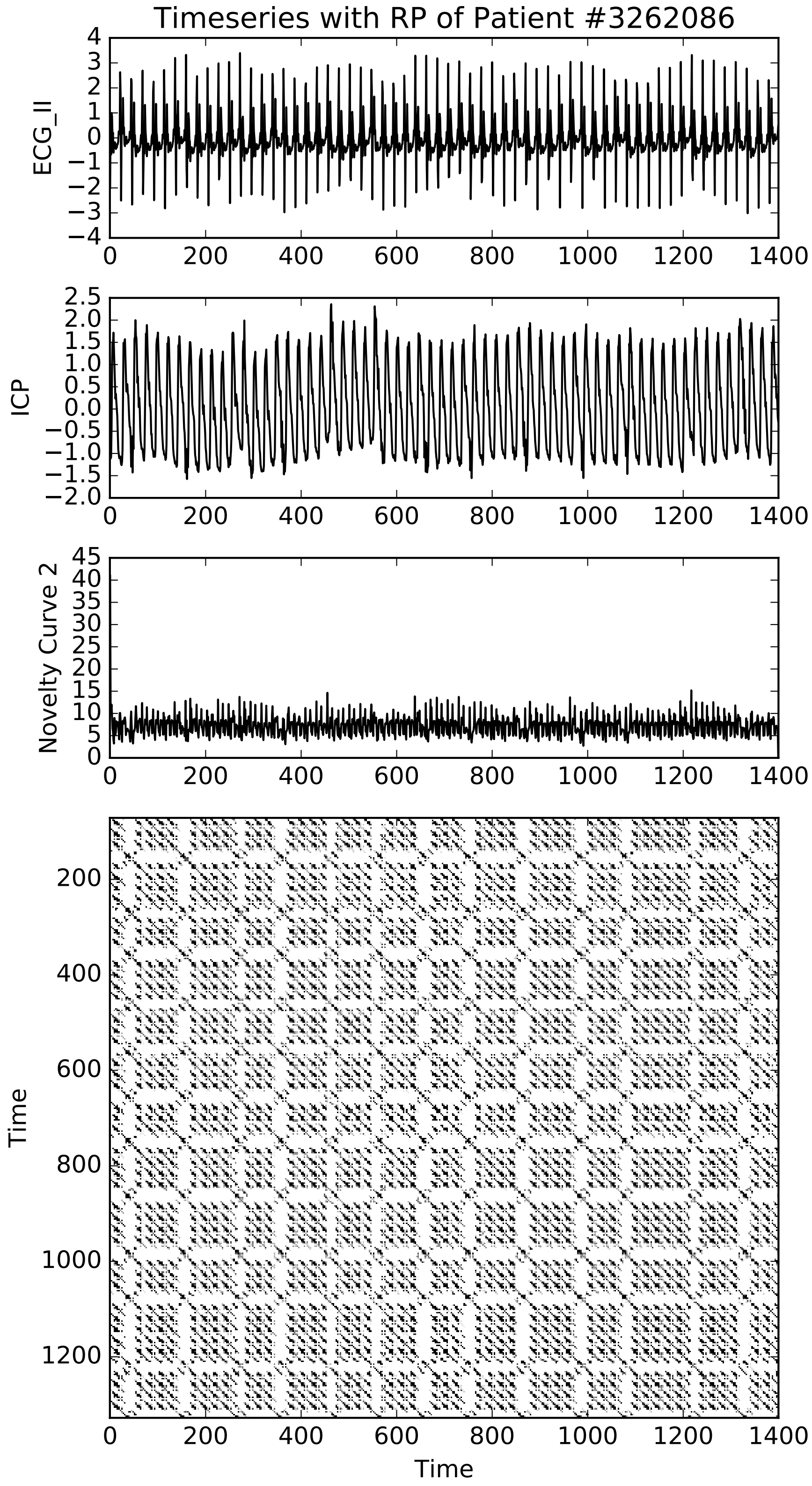

Figure A.70: RP and novelty curve of subject 3262086

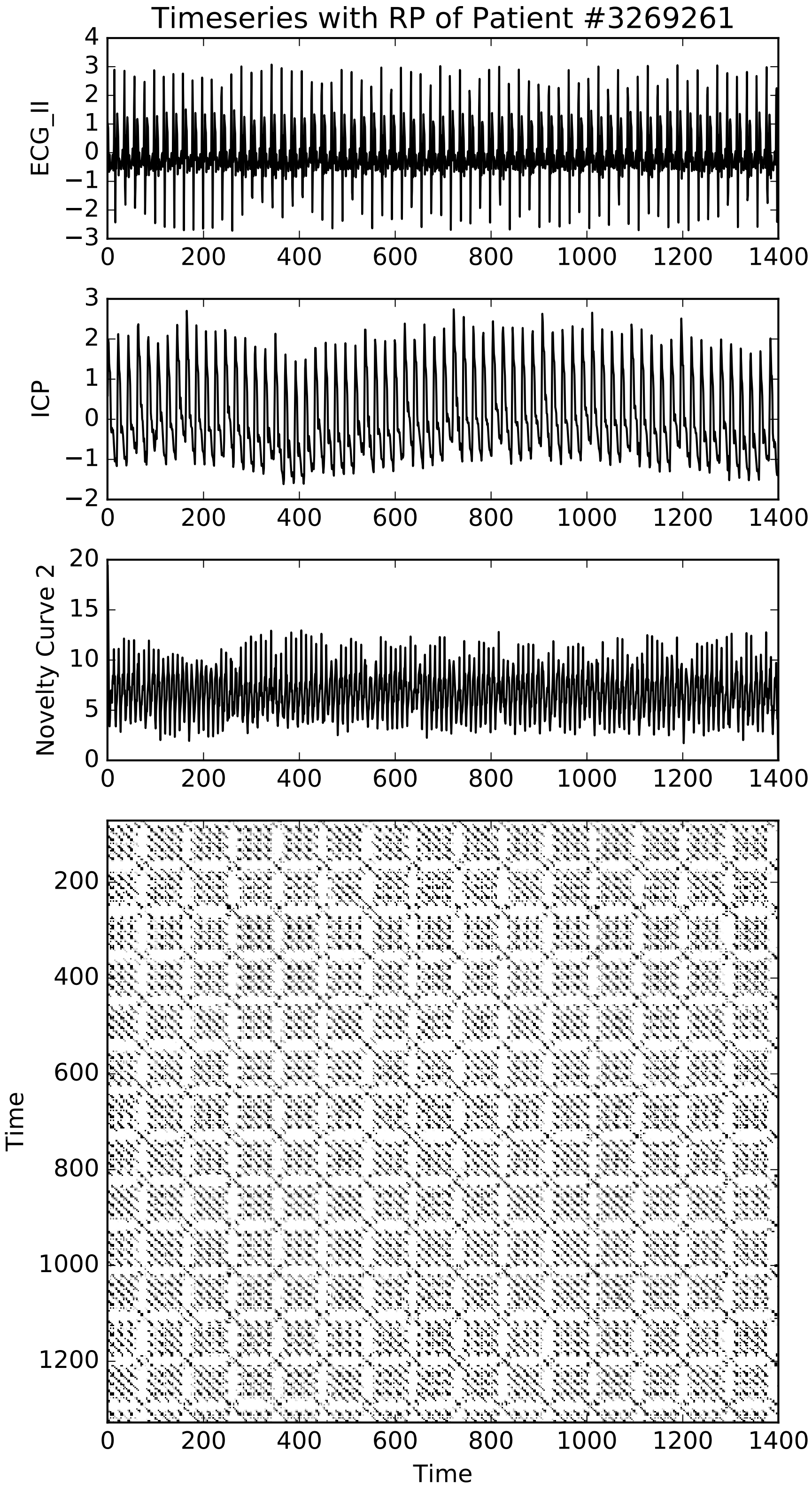

Figure A.71: RP and novelty curve of subject 3269261

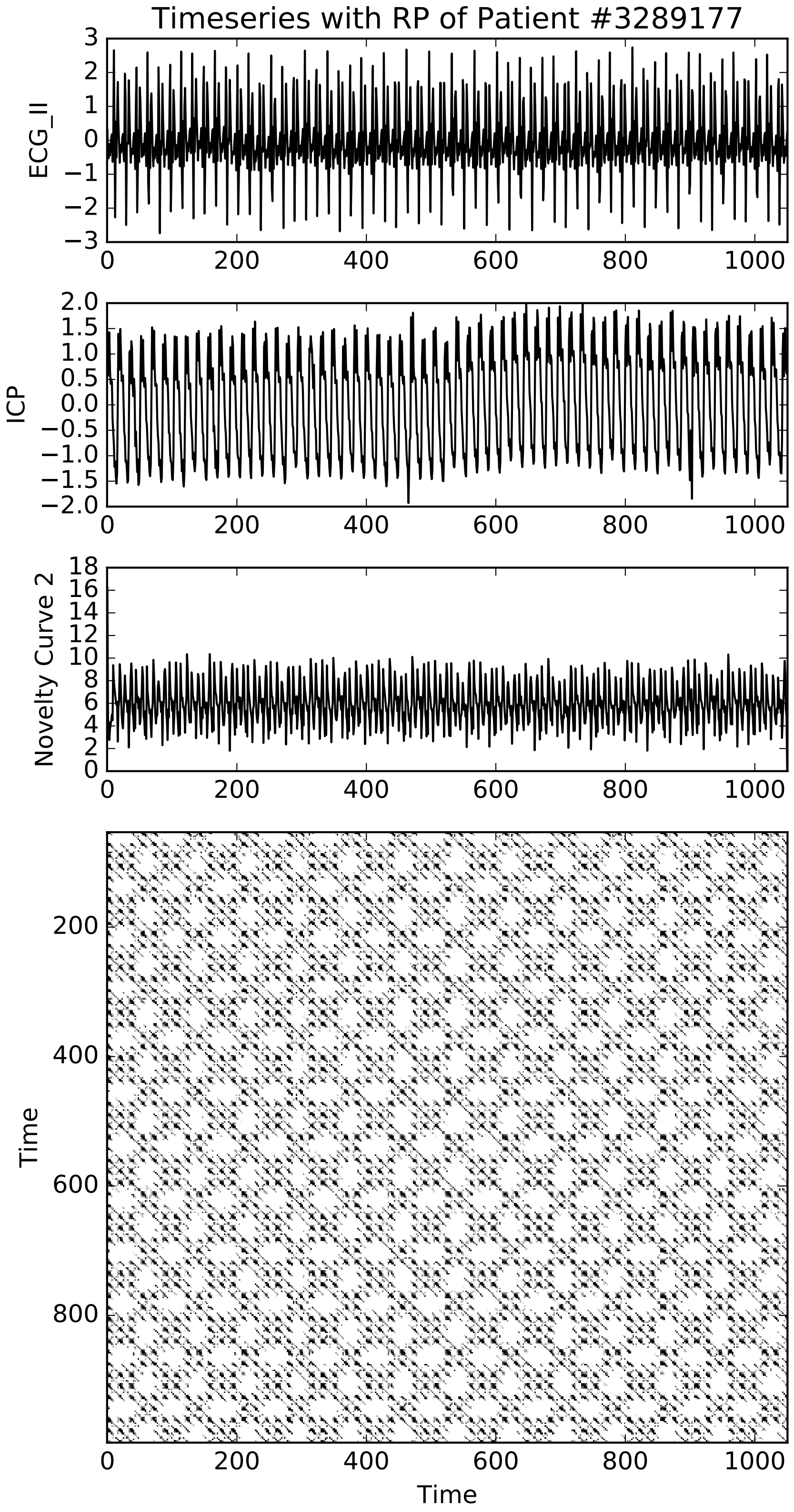

Figure A.72: RP and novelty curve of subject 3289177

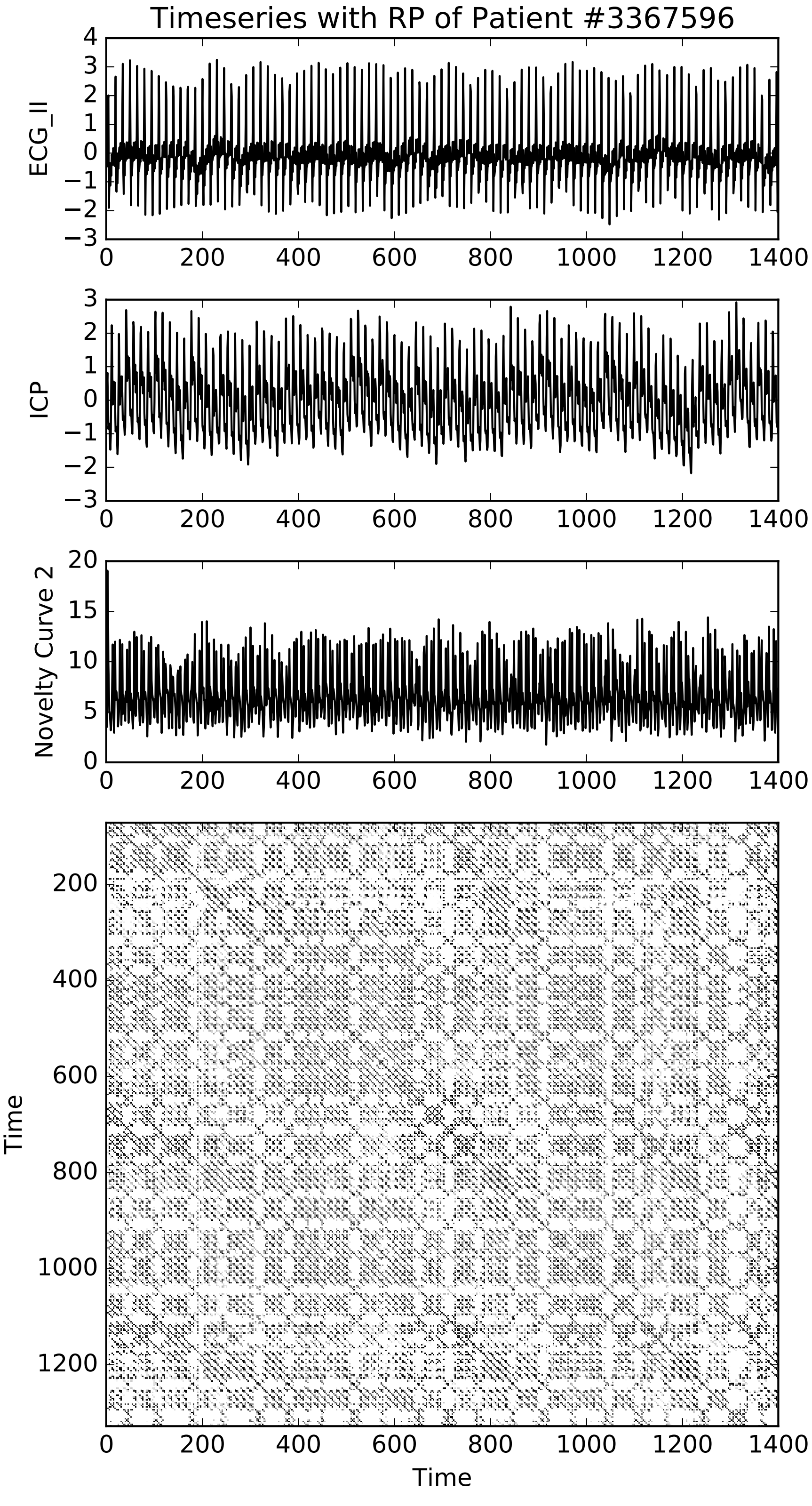

Figure A.73: RP and novelty curve of subject 3367596

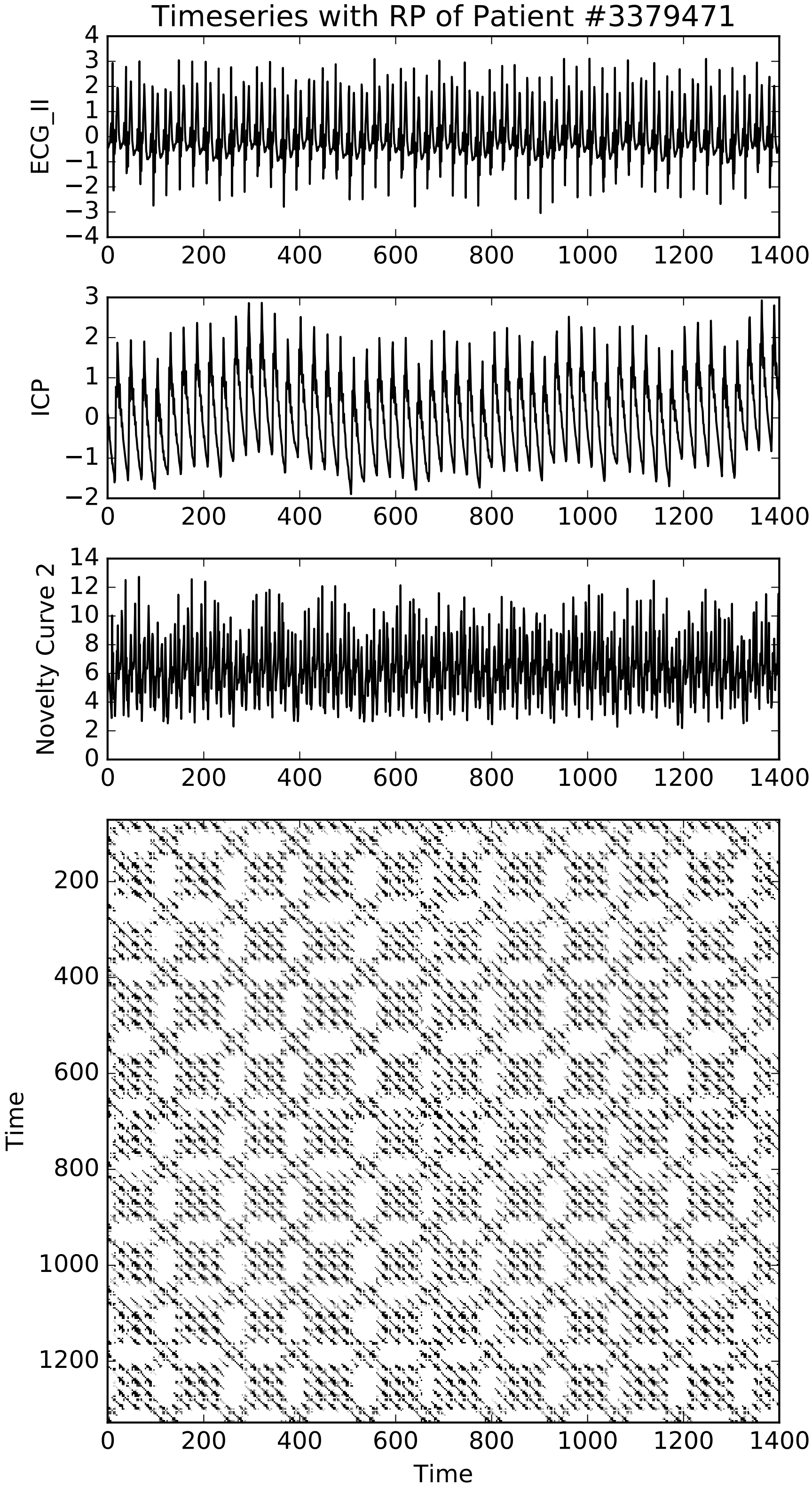

Figure A.74: RP and novelty curve of subject 3379471

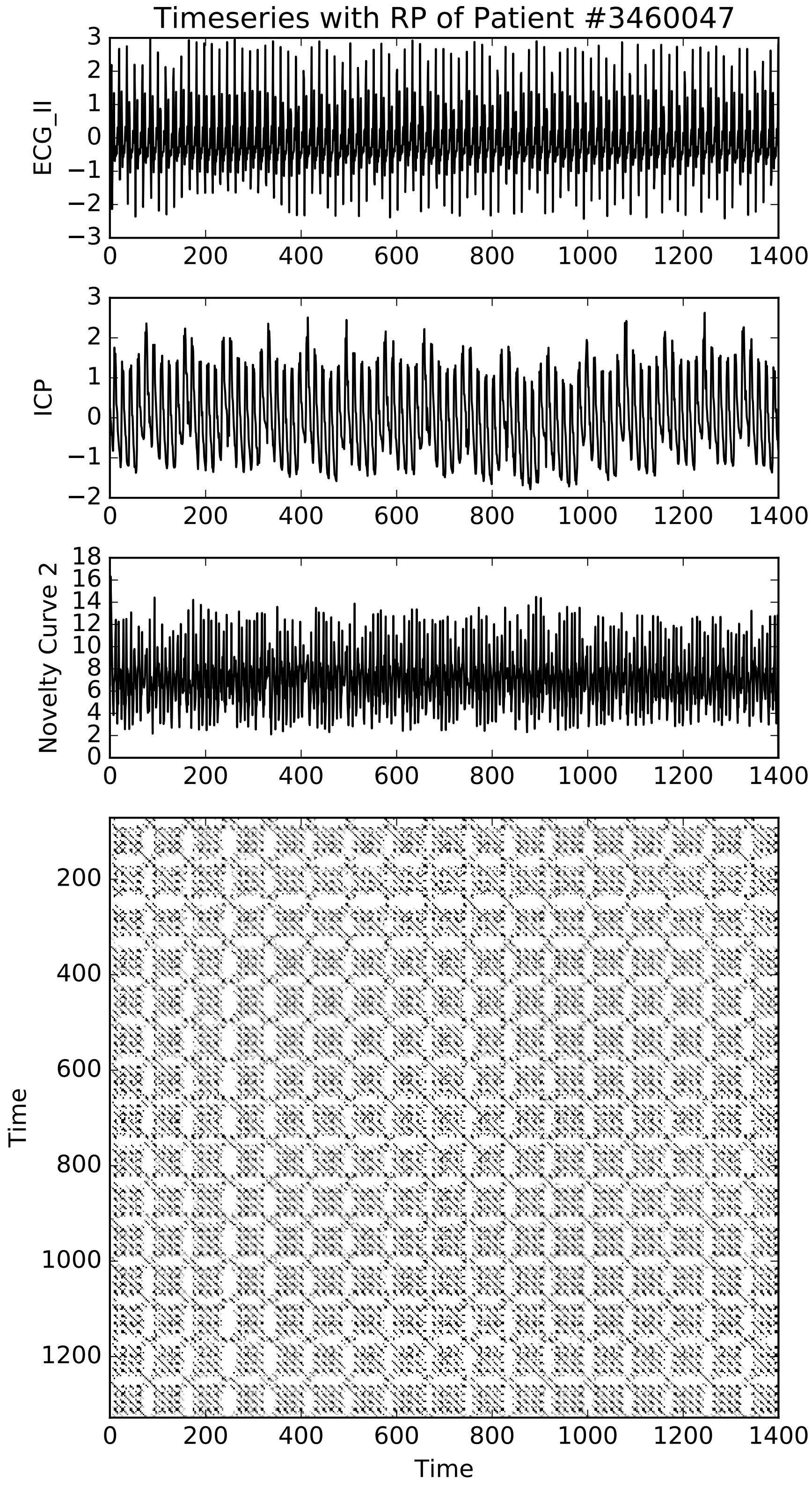

Figure A.75: RP and novelty curve of subject 3460047

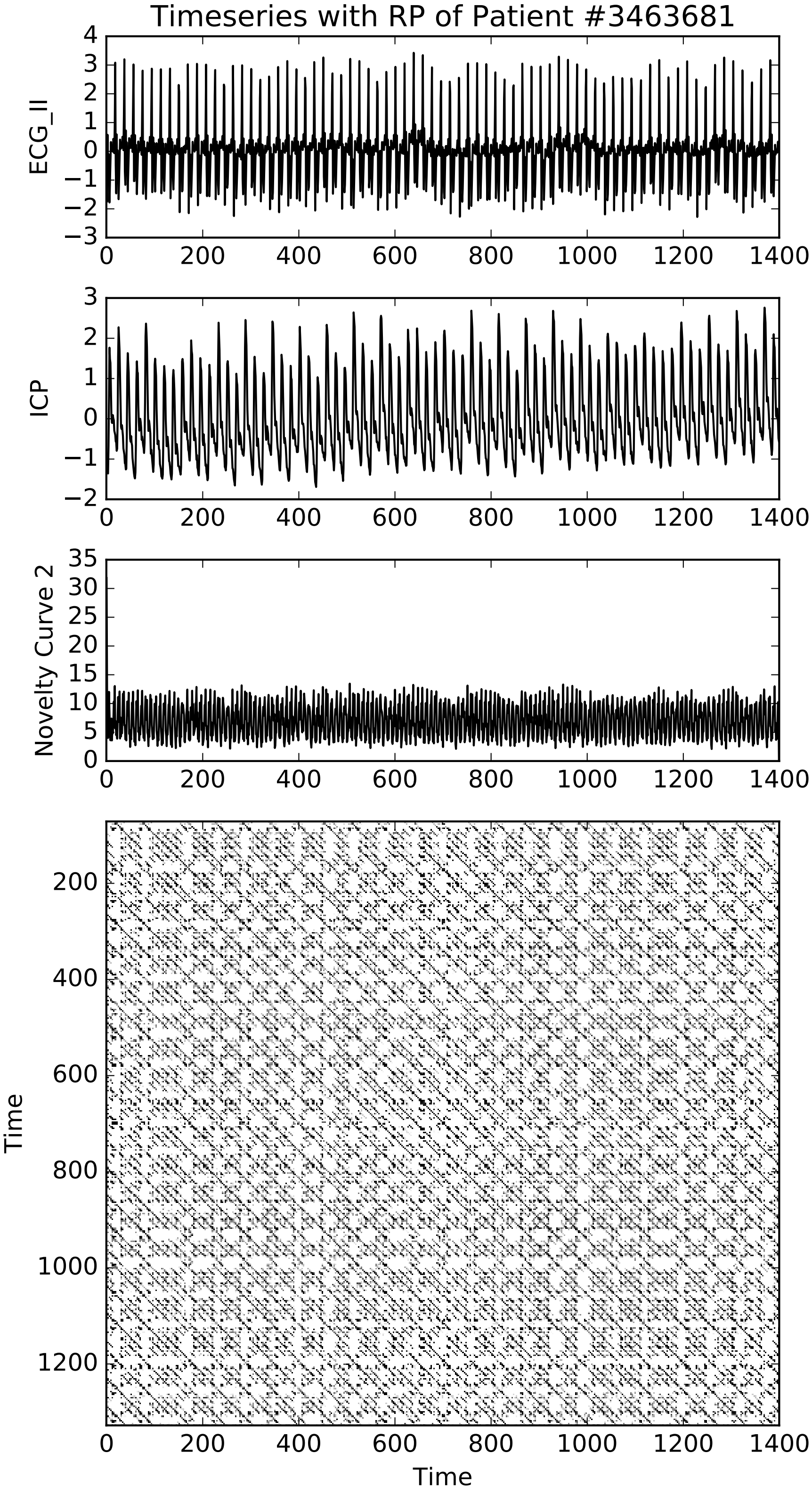

Figure A.76: RP and novelty curve of subject 3463681

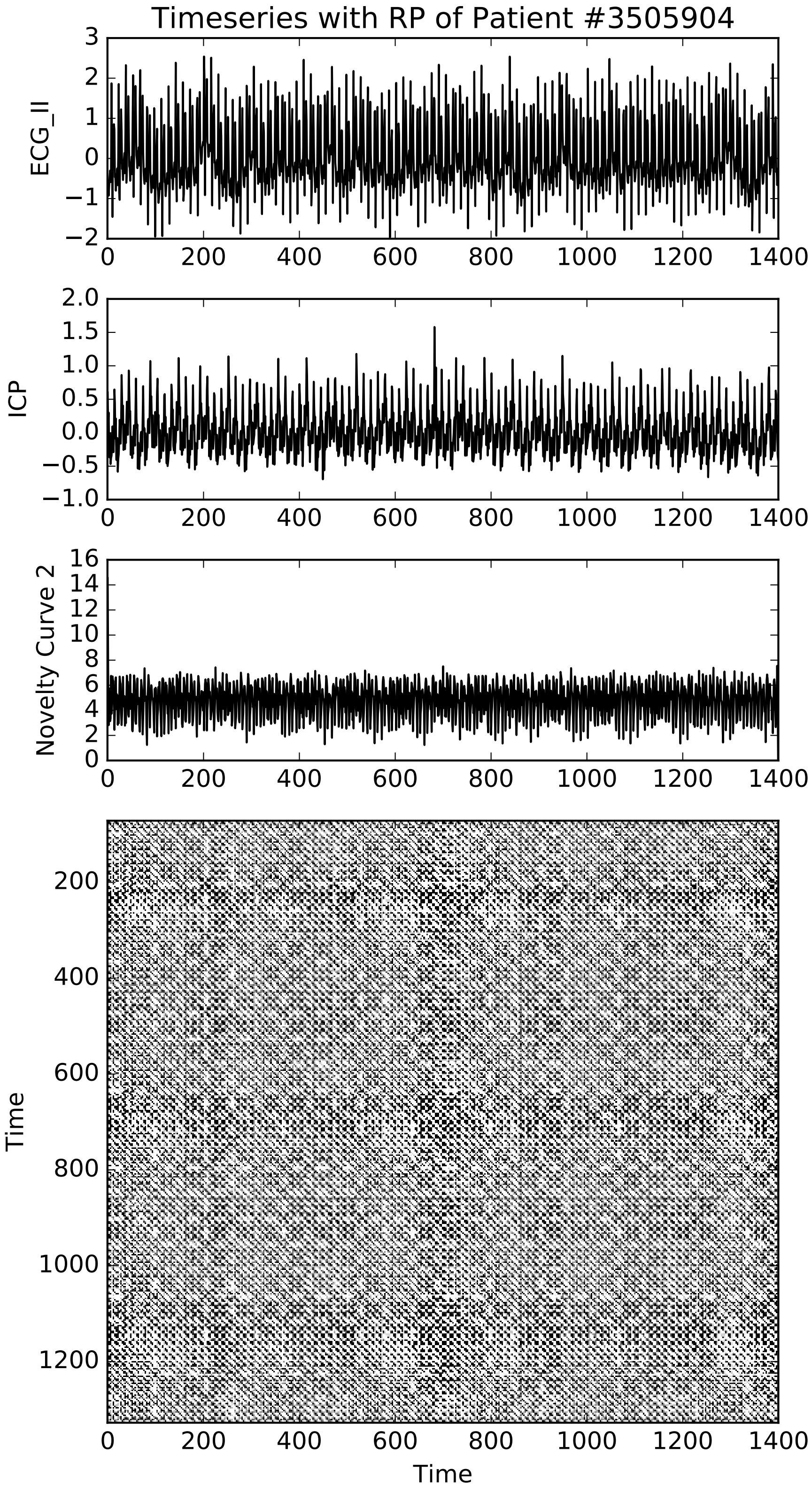

Figure A.77: RP and novelty curve of subject 3505904

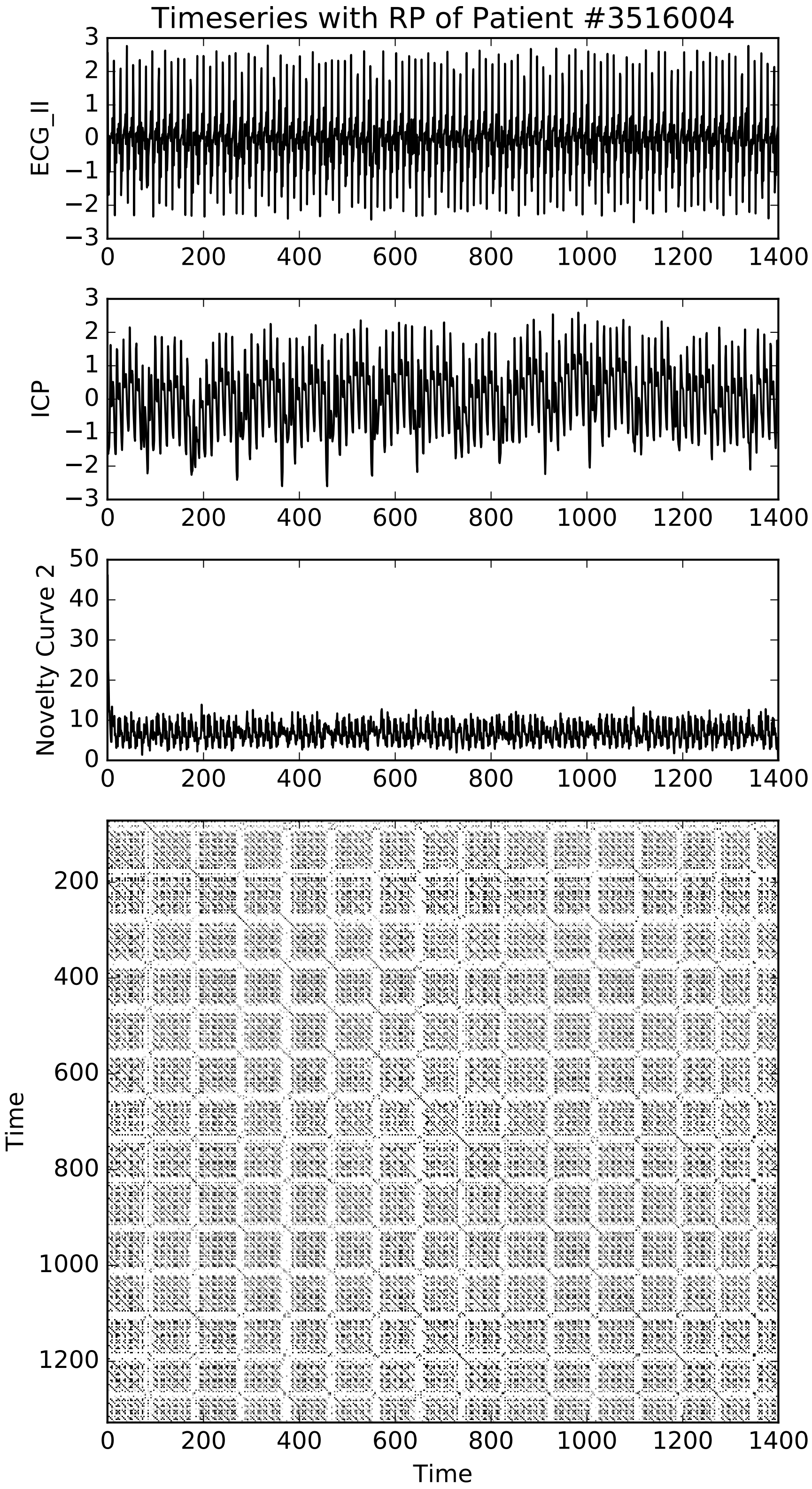

Figure A.78: RP and novelty curve of subject 3516004

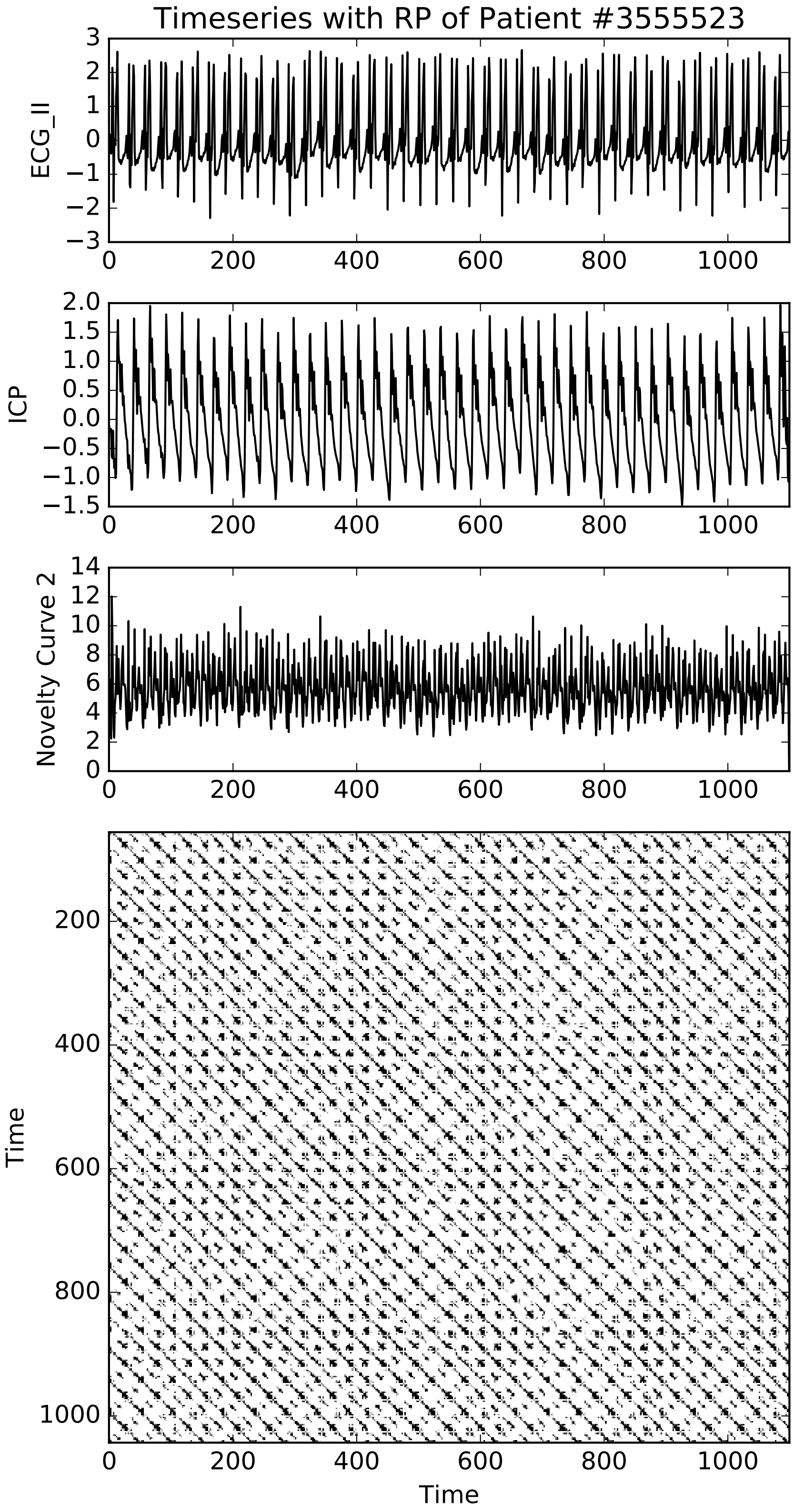

Figure A.79: RP and novelty curve of subject 3555523

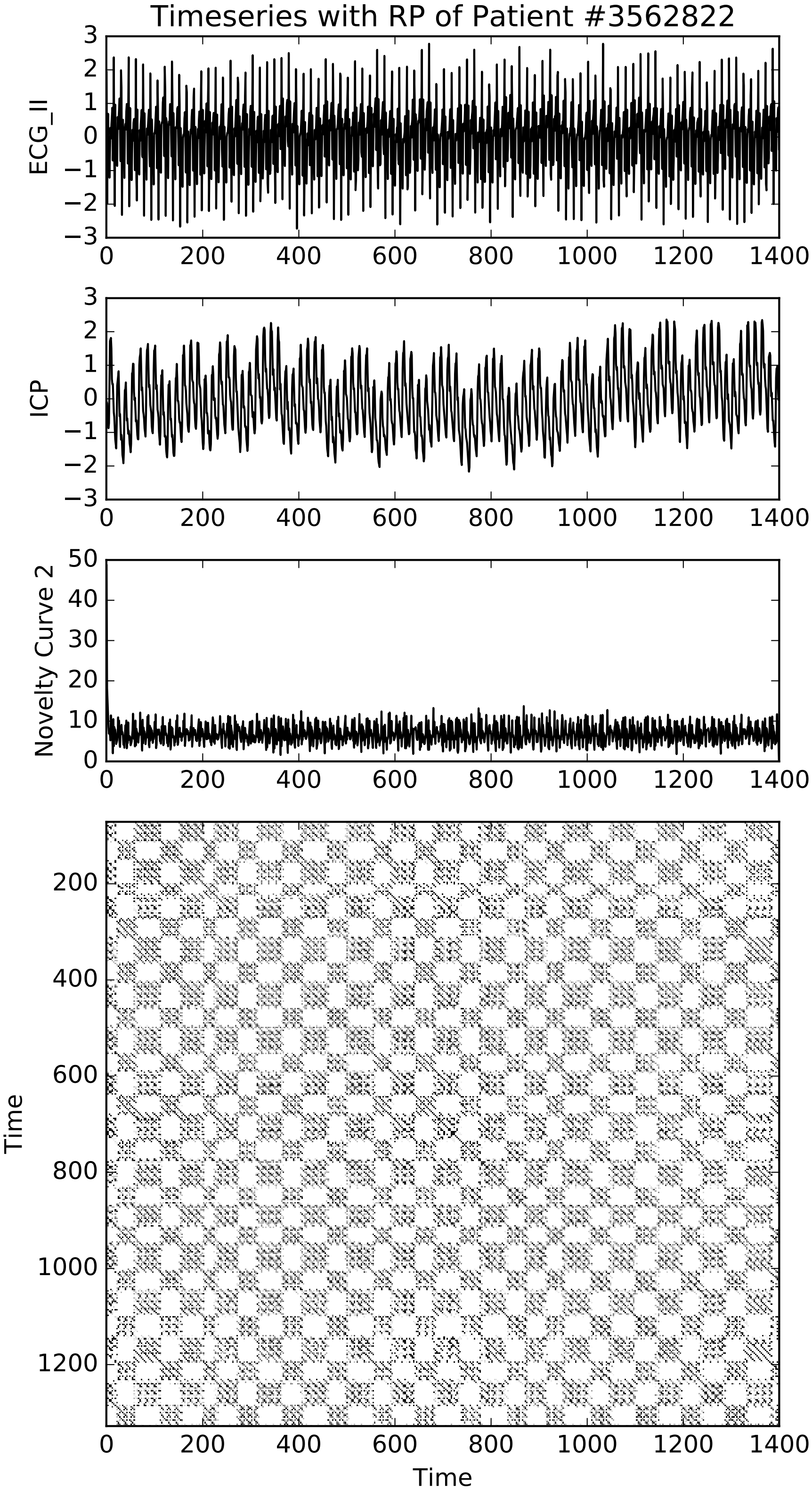

Figure A.80: RP and novelty curve of subject 3562822

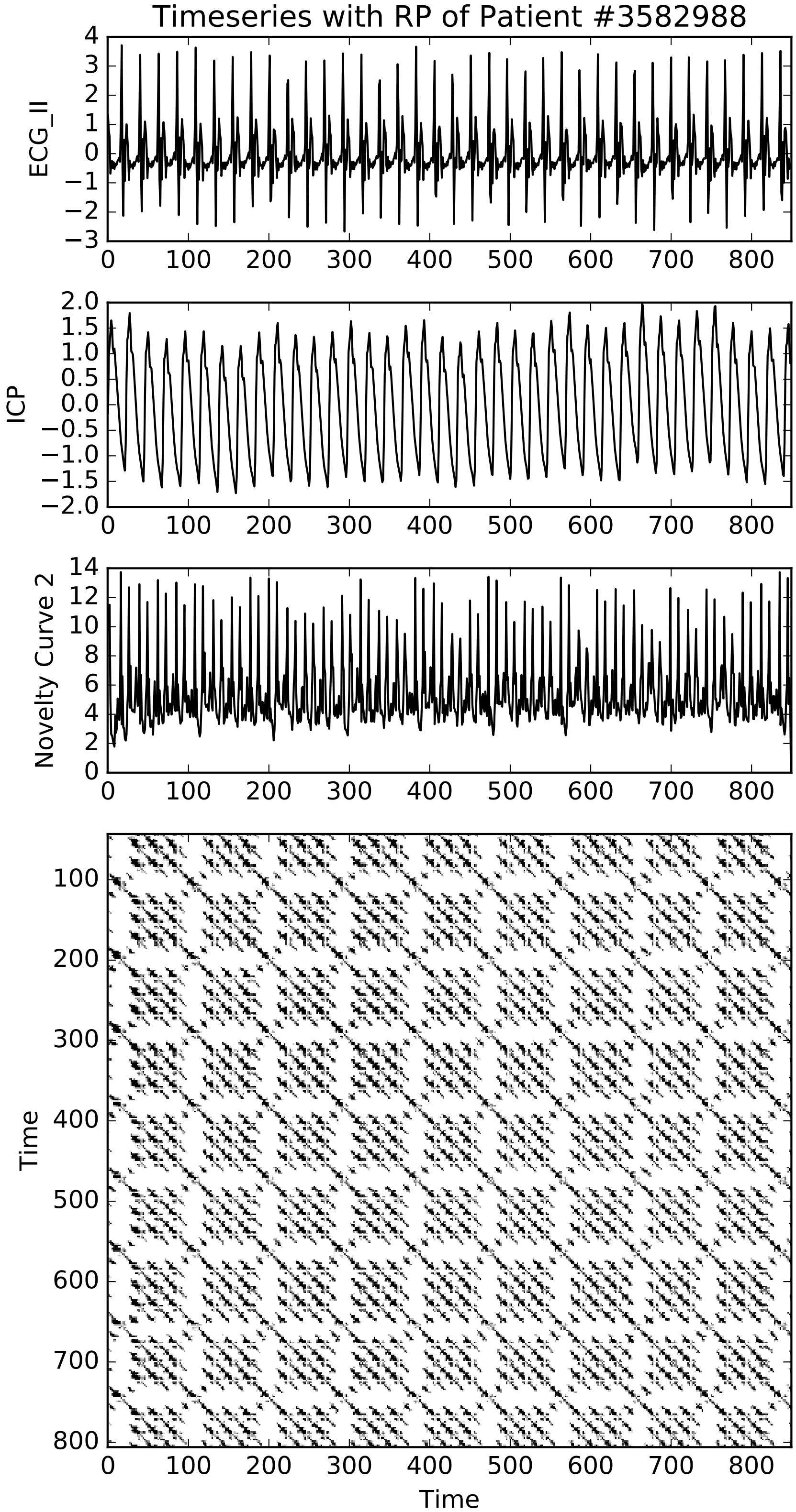

Figure A.81: RP and novelty curve of subject 3582988

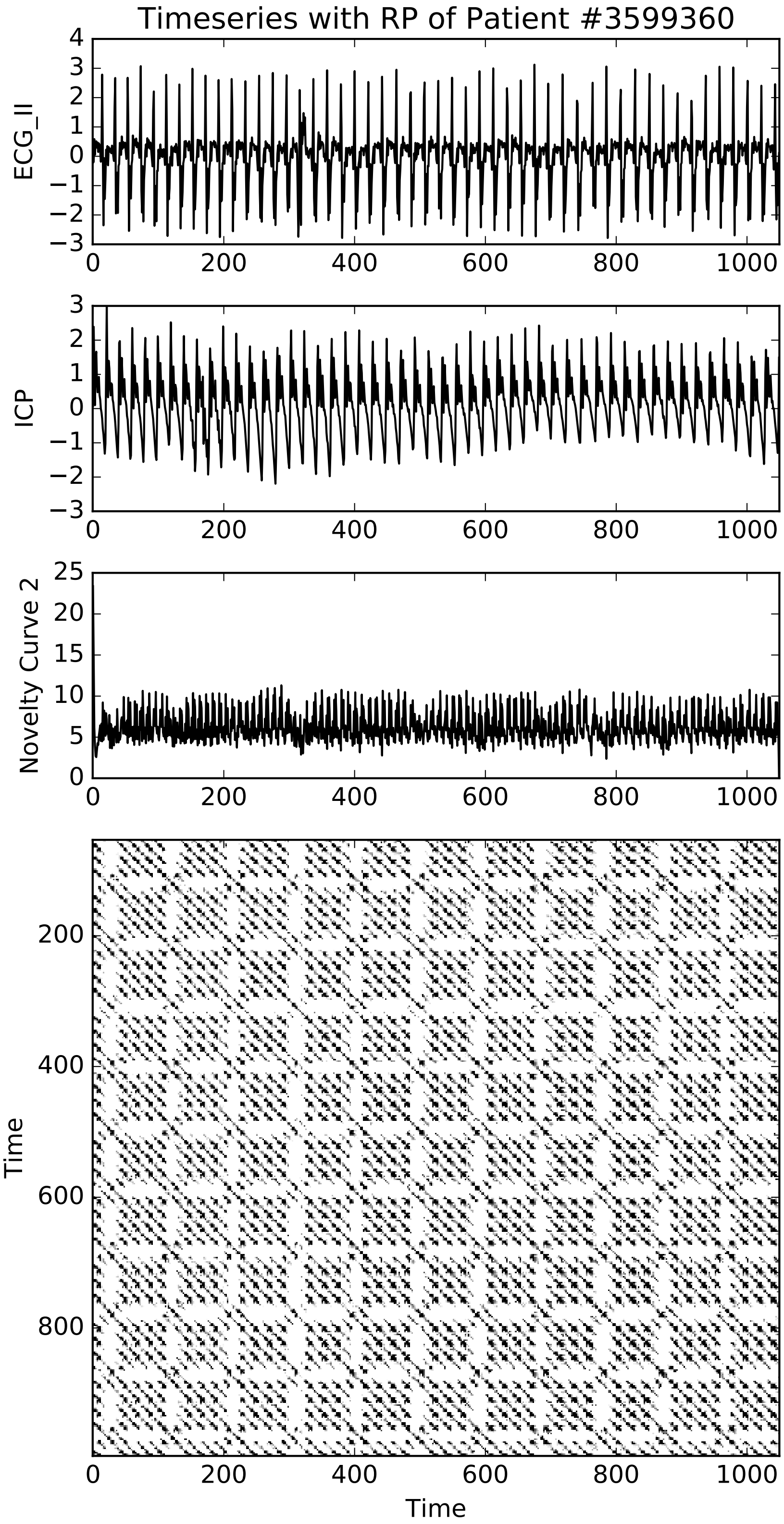

Figure A.82: RP and novelty curve of subject 3599360

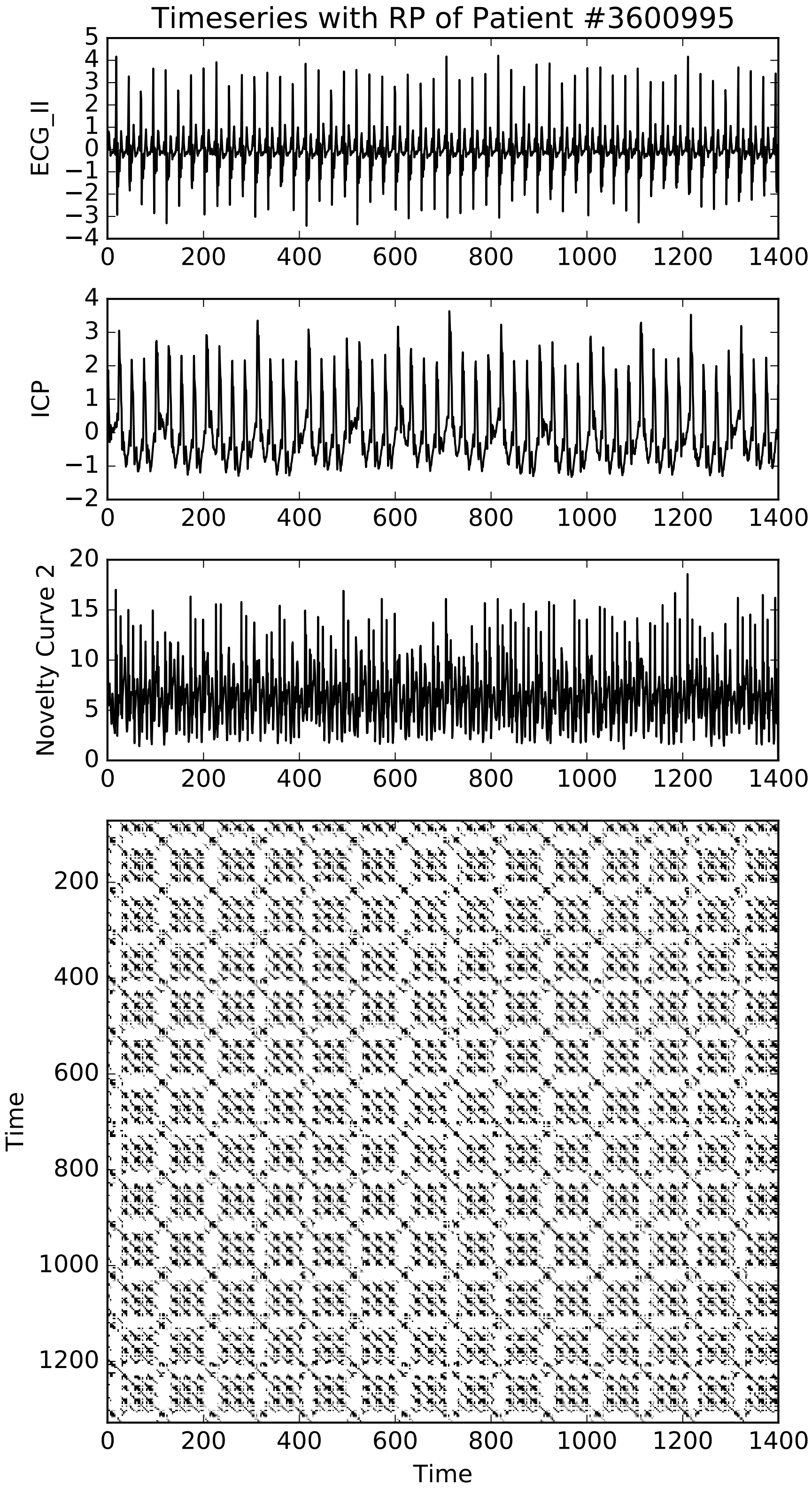

Figure A.83: RP and novelty curve of subject 3600995

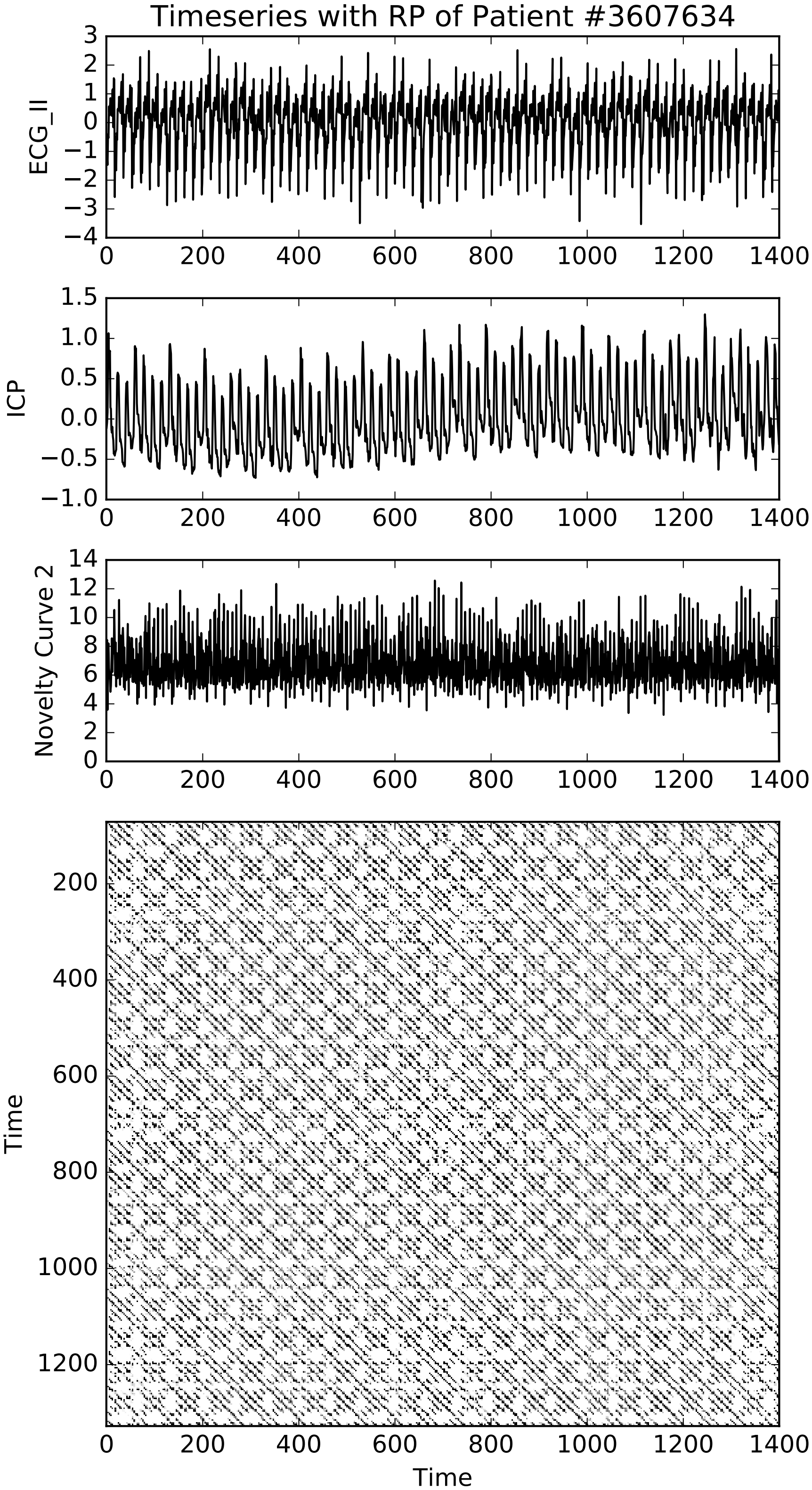

Figure A.84: RP and novelty curve of subject 3607634

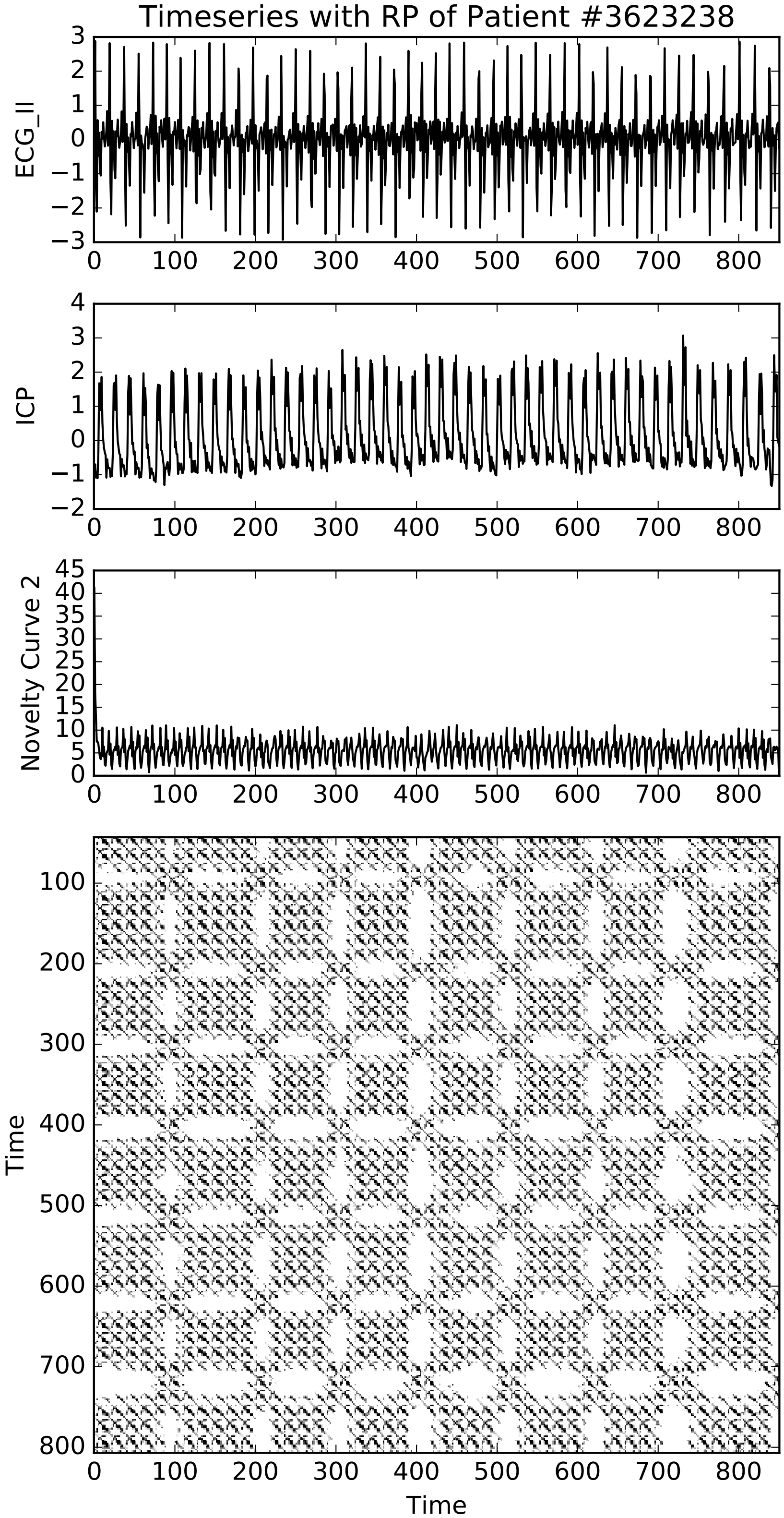

Figure A.85: RP and novelty curve of subject 3623238

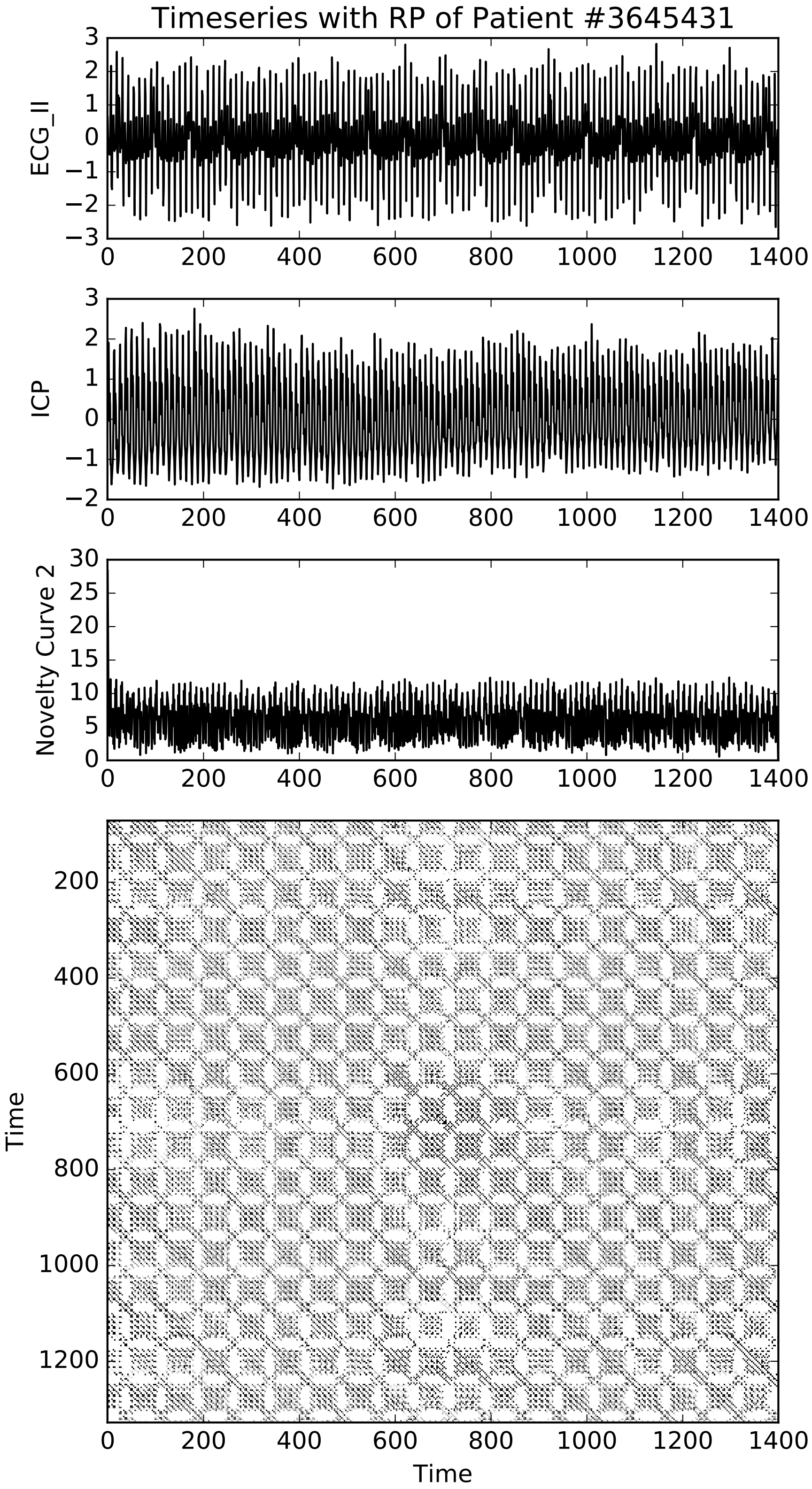

Figure A.86: RP and novelty curve of subject 3645431

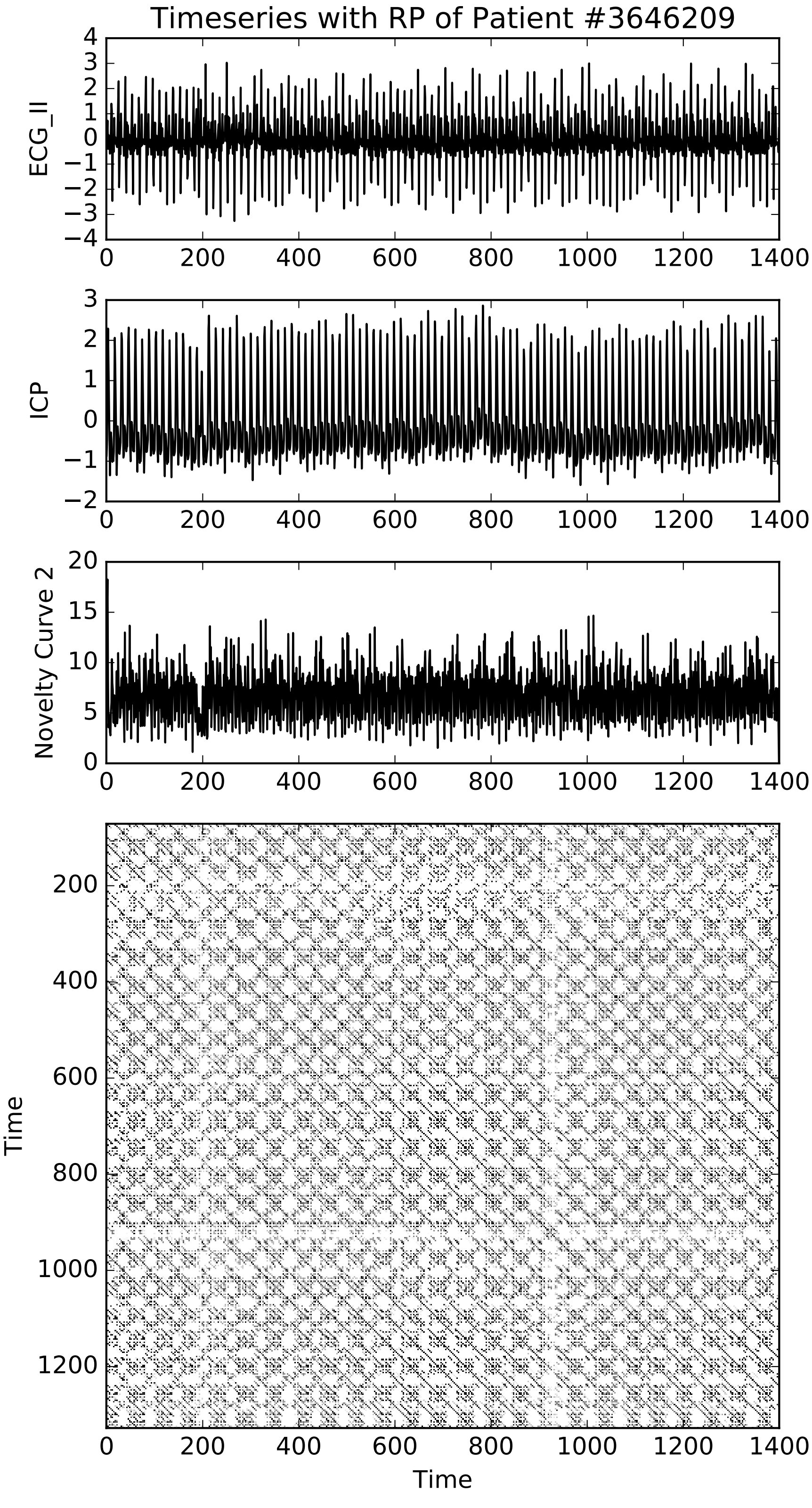

Figure A.87: RP and novelty curve of subject 3646209

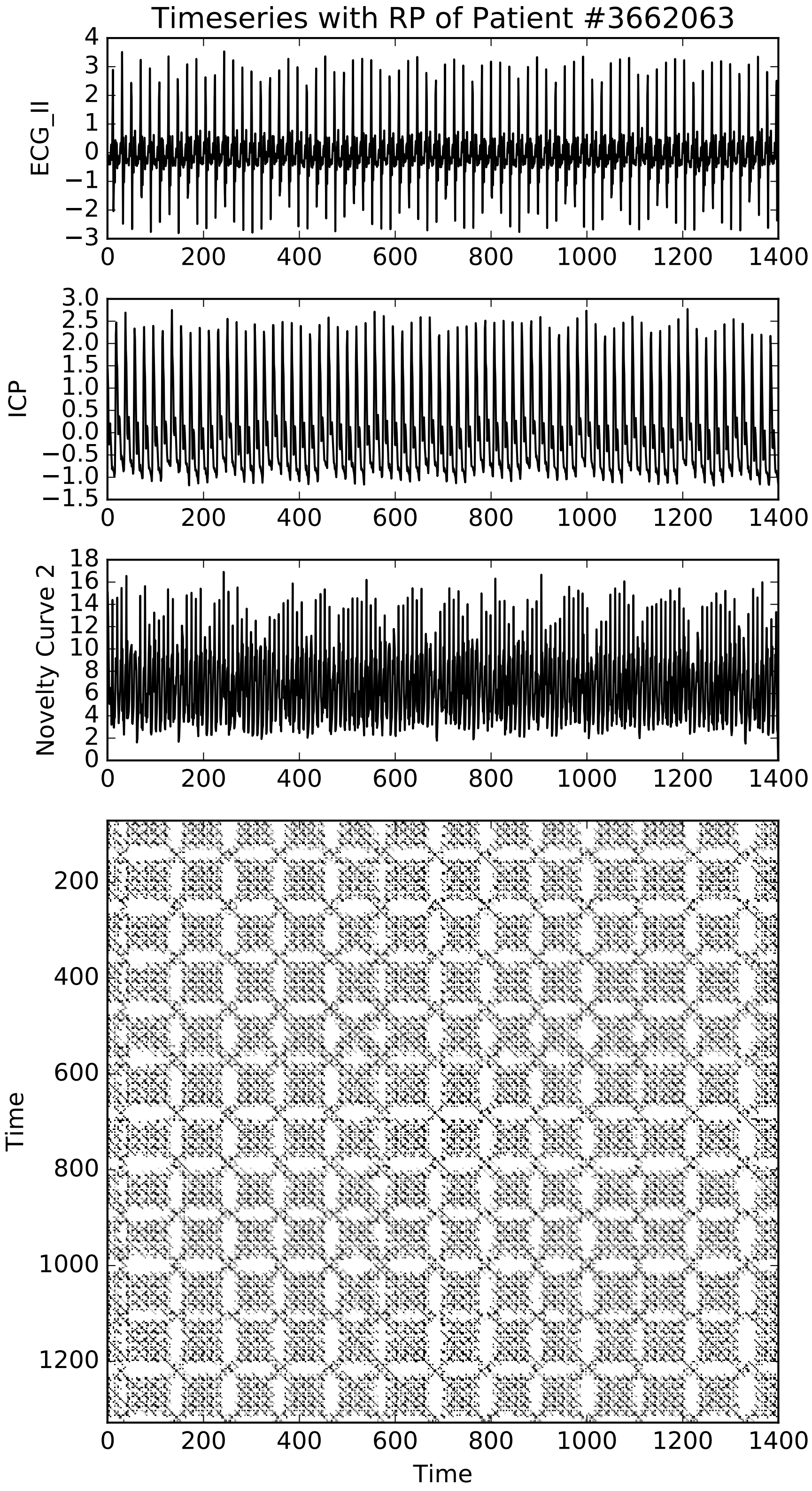

Figure A.88: RP and novelty curve of subject 3662063

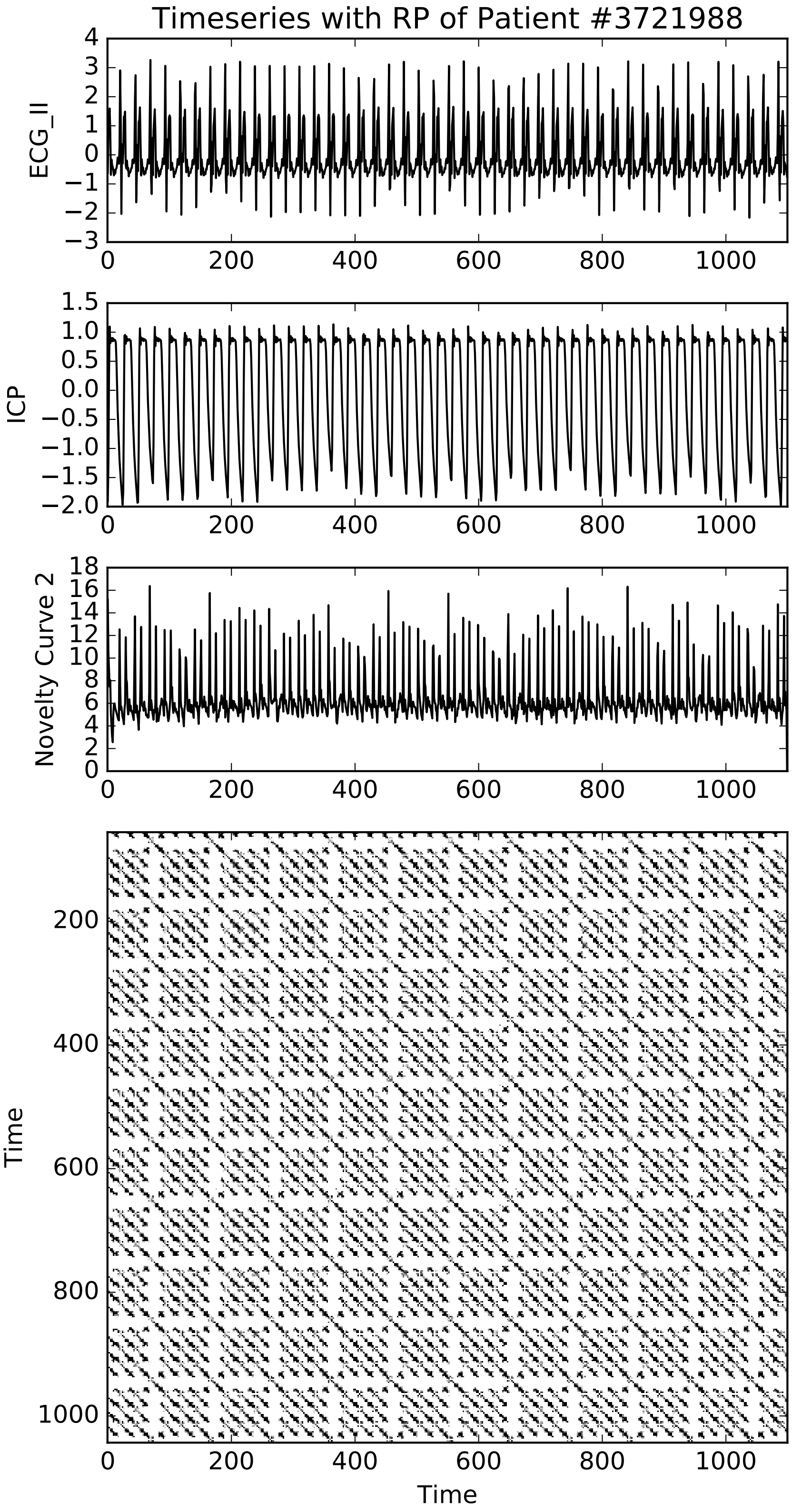

Figure A.89: RP and novelty curve of subject 3721988

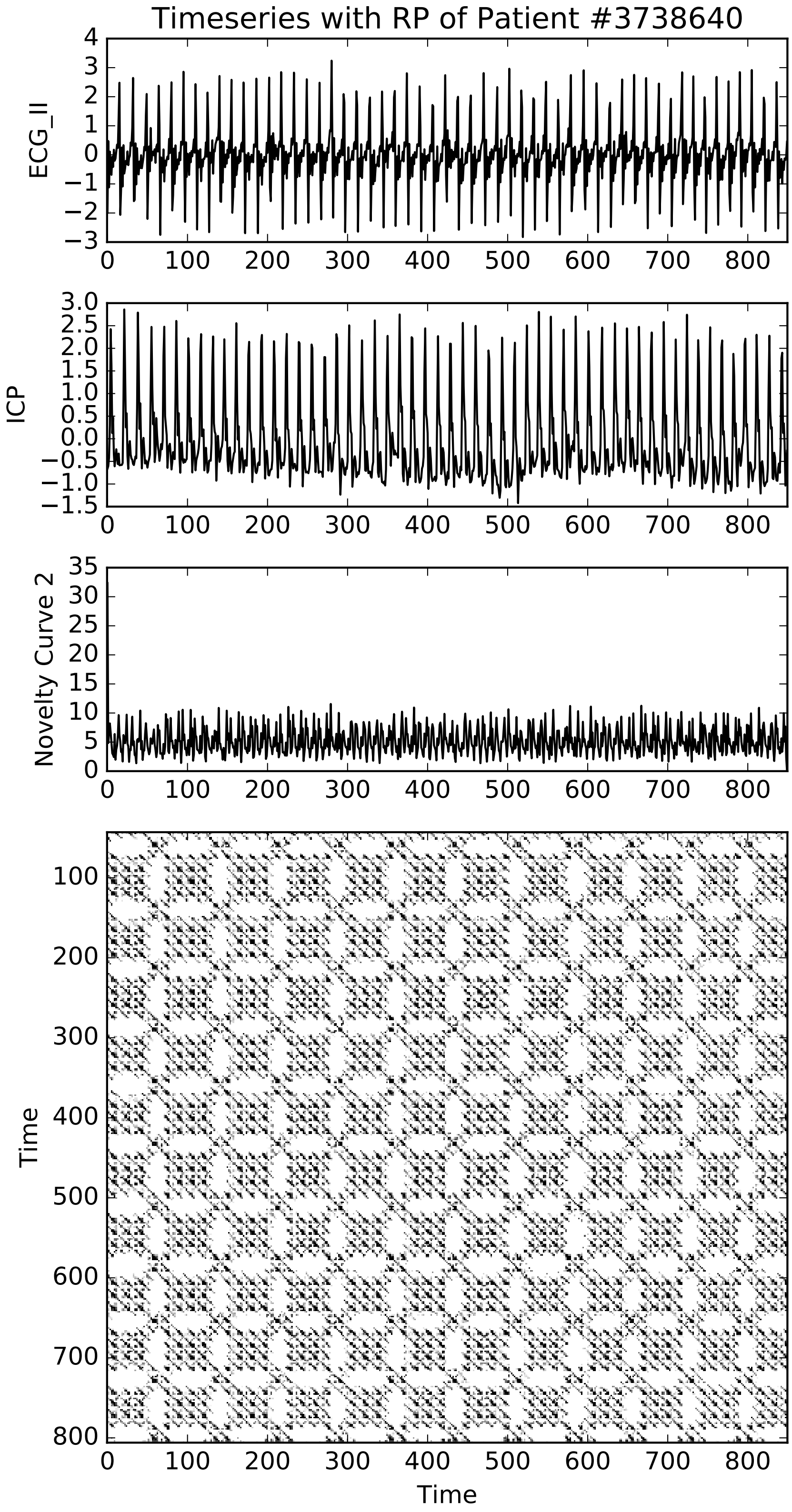

Figure A.90: RP and novelty curve of subject 3738640

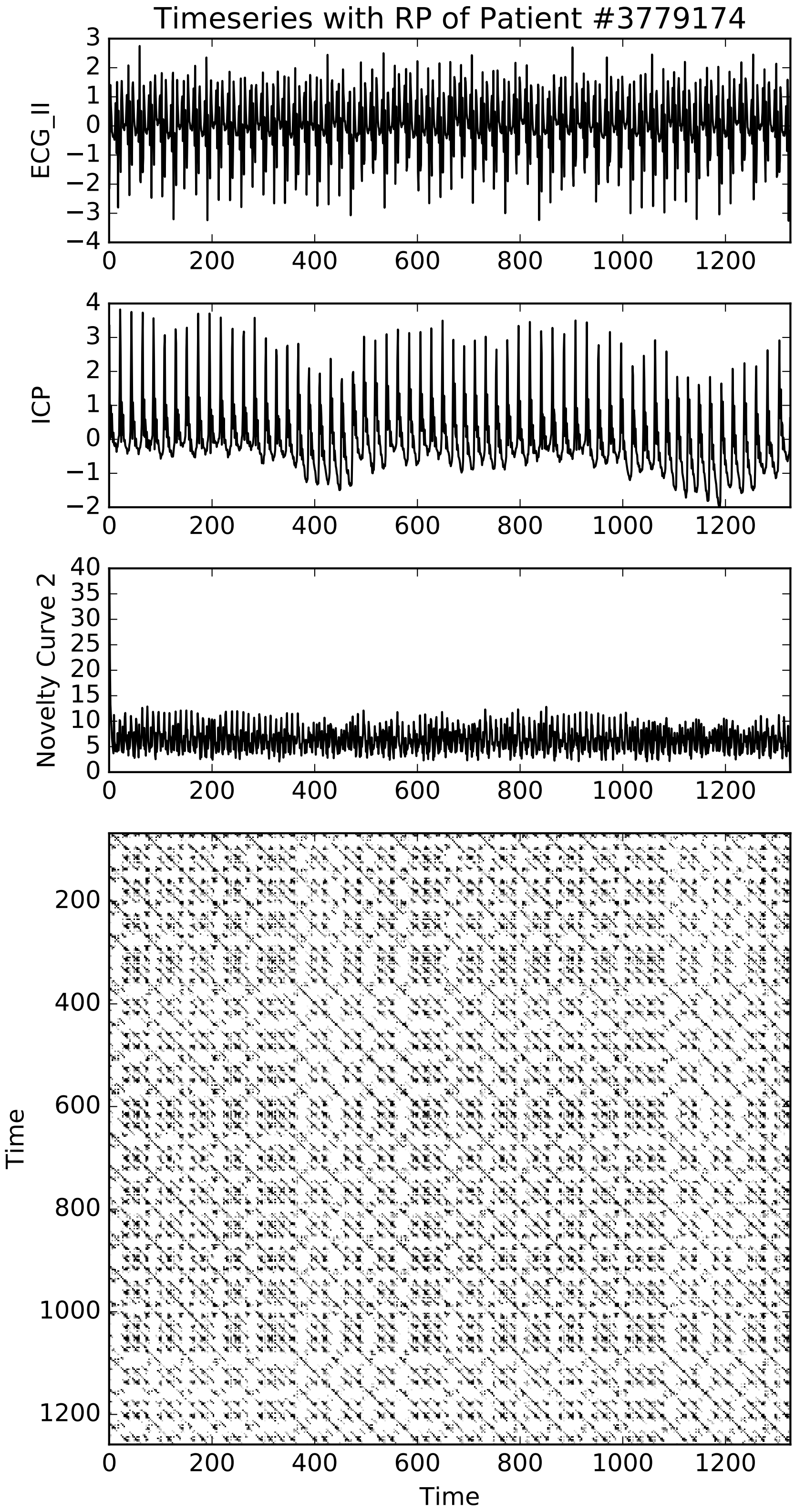

Figure A.91: RP and novelty curve of subject 3779174

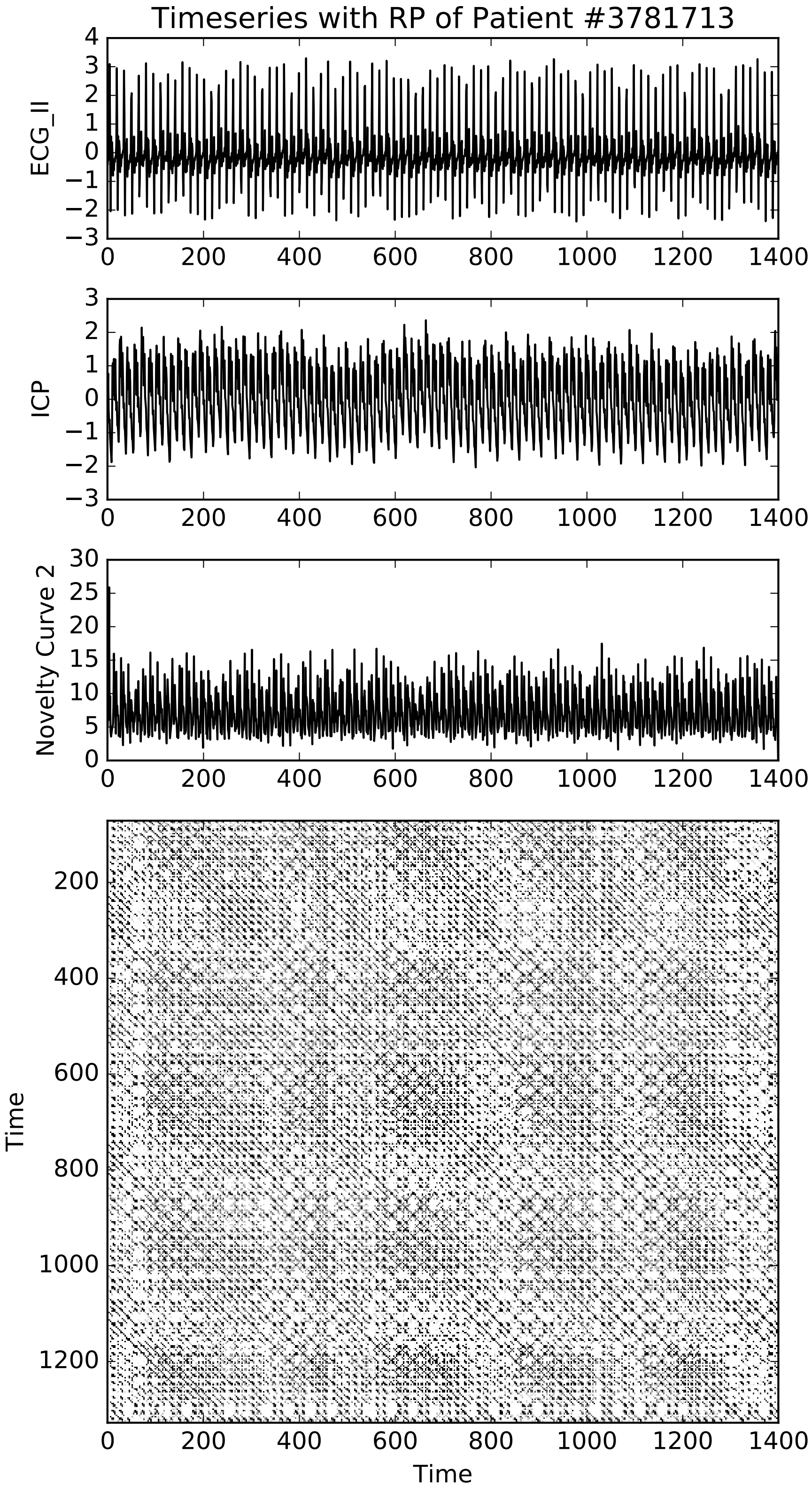

Figure A.92: RP and novelty curve of subject 3781713

Curriculum Vitae

Name:	Mahnaz Rabbani	
Post-Secondary Education:	Master of Science in Computer Science , The University of Western Ontario, London, Canada	2015-present
	Master of Science in Applied Mathematics, The University of Western Ontario, London, Canada	2013-2015
	Bachelor of Science in Mathematics, The KNT University of Technology, Tehran, Iran	2007-2012
Related Work Experience:	Teaching Assistant, The University of Western Ontario	2013-present
	Research Assistant, The University of Western Ontario	2013-present
Publication and Presentations:	The Recurrence-Based Approach for Brain Data Analysis; Oral presentation at the 2017 AMMCS Interdisciplinary Congress; Waterloo, Ontario, Canada; August 20-25, 2017	
	Statistical Data Analysis for Genomics and Neurology: Example Cases of Analysis of Prokaryotic Genome Evolution and Intracranial Pressure Signals; Poster presentation at the Fallona Interdisciplinary Showcase; London, Ontario; January 16, 2017	
	Rabbani, Mahnaz, and Lindi M. Wahl. The dynamics of mobile promoters: Enhanced stability in promoter regions. Published article in the Journal of Theoretical Biology 407: 401-408, 2016	
	Evolution of Mobile Promoters in Prokaryotic Genomes. Master's degree dissertation, The University of Western Ontario, 2015.	